

A Manifestly Gauge Invariant and Universal Calculus for $SU(N)$ Yang-Mills

Oliver J. Rosten

School of Physics and Astronomy, University of Southampton, Highfield,
Southampton SO17 1BJ, U.K.

E-mail: O.J.Rosten@soton.ac.uk

Abstract. Within the framework of the Exact Renormalization Group, a manifestly gauge invariant calculus is constructed for $SU(N)$ Yang-Mills. The methodology is comprehensively illustrated with a proof, to all orders in perturbation theory, that the β function has no explicit dependence on either the seed action or details of the covariantization of the cutoff. The cancellation of these non-universal contributions is done in an entirely diagrammatic fashion.

PACS numbers: 11.10.Gh, 11.15.-q, 11.10.Hi

Contents

| | | |
|----------|---|------------|
| 1 | Introduction | 3 |
| 2 | Review | 9 |
| 2.1 | Elements of $SU(N N)$ Gauge Theory | 9 |
| 2.2 | Diagrammatics for the Flow Equation | 11 |
| 2.2.1 | The Exact Flow Equation | 11 |
| 2.2.2 | The Ward Identities | 13 |
| 2.2.3 | Taylor Expansion of Vertices | 14 |
| 2.2.4 | Charge Conjugation Invariance | 15 |
| 2.3 | The Weak Coupling Expansion | 16 |
| 2.3.1 | Perturbative Diagrammatics | 16 |
| 2.3.2 | The Effective Propagator Relation | 17 |
| 2.3.3 | Primary Diagrammatic Identities of the Third Type | 18 |
| 3 | Further Diagrammatics | 19 |
| 3.1 | Gauge Remainders, Again | 19 |
| 3.2 | The Secondary Diagrammatic Identities | 27 |
| 3.2.1 | The First Family | 27 |
| 3.2.2 | The Second Family | 36 |
| 3.3 | Subtraction Techniques | 39 |
| 3.3.1 | Introduction | 39 |
| 3.3.2 | General Analysis | 42 |
| 4 | Preliminary Diagrammatics | 48 |
| 4.1 | Additional Notation | 48 |
| 4.1.1 | (Pseudo) Effective Propagators | 48 |
| 4.1.2 | Gauge Remainders | 49 |
| 4.1.3 | Vertices | 51 |
| 4.1.4 | Decoration of Kernels <i>etc.</i> | 52 |
| 4.2 | Diagrammatic Functions | 52 |
| 4.2.1 | The Function $\mathcal{D}_{n\mu\nu}^{a11}(p)$ | 53 |
| 4.2.2 | The Function $\mathcal{D}_{n\mu\nu}^{b11}(p)$ | 60 |
| 4.2.3 | The Function $\mathcal{D}_{n\mu\nu}^{c11}(p)$ | 62 |
| 5 | An Expression for β_n | 68 |
| 5.1 | Initial Manipulations | 68 |
| 5.2 | Gauge Remainders | 79 |
| 5.3 | Terms with an $O(p^2)$ Stub | 97 |
| 5.4 | The α and β Terms | 108 |
| 6 | Conclusion | 112 |

Appendix A 116

Appendix B 119

1. Introduction

Of all the problems in theoretical physics, surely one of the most pressing is a better understanding of Yang-Mills theories, particularly in the non-perturbative domain. A promising framework for addressing this issue is the Exact Renormalization Group (ERG) [1–3], the continuum version of Wilson’s RG.

The essential physical idea behind this approach is that of integrating out degrees of freedom between the bare scale of the quantum theory and some effective scale, Λ . The effects of these modes are encoded in the Wilsonian effective action, S_Λ , which describes the physics of the theory in terms of parameters relevant to the effective scale. Central to this methodology is the ERG equation which determines how the Wilsonian effective action changes under infinitesimal changes of the scale. By relating physics at different scales, this equation provides access to the low energy dynamics of Yang-Mills theories. Indeed, more generally, the ERG has proven itself to be a flexible and powerful tool for studying both perturbative and non-perturbative problems in a range of field theories (see [4–12] for reviews). A particular advantage conferred by the ERG is that renormalization is built in: solutions to the flow equation (in pretty much any approximation scheme), from which physics can be extracted, can be naturally phrased directly in terms of renormalized parameters.

Given that the notion of a momentum cutoff is fundamental to the entire ERG construction, it is clear that a regulator is required which incorporates this feature. Immediately, this presents a problem for Yang-Mills theories, since the direct implementation of a momentum cutoff breaks non-Abelian gauge invariance. Traditional (gauge fixed) approaches, which can be broadly divided into those which employ the background field method [13–20] and those which do not [21–37], accept this breaking, recovering the physical symmetry in the limit that all quantum fluctuations have been integrated out.‡

Nevertheless, in [41], a regulator was constructed for $SU(N)$ Yang-Mills based on a real, gauge invariant cutoff. This is achieved by embedding the physical gauge theory into a spontaneously broken $SU(N|N)$ supergauge theory which is itself regularized by covariant higher derivatives. Combining this with earlier work [42–44] allowed the construction of an ERG for Yang-Mills which respects gauge invariance at all scales [45]. In addition to the obvious advantages this has over the alternative approaches, there is a major additional benefit: the gauge invariance is in fact *manifest*, no gauge fixing being required at any stage in the computation of the Wilsonian effective action. Whilst having considerably novelty value, manifest gauge invariance also provides powerful technical

‡ For an approach based on the geometric effective action see [38, 39] and for a summary of the various approaches see [40].

simplifications: the gauge field is protected from field strength renormalization and the Ward identities take a particularly simple form [43], since the Wilsonian effective action is built only from gauge invariant combinations of the covariant derivative, even at the quantum level. In the non-perturbative domain, not only are Gribov copies [46] entirely avoided, but it should be possible to make statements about *e.g.* confinement in a completely gauge independent way. Furthermore, such a framework has the ability to underlie gauge-fixed ERG formalisms as it should, in principle, be possible to derive all results obtained by the latter by gauge fixing at an appropriate stage.

The key to constructing the manifestly gauge invariant scheme of this paper resides in the immense freedom inherent in the ERG [47–49]: of the infinite number suitable for $SU(N)$ Yang-Mills, an infinite subset allow the Wilsonian effective action to be computed without fixing the gauge. Of these manifestly gauge invariant ERGs, we further specialize to those which allow convenient renormalization to any loop order [49–51]. (By this we mean that the flow equation is of a suitably general form to treat the physical gauge field and an unphysical copy, which is part of the regularizing structure, asymmetrically. Since each of these fields comes with their own coupling, which renormalize separately, allowing the flow equation to distinguish between them facilitates convenient computation.)

Despite these restrictions, there are still an infinite number of admissible ERGs, the differences between them amounting to the following non-universal details. The first two relate to the implementation of a gauge invariant cutoff: the exact forms of both the cutoff functions and their covariantizations amount to non-universal choices. The final source of non-universal differences between the ERGs with which we work is the ‘seed action’, \hat{S} [45, 49–51, 54–56]: a functional which respects the same symmetries as the Wilsonian effective action, S , and has the same structure. However, whereas our aim is to solve the flow for S , \hat{S} acts as an input. Physically, the seed action can be thought of as (partially) parameterizing a general Kadanoff blocking [57] in the continuum [47–49]. Crucially, these non-universal details need never be explicitly specified, instead just satisfying general constraints to ensure that the flow equation is well defined. We turn this residual freedom in the construction to our advantage by recognizing that since all non-universal details must cancel out in the computation of a universal quantity, they can be efficiently absorbed into diagrammatic rules. This observation formed the basis for the manifestly gauge invariant and universal calculus proposed in [45], in which a scheme was developed whereby these non-universal contributions can be iteratively cancelled out, in perturbative calculations.

In the original work [45], a small subset of the diagrammatic rules now known to exist were uncovered and were used in the initial stages of a manifestly gauge invariant computation of the one-loop β function. In a series of works since then [49–51, 55, 56], these diagrammatic rules were extended, allowing both the one and two-loop β functions (in a variety of Quantum Field Theories (QFTs)) to be reduced to manifestly universal diagrammatic expressions, from which the correct numerical coefficients were directly extracted. In this paper, working in $SU(N)$ Yang-Mills, we bring together and complete

the overlapping sets of ideas from this collection of works, developing the diagrammatic calculus to a stage where it is applicable at any number of loops. The calculus is then comprehensively illustrated by deriving an expression for the n -loop β function, β_n , which has no explicit dependence on either the seed action or the details of the covariantization of the cutoff.

This result is, in itself, interesting for several reasons. First, let us recall the standard argument as to why the coefficients β_1 and β_2 , but not $\beta_{\geq 3}$, are guaranteed to agree between certain renormalization schemes [58]. It is important to recognize that each choice of the non-universal details within our ERG corresponds, in general, to a different renormalization scheme. Focusing on one such scheme, we take the coupling of the physical $SU(N)$ gauge field to be $g(\Lambda)$.[§] Now consider a second scheme—either corresponding to some other choice of non-universal details within our ERG or to an entirely independent scheme such as \overline{MS} —with coupling $\tilde{g}(\mu \mapsto \Lambda)$. Given the dimensionless coefficient, η , we can perturbatively match the two couplings:

$$\frac{1}{\tilde{g}^2} = \frac{1}{g^2} + \eta + \mathcal{O}(g^2). \tag{1}$$

Using the usual definition for the β function of g

$$\beta \equiv \Lambda \partial_\Lambda g = \sum_{i=1}^{\infty} g^{2i+1} \beta_i,$$

and a similar definition for $\tilde{\beta}(\tilde{g})$, we can differentiate (1) with respect to Λ to obtain

$$\tilde{\beta}_1 + g^2 \tilde{\beta}_2 = \beta_1 + g^2 \beta_2 + \Lambda \partial_\Lambda \eta + \mathcal{O}(g^4). \tag{2}$$

Therefore, if $\Lambda \partial_\Lambda \eta = 0$ (or, at any rate, does not contribute until $\mathcal{O}(g^4)$), we will obtain $\tilde{\beta}_1 = \beta_1$ and $\tilde{\beta}_2 = \beta_2$. We can expect this agreement to be spoiled, however, if there exist running, dimensionless couplings, besides g (which is equivalent to the introduction of additional mass scales).

Indeed, within our setup there generically exist dimensionless couplings which run even at tree level level [45], spoiling agreement between β -function coefficients at one loop. Of course, this is not a sign of a sick formalism, just a sign that β_1 and β_2 are not physically observable and can be scheme dependent. Nonetheless, it is possible to recover the universal values of β_1 and β_2 by suitably tailoring the setup. The running of η has two sources. The first is \hat{S} , which contributes to the running of η at all orders, including tree level. However, through an implicit choice of \hat{S} , this running can be removed, not just at one-loop, but actually to all orders [50, 51]. Indeed, we now assume that this has been done, and promote this choice to a requirement, necessary in the specification of the subset of manifestly gauge invariant ERGs with which we choose to work.

The second contribution to $\Lambda \partial_\Lambda \eta$ comes from an unphysical, dimensionless coupling, g_2 , associated with the regularizing structure [41, 49–51]. The running of this coupling, which occurs from the one-loop level onwards, cannot be removed through a choice of

[§] Beyond this discussion, we will take $g(\Lambda)$ to represent the coupling for all renormalization schemes implicitly defined by our approach.

\hat{S} ; the solution is to tune it to zero at the end of a calculation. In this manner, β_2 can be arranged to coincide with its standard value [50, 51]. For convenience, we work not with g_2 directly but with

$$\alpha := g_2^2/g^2 \tag{3}$$

and so it is α , in practise, which is tuned to zero.

Beyond two loops, it is apparent from (2) that there is no reason to expect any agreement between β function coefficients. In light of this, it is surprising not only that all contributions to $\Lambda\partial_\Lambda\eta$ coming from \hat{S} can be removed to all orders but also that all dependence of β_n on the seed action and details of the covariantization of the cutoff cancels out, to all orders. (For speculations on whether it may be possible to push the removal of non-universal details further still, see [53].) That we do find such cancellations is perhaps indicative that there is a more direct framework for performing calculations in QFTs which retains the advantages of the ERG approach whilst removing some or all of the redundancy inherent in the approach. In particular, these observations could inspire a manifestly gauge invariant formalism where the seed action and details of the covariantization of the cutoff are relegated to a background role.

The second point to make about the derivation of an expression for β_n which has no explicit dependence on either the seed action or the details of the covariantization of the cutoff is that this is a huge step forward in turning this formalism into a practical computational scheme. The calculation of β_1 and β_2 in this ERG approach was, up until now, an arduous task; just getting to the expression from which the universal value can be extracted was extremely difficult. Now, however, this step is trivial as we simply specialize the new formula for β_n to the appropriate loop order!

To appreciate the various elements of the diagrammatic calculus, it is worth reviewing the procedure for computing β function coefficients employed in [52]. To compute $\beta_{1,2}$, we start by using the flow equation to compute the flow of the two-point vertex corresponding to the physical $SU(N)$ gauge field, A_μ^1 , which we suppose carries momentum, p . Next, we specialize to the appropriate loop order and work at $O(p^2)$; this latter step constrains the equation by allowing the renormalization condition for the physical coupling to feed in. At this point, the equation for $\beta_{1,2}$ contains a small number of diagrams, each of which contains explicit dependence on both the seed action and the details of the covariantization of the cutoff.

Central to the diagrammatic calculus is the ‘effective propagator relation’ [45, 49–52, 54–56]. This convenient computational device arises as a consequence of a choice of seed action we are free to make: we choose the classical, two-point seed action vertices equal to their Wilsonian effective action counterparts. In turn, this ensures that for each independent classical two-point vertex (that cannot be consistently set to zero [51]) there exists an ‘effective propagator’, denoted by Δ , which is the inverse of the given vertex, up to a ‘gauge remainder’. Denoting the classical two-point vertex corresponding to the fields X and Y , which carry indices R and S and momenta p and $-p$, respectively, by

$S_{0RS}^{XY}(p)$ the effective propagator relationship in the A^1 sector reads

$$S_{0\mu\alpha}^{A^1A^1}(p)\Delta_{\alpha\nu}^{A^1A^1}(p) = \delta_{\mu\nu} - \frac{p_\mu p_\nu}{p^2}.$$

Thus, $p_\mu p_\nu/p^2$ is a gauge remainder and it appears as a consequence of the manifest gauge invariance: the effective propagators are inverses of the classical, two-point vertices only in the transverse space. As we will see later, it is convenient to split this gauge remainder into two components, p_ν and p_μ/p^2 .

To proceed, we recognize that certain diagrams generated by the flow comprise exclusively Wilsonian effective action vertices joined together by $\overset{\bullet}{\Delta}$, where we define

$$\overset{\bullet}{X} \equiv -\Lambda\partial_\Lambda|_\alpha X. \quad (4)$$

These terms are processed by moving the $-\Lambda\partial_\Lambda|_\alpha$ from the effective propagator to the diagram as a whole, minus correction terms in which $-\Lambda\partial_\Lambda|_\alpha$ strikes the vertices. The former diagrams are called Λ -derivative terms; the latter can be processed using the flow equation and the resulting set of diagrams simplified, using a set of primary diagrammatic identities, of which the effective propagator relation is one. At this point, we are able to identify cancellations of non-universal contributions, at the diagrammatic level. There is, however, a complication to this diagrammatic procedure: particular classes of sub-diagrams can have two distinct diagrammatic representations. The equivalence of these representations is encoded in the secondary diagrammatic identities.

Iterating the diagrammatic procedure, the expressions for $\beta_{1,2}$ ultimately reduce to the following sets of diagrams:

- (i) Λ -derivative terms, which are built out of Wilsonian effective action vertices, effective propagators and (components of) gauge remainders;
- (ii) ‘ α -terms’, consisting of diagrams built out of the same elements as the Λ -derivative terms but struck by $\partial/\partial\alpha$ (there are no α -terms at one loop [49, 51]);
- (iii) ‘ $O(p^2)$ -terms’, which contain an $O(p^2)$ stub *i.e.* a diagrammatic component which is manifestly $O(p^2)$.

The $O(p^2)$ -terms can be manipulated. In the calculation of β_1 , at any rate, the structure attaching to the stub can be directly Taylor expanded to zeroth order in p —which can once again be done diagrammatically. The above diagrammatic procedure is then iterated. At two loops (and beyond), this procedure is not so straightforward, since naïve Taylor expansion can generate spurious infra-red (IR) divergences [49–51]. The solution is to isolate the components which cannot be Taylor expanded using the ‘subtraction techniques’ of [50, 51]. Now the $O(p^2)$ can be processed, and so $\beta_{1,2}$ can be reduced to just Λ -derivative and α -terms. From these terms, the universal values of $\beta_{1,2}$ can be extracted [45, 50, 51].

Given the diagrammatic representation of the flow equation, the diagrammatic calculus comprises the following elements:

- (i) An operator which implements the flow *i.e.* $-\Lambda\partial_\Lambda$;
- (ii) A diagrammatic rule reflecting the charge conjugation invariance of the theory;

- (iii) The primary diagrammatic identities which allow the direct manipulation of diagrams possessing particular elements;
- (iv) The secondary diagrammatic identities which encode the equivalence of distinct diagrammatic representations of particular classes of sub-diagrams;
- (v) The subtraction techniques.

The primary diagrammatic identities further decompose into three sets. Those of the first type are defined without any reference to perturbation theory, and follow from general constraints such as gauge invariance. The single primary diagrammatic identity of the second type is the effective propagator relation, which we recall follows from the classical flow equation, given a choice we impose on the seed action. Those of the third type follow directly from those of the first and second types. However, it is convenient to give them in their own right, as they are not necessarily obvious and are heavily used in this paper.

The secondary diagrammatic identities decomposes into two families, one of which is applicable only to those diagrams which possess an $O(p^2)$ stub and the other of which is more generally applicable.

It is apparent that, of all the elements of the diagrammatic calculus, only one is reliant on perturbation theory. An obvious question, to which we return in the conclusion, is whether the calculus has a non-perturbative extension. We emphasise that, irrespective of whether or not this is the case, the framework admits standard ERG analyses in the non-perturbative domain, but with the benefits of manifest gauge invariance.

To derive an expression for arbitrary β_n , we could pursue the above strategy (see [51] for an attempt in this direction). However, there is a much more efficient way to proceed, motivated by the form of the Λ -derivative terms at one and two loops. We start by constructing a set of n -loop functions which depend only on Wilsonian effective action vertices, effective propagators and (components of) gauge remainders. Considering the $O(p^2)$ parts of these diagrams (strictly, up to functions not polynomial in p), we compute their flow. Amongst the generated terms is β_n multiplied by a coefficient which is universal as a consequence of specializing to $O(p^2)$. Using the various diagrammatic identities, we then demonstrate that all dependence on the seed action and details of the covariantization cancels out between the remaining terms. By taking the Λ -derivative terms as the starting point for the calculation, we avoid having to iteratively construct them, which reaps better and better dividends with each loop order.

This paper is organized as follows. In section 2, we review the aspects of the manifestly gauge invariant ERG we require for this paper. Following a brief exposition of $SU(N|N)$ gauge theory, the flow equation is introduced via its diagrammatic representation. Some properties of the various diagrammatic elements of the flow equation are discussed and the primary diagrammatic identities of the first type are stated. The section concludes with the examination of the form taken by the flow equation in the perturbative regime; we describe the effective propagator relation and

derive the primary diagrammatic identities of the third type.

Section 3, the basis of which comes from [51], is devoted to developing the diagrammatic techniques to the level sufficient for computing β_n . First, we revisit the gauge remainders, discussing the type of diagrams they can generate in the perturbative domain. Next, we state and prove the secondary diagrammatic identities and finally we describe the subtraction techniques necessary for manipulating the $O(p^2)$ terms. This completes the description of the calculus and concludes the first part of the paper.

The second part of the paper is devoted to a detailed illustration of the calculus. Section 4 begins with a description of some further notation which facilitates the practical application of the calculus, by allowing us to represent sets (with a potentially huge number) of n -loop diagrams in an extremely compact manner. Using this notation, we introduce a set of diagrammatic functions which will play a central role in the treatment of β_n to follow. Various important properties of these functions are analysed, which allows an illustration of many of the diagrammatic techniques in their most natural setting. In section 5 we derive an expression for β_n which is independent of the seed action and the details of the covariantization of the cutoff and we conclude in section 6. The primary and secondary diagrammatic identities are collected together in Appendix A for easy reference.

2. Review

2.1. Elements of $SU(N|N)$ Gauge Theory

Throughout this paper, we work in Euclidean dimension, D . We regularize $SU(N)$ Yang-Mills by embedding it in spontaneously broken $SU(N|N)$ Yang-Mills, which is itself regularized by covariant higher derivatives [41]. The supergauge field, \mathcal{A}_μ , is valued in the Lie superalgebra and, using the defining representation, can be written as a Hermitian supertraceless supermatrix:

$$\mathcal{A}_\mu = \begin{pmatrix} A_\mu^1 & B_\mu \\ \bar{B}_\mu & A_\mu^2 \end{pmatrix} + \mathcal{A}_\mu^0 \mathbb{1}.$$

Here, $A_\mu^1(x) \equiv A_{a\mu}^1 \tau_1^a$ is the physical $SU(N)$ gauge field, τ_1^a being the $SU(N)$ generators orthonormalized to $\text{tr}(\tau_1^a \tau_1^b) = \delta^{ab}/2$, while $A_\mu^2(x) \equiv A_{a\mu}^2 \tau_2^a$ is a second unphysical $SU(N)$ gauge field. When labelling *e.g.* vertex coefficient functions, we often abbreviate $A^{1,2}$ to just 1,2. The B fields are fermionic gauge fields which will gain a mass of order Λ from the spontaneous symmetry breaking; they play the role of gauge invariant Pauli-Villars (PV) fields, furnishing the necessary extra regularization to supplement the covariant higher derivatives. In order to unambiguously define contributions which are finite only by virtue of the PV regularization, a pre-regulator must be used in $D = 4$ [41]. For the time being, we will use dimensional regularization, emphasising that this makes sense non-perturbatively, since it is not being used to renormalize the theory, but rather as a prescription for discarding surface terms in loop integrals [41].

The theory is subject to the local invariance:

$$\delta\mathcal{A}_\mu = [\nabla_\mu, \Omega(x)] + \lambda_\mu(x)\mathbb{1}. \quad (5)$$

The first term, in which $\nabla_\mu = \partial_\mu - i\mathcal{A}_\mu$, generates supergauge transformations. Note that the coupling, g , which we now take to represent the coupling for all renormalization schemes implicitly defined by our approach, has been scaled out of this definition. It is worth doing this: since we do not gauge fix, the exact preservation of (5) means that none of the fields suffer wavefunction renormalization, even in the broken phase [45].

The second term in (5) divides out the centre of the algebra. This ‘no \mathcal{A}^0 shift symmetry’ ensures that nothing depends on \mathcal{A}^0 and that \mathcal{A}^0 has no degrees of freedom. We adopt a prescription whereby we can effectively ignore the field \mathcal{A}^0 , altogether, using it to map us into a particular diagrammatic picture [49, 51].

The spontaneous symmetry breaking is carried by a superscalar field

$$\mathcal{C} = \begin{pmatrix} C^1 & D \\ \bar{D} & C^2 \end{pmatrix},$$

which transforms homogeneously:

$$\delta\mathcal{C} = -i[\mathcal{C}, \Omega]. \quad (6)$$

It can be shown that, at the classical level, the spontaneous symmetry breaking scale (effectively the mass of B) tracks the covariant higher derivative effective cutoff scale, Λ , if \mathcal{C} is made dimensionless (by using powers of Λ) and \hat{S} has the minimum of its effective potential at:

$$\sigma \equiv \begin{pmatrix} \mathbb{1} & 0 \\ 0 & -\mathbb{1} \end{pmatrix}. \quad (7)$$

In this case the classical action S_0 also has a minimum at (7). At the quantum level this can be imposed as a constraint on S by taking $\langle C \rangle = \sigma$ as a renormalization condition. This ensures that the Wilsonian effective action does not possess any one-point vertices, which can be translated into a constraint on \hat{S} [45, 51]. In the broken phase, D is a super-Goldstone mode (eaten by B in the unitary gauge) whilst the C^i are Higgs bosons and can be given a running mass of order Λ [41, 42, 45]. Working in our manifestly gauge invariant formalism, B and D gauge transform into each other; in recognition of this, we define the fields

$$F_M = (B_\mu, D), \quad (8a)$$

$$\bar{F}_N = (\bar{B}_\nu, -\bar{D}), \quad (8b)$$

where M, N are five-indices [49, 51].^{||}

The couplings g and α (recall (3)) are defined through their renormalization conditions:

$$S[\mathcal{A} = A^1, \mathcal{C} = \sigma] = \frac{1}{2g^2} \text{str} \int d^Dx \left(F_{\mu\nu}^1 \right)^2 + \dots, \quad (9)$$

$$S[\mathcal{A} = A^2, \mathcal{C} = \sigma] = \frac{1}{2\alpha g^2} \text{str} \int d^Dx \left(F_{\mu\nu}^2 \right)^2 + \dots, \quad (10)$$

^{||} The summation convention for these indices is that we take each product of components to contribute with unit weight.

where the ellipses stand for higher dimension operators and the ignored vacuum energy. The field strength tensors in the A^1 and A^2 sectors, $F_{\mu\nu}^1$ and $F_{\mu\nu}^2$, should really be embedded in the top left / bottom right entries of a supermatrix, in order for the supertraces in (9,10) to make sense. We will frequently employ this minor abuse of notation, for convenience.

2.2. Diagrammatics for the Flow Equation

2.2.1. The Exact Flow Equation The diagrammatic representation of the flow equation is shown in figure 1 [49, 51]. (For a comprehensive description of the diagrammatics see [49, 51].)

$$\begin{aligned}
 -\Lambda\partial_\Lambda \left[\textcircled{S} \right]^{\{f\}} &= a_0[S, \Sigma_g]^{\{f\}} - a_1[\Sigma_g]^{\{f\}} \\
 &= \frac{1}{2} \left[\begin{array}{c} \textcircled{\Sigma_g} \\ \bullet \\ \textcircled{S} \end{array} - \textcircled{\Sigma_g}^{\bullet} - \textcircled{\Sigma_g}^{\bullet} \right]^{\{f\}}
 \end{aligned}$$

Figure 1. The diagrammatic form of the flow equation.

The left-hand side depicts the flow of all independent Wilsonian effective action vertex *coefficient functions*, which correspond to the set of broken phase fields, $\{f\}$. Each coefficient function has associated with it an implied supertrace structure (and symmetry factor which, as one would want, does not appear in the diagrammatics). For example,

$$\left[\textcircled{S} \right]^{C^1 C^1} \tag{11}$$

represents both the coefficient functions $S^{C^1 C^1}$ and S^{C^1, C^1} which, respectively, are associated with the supertrace structures $\text{str}C^1 C^1$ and $\text{str}C^1 \text{str}C^1$.

The objects on the right-hand side of figure 1 have two different types of component. The lobes represent vertices of action functionals, where $\Sigma_g \equiv g^2 S - 2\hat{S}$ (recall that \hat{S} is the seed action). The object attaching to the various lobes, $\text{---}\bullet\text{---}$, is the sum over vertices of the covariantized ERG kernels [43, 45] and, like the action vertices, can be decorated by fields belonging to $\{f\}$. The appearance of the symbol \bullet is not accidental, meaning $-\Lambda\partial_\Lambda|_\alpha$, as in (4). The dumbbell-like term, which corresponds to the bilinear functional a_0 , is referred to as the classical term. The next two terms, which are both generated by a_1 , are referred to as quantum terms. The second of these contains a kernel which ‘bites its own tail’. This diagram is not properly UV regularized by the $SU(N|N)$ regularization and, in the past, it has been argued that it can and should be

discarded, through an appropriate constraint on the covariantization [42, 43, 45, 49]. ^{\mathcal{P}} Here, though, we will keep these diagrams for as long as possible: as recognized in [51], in any calculation β function coefficients, the explicit ultraviolet divergences in kernel-biting-their-tail diagrams, which can be dimensionally regularized, should be cancelled by divergences hidden in other terms. In this paper, we demonstrate that this is indeed the case: all explicit dependence of β_n on kernel-biting-their-tail diagrams cancels out. Nonetheless, there is an implicit dependence left behind and it seems inevitable that, to further proceed, the covariantization must be suitably constrained, after all.

It is worth drawing attention to the fact that dimensional regularization is thus being used for two entirely independent purposes. On the one hand, it is used as a temporary measure, at intermediate stages of our calculations, to properly define diagrams possessing a kernel which bites its own tail. On the other hand, it is being employed as a pre-regulator. As we will argue in the conclusions, there is evidence to suggest the existence of a purely diagrammatic pre-regulator, which would make sense in $D = 4$.

Embedded within the diagrammatic rules is a prescription for evaluating the group theory factors. Suppose that we wish to focus on the flow of a particular vertex coefficient function, which necessarily has a unique supertrace structure. For example, we might be interested in just the $S^{C^1 C^1}$ component of (11).

On the right-hand side of the flow equation, we must focus on the components of each diagram with precisely the same (implied) supertrace structure as the left-hand side, noting that the kernel, like the vertices, has multi-supertrace contributions (for more details see [49, 51]). In this more explicit diagrammatic picture, the kernel is to be considered a double sided object. Thus, whilst the dumbbell like term of figure 1 has at least one associated supertrace, the next diagram has at least two, on a account of the loop (this is strictly true only in the case that kernel attaches to fields on the same supertrace). If a closed circuit formed by a kernel is devoid of fields then it contributes a factor of $\pm N$, depending on the flavours of the fields to which the kernel forming the loop attaches. This is most easily appreciated by defining the projectors

$$\sigma_+ \equiv \begin{pmatrix} \mathbb{1} & 0 \\ 0 & 0 \end{pmatrix}, \quad \sigma_- \equiv \begin{pmatrix} 0 & 0 \\ 0 & \mathbb{1} \end{pmatrix} \tag{12}$$

and noting that $\text{str}\sigma_{\pm} = \pm N$. In the counterclockwise sense, a σ_+ can always be inserted for free after an A^1 , C^1 or \bar{F} , whereas a σ_- can always be inserted for free after an A^2 , C^2 or F .

The rules thus described receive $1/N$ corrections in the A^1 and A^2 sectors. If a kernel attaches to an A^1 or A^2 , it comprises a direct attachment and an indirect attachment, as shown in figure 2 (see [49, 51] for more detail).

^{\mathcal{P}} These diagrams are artefacts of the flow equation. The $SU(N)$ gauge theory *is* fully regularized by the $SU(N|N)$ scheme. However, regularization of the flow equation does not trivially follow from the regularization of the underlying theory.

Figure 2. The $1/N$ corrections to the group theory factors.

We can thus consider the diagram on the left-hand side as having been unpackaged, to give the terms on the right-hand side. The dotted lines in the diagrams with indirect attachments serve to remind us where the loose end of the kernel attaches in the parent diagram.

2.2.2. The Ward Identities All vertices, whether they belong to either of the actions or to the covariantized kernels are subject to Ward identities which, due to the manifest gauge invariance, take a particularly simple form:

$$q \begin{array}{c} X \\ \swarrow \\ \downarrow^p \\ \searrow \\ Y \\ \swarrow \\ r \end{array} = \begin{array}{c} X \\ \swarrow \\ \downarrow \\ \searrow \\ Y \end{array} + \begin{array}{c} X \\ \swarrow \\ \downarrow \\ \searrow \\ Y \end{array} - \begin{array}{c} X \\ \swarrow \\ \downarrow \\ \searrow \\ Y \end{array} - \begin{array}{c} X \\ \swarrow \\ \downarrow \\ \searrow \\ Y \end{array} + \dots (13)$$

Equation (13) is the first primary diagrammatic identity of the first type. On the left-hand side, we contract a vertex with the momentum of the field which carries p . This field—which we will call the active field—can be either A_ρ^1 , A_ρ^2 , F_R or \bar{F}_R . In the first two cases, the triangle \triangleright represents p_ρ whereas, in the latter two cases, it represents $p_R \equiv (p_\rho, 2)$. (Given that we often sum over all possible fields, we can take the Feynman rule for \triangleright in the C -sector to be null.) In all cases, \triangleright is independent of Λ and α , which is encoded in the second of the primary diagrammatic identities of the first type:

$$\begin{array}{c} \bullet \\ \triangleright \end{array} = 0, \quad (14a)$$

$$\begin{array}{c} \textcircled{\triangleright} \\ \triangleright \end{array} = 0, \quad (14b)$$

where $\textcircled{\triangleright} \equiv \partial/\partial\alpha$.

On the right-hand side of (13), we push the contracted momentum forward onto the field which directly follows the active field, in the counterclockwise sense, and pull back (with a minus sign) onto the field which directly precedes the active field. Since our diagrammatics is permutation symmetric, the struck field—which we will call the target field—can be either X , Y or any of the un-drawn fields represented by the ellipsis. Any field(s) besides the active field and the target field will be called spectators. Note that we can take X and $/$ or Y to represent the end of a kernel. In this case, the struck field is determined to be unambiguously on one side of the (double sided) kernel; the contributions in which the struck field is on the other side are included in the ellipsis. This highlights the point that allowing the active field to strike another field necessarily involves a partial specification of the supertrace structure: it must be the case that the struck field either directly followed or preceded the active field. In turn, this means that the Feynman rule for particular choices of the active and target fields can be zero. For example, an F can follow, but never precede an A_μ^1 , and so the pull back of an A_μ^1 onto

the field X , whilst holding the momentum of the preceding field fixed (we assume for the time being that both X and the preceding field carry non-zero momentum). Of course, using our current diagrammatic notation, this latter field can be any of those which decorate the vertex, and so we sum over all possibilities. Thus, each cyclically ordered push forward like term has a partner, cyclically ordered pull back like term, such that the pair can be interpreted as

$$\left(\partial_\mu^r \Big|_s - \partial_\mu^s \Big|_r\right) \text{Vertex}, \tag{18}$$

where r and s are momenta entering the vertex. In the case that $r = -s$, we can and will drop either the push forward like term or pull back like term, since the combination can be expressed as ∂_μ^r ; we interpret the diagrammatic notation appropriately. If any of the fields decorating the vertex carry zero momentum (besides the explicitly drawn A^i), then they are transparent to this entire procedure. Thus, they are never differentiated and, if they precede a field which is, we must look to the first field carrying non-zero momentum to figure out which of the vertex's momenta is held constant. Just as in (13), the fields X and or Y can be interpreted as the end of a kernel. In this case, we introduce some new notation, since it proves confusing in complete diagrams to actually locate the derivative symbol at the end of such an object. The notation for the derivative with respect to the momentum entering the end of a kernel is introduced in figure 3.

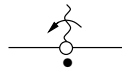


Figure 3. Notation for the derivative with respect to the momentum entering an undecorated kernel.

Recalling that a kernel, whose fields are explicitly cyclically ordered, is a two-sided object, we note that the field whose momentum we have expanded in is sat on the top-side of the vertex. The derivative is taken to be with respect to the momentum which flows *into* the end of the vertex which follows the derivative, in the sense indicated by the arrow on the derivative symbol. It is clear that the direction of the arrow on the derivative symbol can be reversed at the expense of a minus sign.

2.2.4. Charge Conjugation Invariance Charge conjugation invariance can be used to simplify the diagrammatics, by allowing us to discard certain terms and to combine others. The diagrammatic prescription for replacing a diagram which possesses exclusively bosonic external fields with its charge conjugate is [49, 51] to reflect the diagram, picking up a sign for each

- (i) external A^i ,
- (ii) *performed* gauge remainder,
- (iii) momentum derivative symbol (note that the direction of the arrow accompanying such symbols is reversed by the reflection of the diagram).

2.3. The Weak Coupling Expansion

2.3.1. *Perturbative Diagrammatics* In the perturbative domain, we have the following weak coupling expansions [43, 45, 49, 51]. The Wilsonian effective action is given by

$$S = \sum_{i=0}^{\infty} (g^2)^{i-1} S_i = \frac{1}{g^2} S_0 + S_1 + \dots, \quad (19)$$

where S_0 is the classical effective action and the $S_{i>0}$ the i th-loop corrections. The seed action has a similar expansion:

$$\hat{S} = \sum_{i=0}^{\infty} g^{2i} \hat{S}_i. \quad (20)$$

Recalling (3) we have:

$$\beta \equiv \Lambda \partial_{\Lambda} g = \sum_{i=1}^{\infty} g^{2i+1} \beta_i(\alpha) \quad (21)$$

$$\gamma \equiv \Lambda \partial_{\Lambda} \alpha = \sum_{i=1}^{\infty} g^{2i} \gamma_i(\alpha). \quad (22)$$

Defining $\Sigma_i = S_i - 2\hat{S}_i$, the weak coupling flow equations follow from substituting (19)–(22) into the flow equation, as shown in figure 4 [49, 51].

$$\left[\begin{array}{c} \bullet \\ \circlearrowleft n \end{array} \right]^{\{f\}} = \left[\begin{array}{c} \sum_{r=1}^n \left[2(n_r - 1) \beta_r + \gamma_r \frac{\partial}{\partial \alpha} \right] \begin{array}{c} \bullet \\ \circlearrowleft n_r \end{array} \\ + \frac{1}{2} \left(\sum_{r=0}^n \begin{array}{c} \bullet \\ \circlearrowleft \bar{n}_r \\ \bullet \\ \circlearrowleft \bar{r} \end{array} - \begin{array}{c} \bullet \\ \circlearrowleft \Sigma_{n-} \end{array} - \begin{array}{c} \bullet \\ \circlearrowleft \Sigma_{n-} \end{array} \right) \end{array} \right]^{\{f\}} \quad (23)$$

Figure 4. The weak coupling flow equations.

We refer to the first two terms on the right-hand side of (23) as β and α -terms, respectively. The symbol \bullet , as in equation (4), means $-\Lambda \partial_{\Lambda}|_{\alpha}$. A vertex whose argument is an unadorned letter, say n , represents S_n . We define $n_r \equiv n - r$ and $n_{\pm} \equiv n \pm 1$. The bar notation of the dumbbell term is defined as follows:

$$a_0[\bar{S}_{n-r}, \bar{S}_r] \equiv a_0[S_{n-r}, S_r] - a_0[S_{n-r}, \hat{S}_r] - a_0[\hat{S}_{n-r}, S_r]. \quad (24)$$

The renormalization condition for g , equation (9), constrains the two-point vertex of the physical field $S_{\mu}^{A^1 A^1}(p)$ as follows:

$$S_{0\mu\nu}^{11}(p) = 2(p^2 \delta_{\mu\nu} - p_{\mu} p_{\nu}) + O(p^4) \equiv 2\Box_{\mu\nu}(p) + O(p^4) \quad (25)$$

$$S_{n>0\mu\nu}^{11}(p) = O(p^4), \quad (26)$$

where we have abbreviated A^1 by just ‘1’.

2.3.2. *The Effective Propagator Relation* The effective propagator relation (which we recall is the sole primary diagrammatic identity of the second type) arises from examining the flow of all two-point, tree level vertices. This is done by setting $n = 0$ in (23) and specializing $\{f\}$ to contain two fields, as shown in figure 5. We note that we can and do choose all such vertices to be single supertrace terms [49, 51].

$$\text{Diagram} = \text{Diagram}_1 - \text{Diagram}_2 - \text{Diagram}_3 \tag{27}$$

Figure 5. Flow of all possible two-point, tree level vertices.

Following [42–45, 49, 51, 55] we use the freedom inherent in \hat{S} by choosing the two-point, tree level seed action vertices equal to the corresponding Wilsonian effective action vertices. Equation (27) now simplifies. Rearranging, integrating with respect to Λ and choosing the appropriate integration constants [49, 51], we arrive at the following relationship between the integrated ERG kernels—*a.k.a.* the effective propagators—and the two-point, tree level vertices.

$$M-\text{Diagram} = M-\text{Diagram}_1 - M-\text{Diagram}_2 = M-\text{Diagram}_3 - M-\text{Diagram}_4 \tag{28}$$

Note that we have attached the effective propagator, which only ever appears as an internal line, to an arbitrary structure. The field labelled by M can be any of the broken phase fields. The object $\blacktriangleright \equiv \triangleright$ is a gauge remainder. The individual components of \triangleright will often be loosely referred to as gauge remainders; where it is necessary to unambiguously refer to the composite structure, we will use the terminology ‘full gauge remainder’.

The various components on the right-hand side of (28) can be interpreted, in the different sectors, according to table 1, where we take the gauge remainder to carry momentum p (as denoted by the subscripts carried by the gauge remainder components).

| | δ_{MN} | \triangleright_p | \triangleright_p |
|--------------|-------------------|--------------------------------|--------------------|
| F, \bar{F} | δ_{MN} | $(f_p p_\mu / \Lambda^2, g_p)$ | $(p_\nu, 2)$ |
| A^i | $\delta_{\mu\nu}$ | p_μ / p^2 | p_ν |
| C^i | $\mathbb{1}$ | — | — |

Table 1. Prescription for interpreting (28).

From (25) and table 1, it follows that

$$\Delta_{\rho\sigma}^{11}(p) = \frac{\delta_{\rho\sigma}}{2p^2} + \mathcal{O}(p^0), \quad (29)$$

which we will need later. The functions $f(p^2/\Lambda^2)$ and $g(p^2/\Lambda^2)$ need never be exactly determined (though for a concrete realization, see [51]); rather, they must satisfy general constraints enforced by the requirements of proper UV regularization of the physical $SU(N)$ theory and gauge invariance. We will see the effects of the latter shortly.

Generally speaking, when we encounter components of gauge remainders in complete diagrams, we will either sum over flavours, or the flavour will be obvious, from the context. However, there is one place where we will find it useful to explicitly indicate the flavour (and momenta) of both \triangleright and \triangleright . Thus we introduce the notation

$$\triangleright_p^i, \quad \triangleright_q^j. \quad (30)$$

The superscript indices take the values 0 or 1, denoting a (non-null) bosonic or fermionic gauge remainder, respectively. Later, we will find it useful to form logical expressions with these indices.

2.3.3. Primary Diagrammatic Identities of the Third Type We recall that the primary diagrammatic identities of the third type follow directly from those of the first and second types but are given explicitly nonetheless due to the central role they will play in this paper. The first of these identities is simply the classical part of (16):

$$-\triangleright \circlearrowleft = 0. \quad (31)$$

From the effective propagator relation and (31), two further diagrammatic identities follow. First, consider attaching an effective propagator to the right-hand field in (31) and applying the effective propagator before \triangleright has acted. Diagrammatically, this gives

$$\triangleright \circlearrowleft = 0 = \triangleright - \triangleright \triangleright \triangleright,$$

which implies the following diagrammatic identity:

$$\triangleright \triangleright = 1. \quad (32)$$

Notice that this means that the f and g of table 1 are related by

$$x_p f_p + 2g_p = 1, \quad (33)$$

where we have defined $x_p = p^2/\Lambda^2$.

The effective propagator relation, together with (32), implies that

$$-\circlearrowleft \longrightarrow = \triangleright - \triangleright \triangleright \triangleright = 0.$$

In other words, the (non-zero) structure \longrightarrow kills a classical, two-point vertex. But, by (31), this suggests that the structure \longrightarrow must be equal, up to some factor, to \triangleleft . Hence, the last of the primary diagrammatic identities is

$$\longrightarrow \equiv \triangleleft \cdots \cdots, \quad (34)$$

where the dot-dash line represents the pseudo effective propagators of [49, 51], also denoted by $\tilde{\Delta}$.

3. Further Diagrammatics

3.1. Gauge Remainders, Again

The various additional properties of gauge remainders which we require are most readily introduced by example. To this end, consider the three diagrams shown in figure 6.

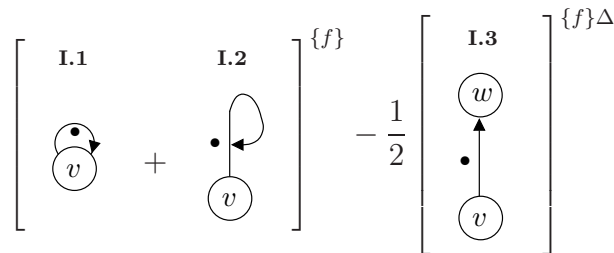


Figure 6. Examples of diagrams possessing a gauge remainder.

There are a number of things to note. First, since these diagrams are used for illustrative purposes, they are labelled **I.#**; for the β_n diagrammatics, the labels will be **D.#**. Secondly, v and w are just vertex arguments, and so take the values of non-negative integers. Since these arguments do not carry a hat or a bar (see 24), the vertices belong to the Wilsonian effective action. Thirdly, the decorations of diagram I.3 include not just the set of fields, $\{f\}$, but also an effective propagator, Δ , which can be in any sector. The rules for decorating diagram I.3 with the effective propagator are simple: if each end attaches to a different object, then the combinatoric factor of the attachment is two, recognizing that the effective propagator can attach either way around. If the two ends attach to the same object, then the combinatoric factor is unity, recognizing that each vertex represents a sum over all permutations of the fields arranged into all possible supertrace structures. Whilst the effective propagator and fields, $\{f\}$, are not explicitly drawn on the diagrams, they will be referred to as implicit, or unrealized decorations.

Let us now consider what happens when the gauge remainders in each of the diagrams I.1–I.3 act. Since no other gauge remainders have acted and since no Taylor expansions have been performed, we can use charge conjugation to collect together the push forward and the pull back (see section 2.2.4). In diagram I.1, the gauge remainder can strike one of two things: either the field to which the kernel attaches or one of the fields, $\{f\}$. It proves to be technically very convenient not to specify precisely which field the gauge remainder hits in the latter case, only that it hits something. Consequently, we take the gauge remainder to strike a ‘socket’, which we suppose can be filled by any of the fields, $\{f\}$. In diagram I.2, the gauge remainder can strike a socket, the top end of the kernel or the bottom end of the kernel. In diagram I.3, the gauge remainder can only strike a socket, though we note that this socket can be filled not only by $\{f\}$ but also by an end of the effective propagator. Figure 7 shows the result of processing the gauge remainders of diagrams I.1–I.3.

$$\begin{aligned}
 \left[\begin{array}{c} \text{Diagram 1} \\ v \end{array} \right]^{\{f\}} &= 2 \left[\begin{array}{cc} \{ \text{I.4} \text{ I.6} \} & \{ \text{I.5} \text{ I.14} \} \\ \text{Diagram 2} & - \text{Diagram 3} \end{array} \right]^{\{f\}} \\
 \left[\begin{array}{c} \text{Diagram 4} \\ v \end{array} \right]^{\{f\}} &= -2 \left[\begin{array}{ccc} \{ \text{I.6} \text{ I.4} \} & \{ \text{I.7} \text{ I.16} \} & \text{I.8} \\ \text{Diagram 5} & + \text{Diagram 6} & - \text{Diagram 7} \end{array} \right]^{\{f\}} \\
 -\frac{1}{2} \left[\begin{array}{c} \text{Diagram 8} \\ w \\ \bullet \\ v \end{array} \right]^{\{f\}\Delta} &= \left[\begin{array}{c} \text{I.9} \\ \text{Diagram 9} \\ v \end{array} \right]^{\{f\}\Delta}
 \end{aligned}$$

Figure 7. The result of allowing the gauge remainders of diagrams I.1–I.3 to act. In all diagrams with the same (opposite) sign to the parent, the push forward and pull back have been collected into twice the push forward (pull back).

Notice that, rather than terminating the pushed forward / pulled back field-line with a half arrow (*cf.* (13)), we just utilize the fact that the corresponding field line already ends in a $>$ and use this to indicate the field hit.⁺ Immediately, we find a cancellation, which we indicate by enclosing the reference number of the cancelled diagram in curly brackets, together with the reference number diagram against which it cancels.

Illustrative Cancellation 1 *Diagram I.6 exactly cancels diagram I.4. Although these diagrams look exactly the same, one might worry that they are different: in diagram I.6, the gauge remainder pulls back along the kernel, whereas in diagram I.4 the gauge remainder has nothing to do with the kernel, instead pushing forward around the vertex. However, gauge invariance ensures that these two diagrams are indeed equivalent [49, 51], and so they cancel.*

Returning to figure 7, consider next diagram I.8. The line segment which joins the top of the kernel to the $>$ —thereby forming a ‘hook’—performs no role other than to make this join. In other words, it is neither a section of the kernel nor an effective propagator. We could imagine deforming this line segment so that the hook becomes arbitrarily large. Despite appearances, we must always remember that this line segment simply performs the role of a Kronecker delta. When part of a complete diagram, this

⁺ Note that we will not always have a $>$ at our disposal. In particular, we will encounter gauge remainders involving pseudo effective propagators terminating in just \triangleright . In this case, the notation of section 2.2.2 must be used.

line segment can always be distinguished from an effective propagator, to which it can be made to look identical, by the context. This follows because hooks in which the line segment is a Kronecker δ only ever attach to effective propagators or kernels, whereas hook-like structures made out of an effective propagator only ever attach to vertices (this will be particularly clear from the perspective of section 5). When viewed in isolation, we will always take the hook structure to comprise just a line segment and so will draw the hook as tightly as possible.

To conclude our discussion of the hook, we give its algebraic form. First, we note from table 1 that the gauge remainder that forms the hook must be in the D (\bar{D}) sector, else the loop integral over its momenta is odd and vanishes. Consequently, the field to which the hook attaches must be in the C^1 (C^2) sector; a conclusion which could also have been drawn from consideration of charge conjugation invariance. Thus, in the former (latter) case, the gauge remainder of the parent, which is in the F (\bar{F}) sector, strikes the F (\bar{F}) at the top of the kernel, turning it into a C^1 ($-C^2$). The sign in the latter case essentially arises from the minus sign in fifth component of \bar{F}_N (see (8a,8b)) (see [49, 51] for painstaking detail). Our prescription is to absorb any signs associated with the end of the kernel into the definition of the hook.

The final ingredient we need to obtain the algebraic form for the hook is to realize that the inside of the hook constitutes an empty loop and so gives a group theory factor of $\pm N$, depending on flavour. Thus we have:

$$\mathcal{D}_1 = +(-N) \int_l g_l \tag{35a}$$

$$\mathcal{D}_2 = -(N) \int_l g_l. \tag{35b}$$

The numbers at the base of the hook in the above equations indicate the sector of the C^i field to which the hooks attach.

We now see a further advantage to having absorbed signs into the definition of the hook: we can trivially extend the diagrammatic effect of charge conjugation to cover its action on a disconnected hook. Quite simply, we have that

$$\mathcal{D} = - \mathcal{Q}, \tag{36}$$

consistent with our previous definition that we take the mirror image, picking up a sign for every performed gauge remainder.

Now we focus on diagram I.9. This diagram, like I.5 and I.7, possesses a socket; we will now see why it is so useful to leave this socket empty. To process this diagram further, we suppose that the vertex with argument w possesses a classical, two-point component. Of course, in this case, this means that w must be a classical vertex. However, in the computation of β_n , we will generally be summing over vertex arguments, such that w could take all values between zero and some positive integer. In preparation for this, we leave the vertex argument as w rather than explicitly writing it as zero. To separate off the classical, two-point component of w , we define the reduction of a vertex to be the full vertex minus its classical, two-point component (should this component

exist). The reduction is denoted by appending the appropriate vertex argument with a superscript R viz. w^R . This decomposition of diagram I.9 is shown in figure 8.

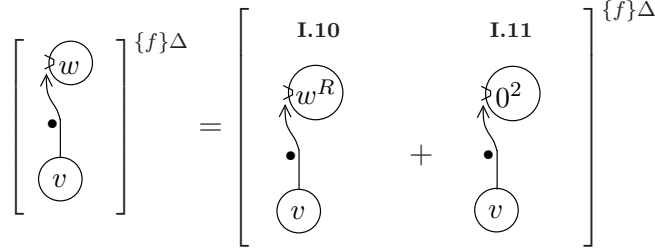


Figure 8. Decomposing the vertex of diagram I.9 (which in this case is implicitly a classical vertex) into a reduced part and a classical, two-point part.

The top vertex of diagram I.10 is reduced. The vertex argument 0^2 of diagram I.11 tells us that this vertex must not only be classical but must also possess precisely two decorations. Thus in addition to the socket, this vertex must have one and only one additional decoration. Clearly, this additional decoration can either be one of the fields $\{f\}$ or one of the ends of the effective propagator. The former case will not concern us here, so we focus on the latter case. Given that one end of the effective propagator decorates the classical, two-point vertex, there are three locations to which the loose end can attach:

- (i) the socket;
- (ii) the vertex with argument v .
- (iii) the kernel;

The first case vanishes by charge conjugation invariance. To see this, consider the parent of diagram I.9, diagram I.3. To generate the diagram corresponding to i, we should consider the component of diagram I.3 in which the top vertex is a three-point vertex, with one of the fields corresponding to the gauge remainder and the other two corresponding to the two ends of the effective propagator. Now, since net fermionic vertices vanish, the gauge remainder must be bosonic. Furthermore, by charge conjugation invariance, the gauge remainder is forced to be in the $C^{1,2}$ sector, in which it is null (see section 2.2.4).

In both cases ii and iii, we can employ the effective propagator relation. This is shown in figure 9. We note that following. First, using the effective propagator to join the classical, two-point vertex to some other object yields a combinatoric factor of two. Secondly, when we henceforth talk of decorating a classical, two-point vertex we always mean that we are explicitly drawing on the second decoration of the vertex, the socket being the first decoration. If we mean to fill the socket, this will be explicitly stated.

Illustrative Cancellation 2 *Diagram I.14 exactly cancels diagram I.5.*

Illustrative Cancellation 3 *Diagram I.16 exactly cancels diagram I.7.*

$$\left[\begin{array}{c} \text{Diagram I.11} \\ \bullet \\ v \end{array} \right]_{\{f\}\Delta} = 2 \left[\begin{array}{c} \text{I.12} \quad \text{I.13} \\ \text{Diagram I.12} + \text{Diagram I.13} \\ \bullet \\ v \end{array} \right]_{\{f\}} + \dots \\
 = 2 \left[\begin{array}{c} \{ \text{I.14} \text{ I.5} \} \quad \text{I.15} \\ \text{Diagram I.14} - \text{Diagram I.15} \\ \bullet \\ v \\ \{ \text{I.16} \text{ I.7} \} \quad \text{I.17} \\ \text{Diagram I.16} - \text{Diagram I.17} \\ \bullet \\ v \end{array} \right]_{\{f\}} + \dots$$

Figure 9. The decoration of the classical, two-point vertex of diagram I.11 by the effective propagator, together with the subsequent application of the effective propagator relation. The ellipses denote diagrams in which the classical, two-point vertex is decorated by one of the fields, $\{f\}$, rather than by the effective propagator.

There are some comments worth making about diagrams I.15 and I.17. First, the $>$ part of the full gauge remainder plays the role of the socket in the parent diagrams. Secondly, these diagrams have a very similar structures to diagrams I.1 and I.2. The only difference is that the full gauge remainder in the new diagrams is nested [51], meaning that it does not attach directly to the kernel, but instead is hit by the gauge remainder component which ends the kernel. Processing nested gauge remainders is much the same as processing un-nested gauge remainders, but charge conjugation invariance cannot generally be used again to collect together the nested push forward and pull back [51, 52]: we must count them separately. However, everything else goes through as before and so we will find that cancellation 1 is repeated twice (twice because we count the nested push forward separately from the nested pull back).

If there were more vertices available, we could imagine iterating the above procedure and thus generating arbitrarily nested gauge remainders. It would then be useful for us to know if there is any simple way of keeping track of which gauge remainders have pushed forward and which have pulled back. With sufficient thought, it is always possible to stare at a complicated diagram and deduce the pattern of pushes forward and pulls back (up to the ambiguity associated with illustrative cancellation 1). However, there is an easier way. Note in diagrams I.15 and I.17 that the $>$ part of the full gauge remainder is bitten on its right-hand edge by the $>$ which terminates the kernel. (We define the right-hand edge to be the edge on our right as we traverse an imaginary line running into

the socket at the apex *viz.* $\frac{L}{R} \longrightarrow$; likewise for sockets on vertices / kernels.) Had we pushed forward, rather than pulled back with the initial gauge remainder, then this bite would have been to the left. With this in mind, consider a string of gauge remainders which bite a socket decorating either a kernel or a vertex; the latter case is shown in figure 10.

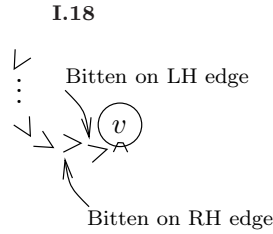


Figure 10. An arbitrarily nested gauge remainder bites a socket on a vertex.

We know from the discussion in illustrative cancellation 1 that, were we to fill the socket of diagram I.18 with the end of a kernel (the other end of which attaches to the gauge remainder at the beginning of the string), then the sense in which the socket is bitten can be interpreted in two ways: either as a push forward around the vertex or as a pull back along the kernel. Given a diagram like I.18, we will always interpret the gauge remainder at the end of the string of gauge remainders as having bitten the vertex, using this to determine the sense in which the gauge remainder acts.

To determine in which sense the nested gauge remainders are bitten we can equate bites on the left with pushes forward and bites on the right with pulls back, the only exception being when a gauge remainder bites the end of kernel to form a hook: the gauge remainder that pushed forward to form the un-nested hook of diagram I.8 can be thought of as biting itself on the right. Thus, moving on to consider the arbitrarily nested hook shown in figure 11, the number of pushes forward is equal to the number of bites on the left, plus one, and the number of pulls back is equal to the number of bites on the right, minus one.



Figure 11. An arbitrarily nested version of the hook.

Structures like those in figure 10 have a compact representation, shown below:

$$\frac{1}{m!} \left\{ \overset{v}{\curvearrowright} \right\} >^m$$

The notation $>^m$ stands for m instances of $>$. These gauge remainder components form a string which bites the socket. We sum over all possible ways in which each gauge remainder can bite, and so diagram I.18 is just one component included our

compact diagrammatic representation. When going from the compact diagrammatic representation to its explicit components, we note that any of the m gauge remainders can bite the socket, and this gauge remainder can, in turn, be bitten by any of the remaining $m - 1$ gauge remainders. This explains the normalization factor of $1/m!$. Denoting the number of bites to the left / right by L / R, the sign of each explicitly drawn diagram is just $(-1)^R$.

Similarly, there is a compact diagrammatic representation of the nested hook—or ring—of figure 11, which is simply

$$\frac{1}{(m - 1)!} \{ \}^{>m}.$$

The rule to go from this compact representation to explicit diagrams is as follows: we draw the set of rings corresponding to all independent sequences bites to the left / right. The normalization factor follows from noting that a ring is invariant under a cyclic permutations of the gauge remainders. The sign of each explicitly drawn ring is $(-1)^{R-1}$.

We conclude this discussion of the gauge remainders by examining diagrams possessing two active gauge remainders. The techniques we use to process such terms are exactly the same as the ones detailed already in this section. There is, however, a qualitatively new type of diagram that arises, together with a source of possible confusion. To investigate both of these issues, we focus on an example in which two full gauge remainders bite a kernel*, as shown in figure 12.

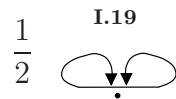


Figure 12. An example of a double gauge remainder diagram.

We proceed by allowing first one gauge remainder to act and then, if possible, allowing the second gauge remainder to act. The qualitatively new type of diagram arises because one of the effects of the first gauge remainder can be to ‘trap’ the second gauge remainder, by biting the field on the kernel to which the second gauge remainder attaches. The remaining full gauge remainder now does not have the same momentum flowing through it as the field it is trying to bite, and so it cannot act. The other diagrams generated are those in which the processed gauge remainder bites one of the ends of the kernel. The result of allowing the first gauge remainder to act is shown in figure 13, where we have collected pulls back and pushes forward, as usual.

Diagram I.21 possesses the trapped gauge remainder. In diagram I.22 we have recognized that the kernel ends where it attaches to the active gauge remainder and so

* Double gauge remainder diagrams are not restricted to those in which both gauge remainders bite a kernel; one or both of the gauge remainders can bite a vertex.

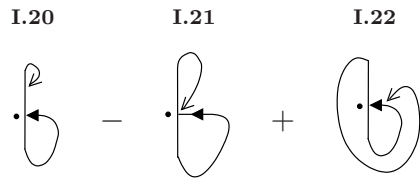


Figure 13. Result of allowing one gauge remainder in diagram I.19 to act.

this is where the processed gauge remainder bites. Note that we can trivially redraw this diagram, as shown in figure 14.



Figure 14. A trivial redrawing of diagram I.22.

Diagram I.23 highlights how one must be very careful when drawing which end of an active gauge remainder a processed gauge remainder bites; diagrams I.23 and I.21 are clearly different. Notice, however, that if the active gauge remainder were *absent*, then diagram I.22 would cancel diagram I.21; we will exploit this later.

Finally, consider allowing the active gauge remainder to act in diagrams I.20 and I.23. We are not interested in all the contributions. Rather, we just want to focus on

- (i) the term produced by diagram I.20 where the gauge remainder pulls back along the kernel, to the same end as the hook;
- (ii) the term produced by diagram I.23 in which the gauge remainder pulls back to the bottom of the kernel.

Reflecting the former diagram about a horizontal line, we arrive at the two diagrams of figure 15. (The reflection does not yield a net sign as we pick up one for each of the processed gauge remainders.)

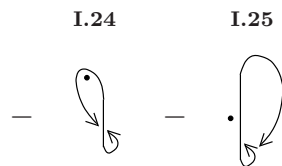


Figure 15. Two of the terms produced by processing diagrams I.20 and I.23.

From the way in which these two diagrams have been drawn, it is clear that they are distinct and that they must be treated as such. We can, however, redraw diagram I.25 by sliding the outer gauge remainder round the hook to where the inner gauge remainder bites the kernel. This is shown in figure 16.



Figure 16. A trivial redrawing of diagram I.25.

Diagram I.26 is, of course, still the same as diagram I.25 but it is starting to look very similar to diagram I.24. Indeed, we must make sure that we never slide the gauge remainder so far round the hook that it appears to bite the kernel at the same point as the gauge remainder which forms the hook. If this were to happen, then such a diagram would be ambiguous.

3.2. The Secondary Diagrammatic Identities

There are two families of secondary diagrammatic identities. Members of the first family are generally applicable, whereas members of the second family are applicable only to diagrams which have been manipulated at $O(p^2)$.

3.2.1. The First Family The first diagrammatic identity in this family is trivial:

$$\text{hook} = 0. \tag{37}$$

This follows directly from charge conjugation invariance: the field attaching to the hook must be in the C^i sector, but in this sector the gauge remainder contracted into the hook is null. Before moving on, notice that the diagram contains one empty socket, corresponding to the $>$ part of the full gauge remainder.

There is a second trivial identity involving a diagram possessing a single socket, which we have seen already. We re-draw it here in what will become a suggestive form:

$$\text{circle with } 0^2 \text{ and arrow} = 0, \tag{38}$$

recalling that this identity follows as a consequence of the effective propagator relation and (A.8). We explicitly indicate that the vertex is a two-point vertex, since such structures will generically occur as sub-diagrams in diagrams with unrealized decorations.

To uncover the next diagrammatic identity, which is the first we will encounter involving two sockets, consider the pair of diagrams in figure 17.

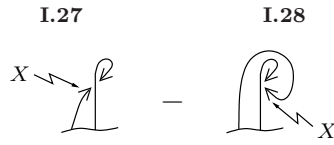


Figure 17. A pair of diagrams whose sum vanishes.

These diagrams naturally arise from a common parent: the differences between the two diagrams come from the sense in which the full gauge remainder of the parent, of which the component labelled X is left behind, acts. The point now is that diagrams I.27 and I.28 cancel. By construction, the unspecified structure at the bottom of both diagrams is common. Furthermore, the gauge remainder labelled X and its attachment to the common structure is the same between the two diagrams. From (35a,35b), the two hooks yield the same algebraic contribution. The only difference between the two diagrams is the sense in which the gauge remainder labelled X acts. However, effectively all that this gauge remainder does is determine whether the hook is of type (35a) or (35b); and we know that the hook is just a common algebraic factor between the two diagrams. Therefore, diagrams I.27 and I.28 are in fact identical up to a sign and so cancel.

This leads us to the following diagrammatic identity:

$$\overrightarrow{\mathcal{R}} - \mathcal{R} \equiv 0, \tag{39}$$

where we understand that this diagram should be viewed as part of some larger diagram, attached via internal fields. Note that in this diagrammatic identity, and all that follow, we can strip off the common $>$ which attaches to some other part of a larger diagram, replacing it with the half arrow notation of (13).

The non-trivial diagrammatic identities which now follow can be thought of as arising from versions of (37) and (39) in which the hook is nested and versions of (38) in which the gauge remainder is nested. To be specific, we will find relationships between the nested versions of (37)–(39) for which the numbers of sockets are equal; equivalently, these relationships are between diagrams with an equal number of *performed* gauge remainders.

The key to proving the non-trivial diagrammatic identities resides in the following relationship between gauge remainder components. Using the notation described around (30), and taking $j_2 = j_1$ **xor** j_3 we have:

$$1 - \triangleright_{l-m_1-k}^{j_1} >_{l-m_1}^{j_2} - \triangleright_k^{j_3} >_{l-m_1}^{j_2} = 0. \tag{40}$$

To demonstrate this, we simply substitute for the gauge remainder components using table 1 and employ (33), as shown in table 3.2.1.

The first non-trivial relationship involves versions of (37)–(39) with two sockets. This identity is, in some sense, still a special case, since the two-socket version of (39) is of course trivial. Consequently, we treat the two-socket case—which is shown in figure 18—separately from the rest.

| j_1 | j_3 | j_2 | |
|-------|-------|-------|--|
| 0 | 0 | 0 | $1 - \frac{(l-m_1-k) \cdot (l-m_1)}{(l-m_1)^2} - \frac{k \cdot (l-m_1)}{(l-m_1)^2} = 0$ |
| 0 | 1 | 1 | $1 - f_{l-m_1} \frac{(l-m_1-k) \cdot (l-m_1)}{\Lambda^2} - f_{l-m_1} \frac{k \cdot (l-m_1)}{\Lambda^2} - 2g_{l-m_1} = 0$ |
| 1 | 0 | 1 | $1 - f_{l-m_1} \frac{(l-m_1-k) \cdot (l-m_1)}{\Lambda^2} - 2g_{l-m_1} - f_{l-m_1} \frac{k \cdot (l-m_1)}{\Lambda^2} = 0$ |
| 1 | 1 | 0 | $1 - \frac{(l-m_1-k) \cdot (l-m_1)}{(l-m_1)^2} - \frac{k \cdot (l-m_1)}{(l-m_1)^2} = 0$ |

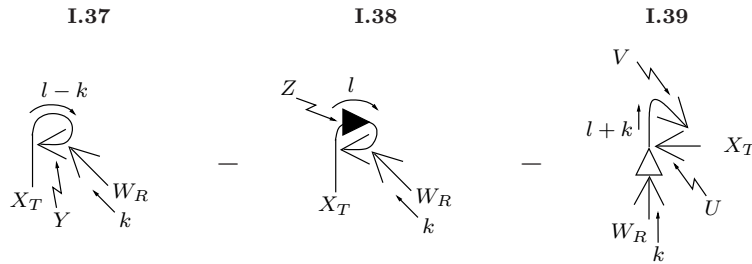
Table 2. Break down of (40) into the different sectors.

$$\begin{array}{cccc}
 \text{I.29} & \text{I.30} & \text{I.31} & \text{I.32} \\
 \begin{array}{c} \text{Diagram I.29} \\ \text{Diagram I.30} \end{array} & - & \begin{array}{c} \text{Diagram I.31} \\ \text{Diagram I.32} \end{array} & \\
 \text{I.33} & \text{I.34} & \text{I.35} & \text{I.36} \\
 - \begin{array}{c} \text{Diagram I.33} \\ \text{Diagram I.34} \end{array} & + & \begin{array}{c} \text{Diagram I.35} \\ \text{Diagram I.36} \end{array} & = 0
 \end{array} \tag{41}$$

Figure 18. Two sets of diagrams, each of which will be shown to sum individually to zero.

Diagrams I.31, I.33 and I.35 can each be obtained from diagram I.29 by changing the senses in which the gauge remainders bite (the remaining four diagrams are similarly related). There are actually some stronger relationships than the one given above. For example, the first four diagrams only ever cancel amongst themselves. However, for our analysis of β_n , only the statement (41) is required.

To prove (41), we begin by focusing on the first pair of diagrams, which we redraw in figure 19. Notice that we have used the effective propagator relation in diagram I.29, have filled the sockets with fields of a specific flavour and have chosen a convenient momentum routing for each of the diagrams.


Figure 19. Re-expression of diagrams I.29 and I.30.

The letters $U-Z$ denote field flavour, and the subscripts T and R represent indices. It is straightforward to verify, and intuitively obvious, that W_R and X_T must be either

both bosonic or both fermionic. In the former case, the internal fields U, V, Y and Z are all of the same flavour, being either all bosonic or all fermionic. In the case that the internal fields are all bosonic, diagrams I.37–I.39 reduce to a common factor multiplied by

$$1 - \triangleright_l^0 >_{l+k}^0 - \triangleright_k^0 >_{l+k}^0, \tag{42}$$

whereas, in the case that the internal fields are all fermionic, they reduce to some other common factor multiplied by

$$1 - \triangleright_l^1 >_{l+k}^1 - \triangleright_k^0 >_{l+k}^1. \tag{43}$$

It is immediately apparent from (40) that both (42) and (43) yield zero, upon identifying $-m_1$ with k . In exactly the same way, diagrams I.31 and I.32, I.33 and I.34, I.35 and I.36 cancel when the external fields are bosonic.

Let us now consider filling the sockets of diagrams I.29–I.36 with fermionic fields. The first thing to realize is that the latter four diagrams do not exist with these decorations, since such decoration is incompatible with the group theory structure [51]. In figure 20, we collect together all surviving terms for which $W_R = \bar{F}$ and $X_T = F$ (and identical analysis can be done for $F \leftrightarrow \bar{F}$), and sum over all possible flavours of the internal fields.

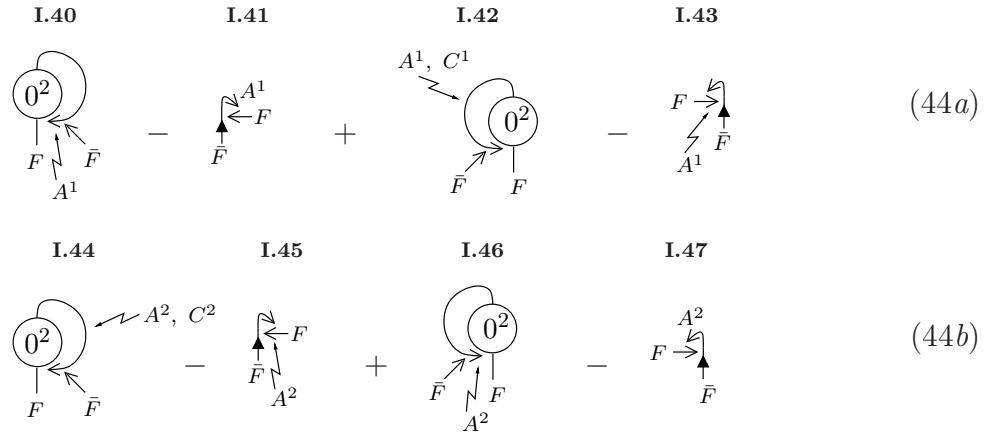


Figure 20. Field decomposition of diagrams I.29–I.32 in the case that the external fields are fermionic.

On the basis of (42,43), we might expect diagram I.40 to cancel diagram I.41 *etc.* However, this expectation is not borne out; rather we find that the Kronecker δ part of I.40 (I.42) combines with the gauge remainder part of I.42 (I.40) and I.43 (I.41), to yield a common factor multiplied by a term of the form (40). In this way, we thus find that each row of diagrams in figure 20 vanishes.

This completes the discussion of diagrammatic identity (41) and so now we move on to the general case, which relates versions of (37)–(39) with any number of sockets ≥ 3

to each other. To begin, we consider by looking at those diagrams with the specific patterns of bites on the left / right shown in figure 21.

Figure 21. A generalized diagrammatic identity.

There are a number of things to note about diagrams I.48–I.52. First, each of the diagrams possesses the fields W , X and Z^1, \dots, Z^r with indices R, T and S_1, \dots, S_r , respectively. The cyclic ordering of these fields is the same in each diagram. In the case that each diagram possesses only three external fields, we should identify Z^1 with Z^r . Secondly, for each of the fields X, Z^1, \dots, Z^r there is, in each diagram, an associated \triangleright . The flavour of this \triangleright , which may of course differ from that of the associated external field, is denoted by $X', Z^{1'}, \dots, Z^{r'}$, as appropriate. Notice that, in diagram I.49, the field line X is associated with not one but two internal objects, the flavours of which are denoted by X' and X'' , as indicated. Diagram I.50 is the only one in which the field line W is associated not only with an external \triangleright (the flavour of which, W' , is just the same as that of W) but also an internal \triangleright , the flavour of which is denoted by W'' . Finally, we comment on the momentum routing, which is taken to be the same each diagram. The external field W is taken to carry momentum k . The external fields Z^1, \dots, Z^r carry momenta m_1, \dots, m_r , respectively; momentum conservation now fixes the momentum carried by X . The loop momentum is l , and is routed such that it is carried by $Z^{1'}$. This now uniquely determines the momenta carried by all other internal fields.

With these points in mind, we now wish to show that the sum of the five diagrams vanishes. Immediately, we notice that, whatever the flavours of the internal and external fields, diagrams I.48 and I.51 cancel. The only difference between these two diagrams is the order in which W and Z^r bite the field line of X , which affects neither the flavours

of the internal fields or the group theory factors (this conclusion will change when we consider versions of these diagrams with different patterns of bites to the left / right).

Now let us consider diagrams I.49, I.50 and I.52. The first thing that we must do to show that these diagrams cancel is demonstrate that the flavours of the external fields and all common internal fields can be arranged to be the same in all three cases. Clearly, we can always choose the external fields to be the same. Assigning a value of 0 (1) to the bosonic (fermionic) fields, as usual, and denoting the statistics of the field V by $[V]$, we see that

$$\begin{aligned} [X'] &= [X] \mathbf{xor} [Z^{r'}], \\ [Z^{1'}] &= [Z^1] \mathbf{xor} [X'] \mathbf{xor} [W'], \\ [Z^{(r-i)'}] &= [Z^{r-i}] \mathbf{xor} [Z^{r-i-1}] \mathbf{xor} \cdots \mathbf{xor} [Z^1], \end{aligned}$$

in all three diagrams, where i is in the range $\{0, r-2\}$. Thus, if in addition to choosing all external fields to be the same in diagrams I.49, I.50 and I.52 we also choose $Z^{r'}$ to be the same, it follows that all flavours W' , X' and $Z^{1'}, \dots, Z^{r'}$ agree. Consequently, we can write the sum of the three diagrams as:

$$\int_l F(k, m_i, l, j_1, j_2, j_3) \left[-\triangleright_{l-m_1-k}^{j_1} \triangleright_{l-m_1}^{j_2} -\triangleright_k^{j_3} \triangleright_{l-m_1}^{j_2} + 1 \right],$$

where $j_2 = j_1 \mathbf{xor} j_3$ and $F(k, m_i, l, j_1, j_2, j_3)$ is common to all three terms. This term vanishes, courtesy of (40).

Our next task is to show that the versions of (45) with different patterns of bites to the left / right also vanish. The first thing to notice is that changing the senses in which the gauge remainder components carrying the labels $Z^{2'}, \dots, Z^{r-1'}$ are bitten induces a change which is common to all five diagrams, and so the cancellations detailed above go through, just the same. In the case that there are at least four external fields—in which case we do not identify Z^r with Z^1 —the sense in which $Z^{r'}$ is bitten factors out as well.

Let us now consider alternatively nested versions of diagrams I.48 and I.51, in which we consider changing the sense in which one and only one gauge reminder is bitten / bites. Changing the sense in which $Z^{1'}$ is bitten induces the same change in both diagrams, and so they still cancel. Next, consider changing the sense in which $Z^{r'}$ bites. This does not induce the same change in each diagram, on account of the differing orders in which $Z^{r'}$ and W' act in each of the diagrams. Moreover, in diagram I.48 we can change the sense in which W' bites. We cannot do this in diagram I.51 since it has, in a sense, been done already: diagrams I.51 and I.52 form a pair of diagrams, essentially differing only in the sense in which W' acts. (This is particularly clear when we consider these diagrams as part of a larger diagram, in which case all indices simply become dummy indices which are summed over).

Similarly, consider alternatively nested versions of diagrams I.49, I.50 and I.52. Changing the sense in which X' is bitten induces the same change in all three diagrams, and so they still cancel. However, changing the sense in which $Z^{1'}$ is bitten does not induce the same change in the final diagram as in the first two. Moreover, in diagram I.49

we can change the sense in which W' bites, and in diagram I.50 we can change the sense in which W'' is bitten. Again, neither of these terms is obviously cancelled.

We collect together the diagrams which no longer cancel after changing the sense in which one of the gauge remainders acts in figure 22.

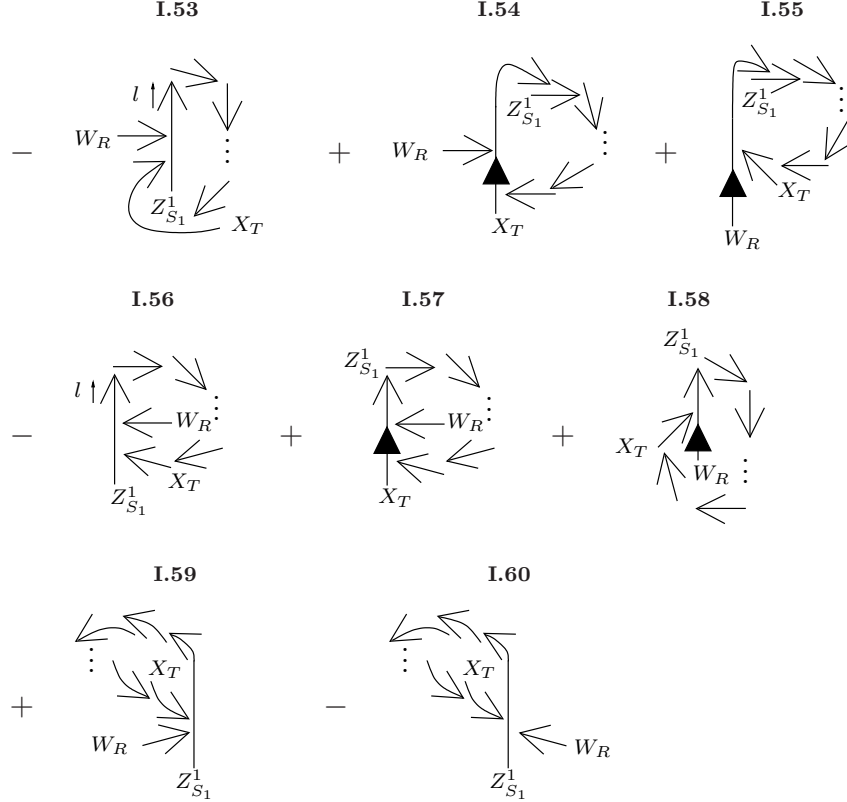


Figure 22. The set of diagrams, obtained from changing the sense in which precisely one of the gauge remainders of diagrams I.48–I.52 bites, which do not cancel in the same way as the diagrams of figure 21.

Notice that, in diagram I.53, we have changed the labelling of the fields, compared to diagram I.48. With the fields labelled in this way, we can repeat the analysis of diagrams I.49, I.50 and I.52 and thus prove that, given a set of common external fields, all internal fields can be chosen to be the same in diagrams I.53–I.55. Furthermore, we see that the group theory structure of these diagrams is identical: in each case the field $Z_{S_1}^1$ is inside the loop, with the remaining field lines having a cyclic order, common to the three diagrams, on the outside. Consequently, we can write the sum of the three diagrams as:

$$\int_l F'(k, m_i, l, j_1, j_2, j_3) \left[1 - \triangleright_{l-m_1-k}^{j_1} \triangleright_{l-m_1}^{j_2} - \triangleright_k^{j_3} \triangleright_{l-m_1}^{j_2} \right],$$

where once again $j_2 = j_1$ **or** j_3 and $F'(k, m_i, l, j_1, j_2, j_3)$ is common to all three terms. Thus, in accord with (40), the sum of diagrams I.53–I.55 vanishes. In exactly the same fashion, we can show that diagrams I.56–I.58 also sum to zero.

This still leaves us with diagrams I.59 and I.60. Let us put these to one side for a moment and consider instead different patterns of bites to the left / right in diagrams I.53–I.58. Let us start with the first three diagrams. The only changes we can make which do not lead to diagrams which cancel in exactly the same way as the parents (or take us back to the diagrams of figure 21) are as follows:

- (i) changing the sense in which W' bites in diagrams I.53 and I.54;
- (ii) changing the sense in which X' bites in diagram I.55.

The resulting diagrams are shown in figure 23.

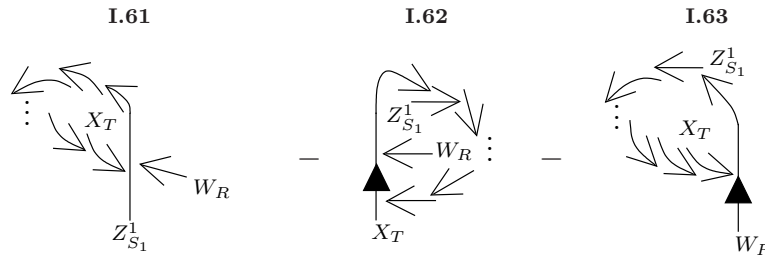


Figure 23. The set of diagrams, obtained from changing the sense in which precisely one of the gauge remainders of diagrams I.53–I.58 acts, which do not cancel in exactly the same way as the parent diagrams or reproduce already drawn diagrams.

Now consider making similar changes to diagrams I.56–I.58. The point is, that the set of diagrams we would draw simply reproduces the pattern of bites to the left / right that we see in diagrams I.61–I.63. In other words, we have taken account of these terms already and so we have no further diagrams to draw. Now, diagram I.61 cancels diagram I.60 and diagrams I.62 and I.63 cancel diagram I.59. Thus everything closes. Any further changes to the pattern of bites to the left / right will simply replicate cancellations we have seen already.

We have therefore demonstrated that, in addition to the diagrams of figure 21 summing to zero, so too do appropriate combinations of their alternatively nested partners. We can use this fact, together with identity (41), to derive a relationship between all diagrams of the basic structure just discussed, possessing between two and m empty sockets. The relationship, which is crucial in our treatment of β_n , is shown in figure 24.

The notation $[]_{ES}$ tells us to sum over Every Sense in which all the gauge remainders can bite. Thus, diagrams I.64 and I.67 have three partners, diagrams I.65, I.66, I.68 and I.69 seven partners *etc.*

It is worth clarifying the diagrams represented by the various ellipses. The ellipsis following diagram I.65 denotes additionally nested diagrams, where the classical, two-point, vertex is still joined to the innermost gauge remainder. The ellipsis after diagram I.66 denotes additionally nested diagrams, where the classical, two-point vertex

$$\begin{aligned}
 & \left[\begin{array}{c} \text{I.64} \\ \text{Diagram with } 0^2 \text{ and } \gamma \end{array} \right] + \left[\begin{array}{c} \text{I.65} \\ \text{Diagram with } 0^2 \text{ and } \gamma \end{array} + \dots \right] \\
 & \quad - \left[\begin{array}{c} \text{I.66} \\ \text{Diagram with } 0^2 \text{ and } \gamma \end{array} + \dots \right] \\
 & \quad \quad \quad \vdots \\
 & \quad \quad \quad \left. \right]_{ES} \\
 = & \left[\begin{array}{c} \text{I.67} \\ \text{Diagram with } \blacktriangle \end{array} \right] - \left[\begin{array}{c} \text{I.68} \\ \text{Diagram with } \blacktriangle \end{array} + \dots \right] \\
 & \quad - \left[\begin{array}{c} \text{I.69} \\ \text{Diagram with } 0^2 \text{ and } \gamma \end{array} - \left[\begin{array}{c} \text{I.70} \\ \text{Diagram with } 0^2 \text{ and } \gamma \end{array} + \dots \right] \right. \\
 & \quad \quad \quad \left. - \left[\begin{array}{c} \text{I.71} \\ \text{Diagram with } 0^2 \text{ and } \gamma \end{array} + \dots \right] \right]_{ES}
 \end{aligned} \tag{46}$$

Figure 24. A relationship between certain diagrams possessing between two and m empty sockets.

joins to the innermost but one gauge remainder. The vertical dots on the next line represent additionally nested diagrams in which the classical, two-point vertex joins to gauge remainders successively further away from the innermost one. Note, though, that we never make the join to the outermost gauge remainder. Thus, we have arranged things such that all diagram in a given column possess the same number of sockets. The relationship between the top set of diagrams and the bottom set holds for any number of columns, so long as this number is the same for both sets of diagrams.

We now expound on how the diagrammatic identities of this section combine to yield (46). Diagram I.64 and its partners are clearly equal to I.67 and its partners by diagrammatic identity (41). Applying the effective propagator relationship to diagram I.69 and its partners, the Kronecker δ part combines with diagram I.68 to give diagram I.66, via diagrammatic identity (45) (and its alternatively nested versions). On the other hand, the gauge remainder term and its partners are just equal to diagram I.65 and its partners courtesy of diagrammatic identity (41).

Using the notation described under figure 11, we can represent (46) in the compact form shown in figure 25.

$$\begin{aligned}
 \sum_{m'=1}^{m-1} \frac{1}{m'!} \left(\text{Diagram: a circle with a vertex labeled } 0^2 \text{ and a gauge remainder } \{ \} >_{\wedge}^{m'} \right) &= \sum_{m'=1}^{m-1} \frac{1}{(m'+1)!} \left\{ \right\} >_{\blacktriangle}^{m'+1} \\
 &- \sum_{m'=2}^{m-1} \sum_{m''=0}^{m'-2} \frac{1}{(m'-m'')!m''!} \left(\text{Diagram: a circle with a vertex labeled } 0^2 \text{ and a gauge remainder } \{ \} >_{\wedge}^{m''} \right) \left\{ \right\} >_{\wedge}^{m'-m''}
 \end{aligned} \tag{47}$$

Figure 25. A compact form of (46).

The loose end of the effective propagator in the first diagram can attach to any of the m' gauge remainder components. We need not strictly prohibit it from attaching to the socket on the vertex since such a diagram vanishes by charge conjugation invariance, anyway. The relationship (47) is, of course, valid separately for every integer value of m from one to infinity. The explicitly drawn $>$ in the first and third diagrams can bite in either sense. Notice that, since the explicitly drawn $>$ is common to each diagram (in the second diagram it just sits at the bottom end of the full gauge remainder), we could strip it off completely, replacing it where necessary with the half arrow notation of (13) (*i.e.* we could remove the $>$ completely from the second diagram, where it does not push forward or pull back on to another field, but would have to replace it with a half arrow in the first and third diagrams).

3.2.2. The Second Family The first diagrammatic identity in this family follows from the two equivalent way of processing the diagram on the left-hand side of figure 26: our first operation can either be to process the gauge remainder or to Taylor expand the vertex (we assume that the socket is decorated by an A^i sector field). In the former case, although we do not explicitly indicate it at this stage, it is understood that the socket in the daughter diagrams is filled by an A^i sector field carrying zero momentum, just as in the parent. In the latter case, we can move the momentum derivative from the vertex to the \triangleright which bites the vertex, at the expense of a minus sign, courtesy of diagrammatic identity (A.7).

The factor of two on the second line arises from using charge conjugation invariance to collect together momentum derivative terms; we have not used charge conjugation to collect together pushes forward and pulls back on the first line. By equating the two expressions with each other, we are lead to the following diagrammatic identity:

$$\frac{1}{m} \left\{ \right\} >_{\vee}^m = -2 \left\{ \right\} >_{\blacktriangleright}^{m-1} \tag{48}$$

where, in both diagrams, the socket must be decorated by an A^i sector carrying zero momentum. In the special case that the socket of the first diagram can be identified

Figure 26. Deducing a secondary diagrammatic identity; the socket must be decorated by an A^i sector field which carries zero momentum.

with the sockets of one of the m gauge remainders (48) becomes:

$$2m(m-1) \{ \text{diagram with } \star \text{ and } \circlearrowleft \}^{>^{m-2}} = - \{ \text{diagram with } \cup \}^{>^m}. \quad (49)$$

Notice that, in the second diagram, even though the socket is identified with one of the gauge remainders, we have kept it to remind us that the relationship (49) holds only if the sockets on each side of the equation are filled with an A^i field carrying zero momentum.

The second diagrammatic identity in this family follows as a consequence of diagrammatic identities (A.1) and (A.7). Defining

$$\star \equiv \text{diagram with } \star \text{ and } \circlearrowleft \equiv \text{diagram with } \star \text{ and } \circlearrowleft \text{ and } \uparrow - \frac{1}{2} \text{diagram with } \star \text{ and } \circlearrowleft \text{ and } \downarrow \quad (50)$$

we have

$$\text{diagram with } 0^2 \text{ and } \star \text{ and } \circlearrowleft = \text{diagram with } 0^2 \text{ and } \star \text{ and } \circlearrowleft = - \text{diagram with } 0 \text{ and } \star \text{ and } \circlearrowleft. \quad (51)$$

A number of comments are in order. Strictly speaking, the presence of \star (as opposed to some other internal line involving a momentum derivative) is not necessary for either this diagrammatic identity or those that follow. However, in practise, it is a \star that most commonly occurs in such scenarios. Note that each diagram effectively possesses two external A^1 's (after decoration of the socket associated with the \star), which we suppose to be the only external fields. We understand that the socket possessed by the $>$ and the loose end of the \star are internal fields, which are somehow tied up into a complete diagram. In the second diagram, if the right-most gauge remainder pushes forward onto the internal field, we recover the parent. If this gauge remainder were instead to pull back onto the internal field, then the supertrace structure of the diagram would be uniquely determined to be $\text{str} A_\mu^1 \text{str} A_\nu^1 = 0$. If either gauge remainder strikes the external field, then the other gauge remainder kills the diagram, courtesy of (A.7). To

go from the second diagram to the third, we allow the left-most gauge remainder to act; the only surviving contribution is the pull back onto the internal field.

The next diagrammatic identity is the first of this family which necessitates consideration of the algebraic form of gauge remainders, and is shown in figure 27. Notice that, in the first diagram, both the \star and the $>$ bite the socket.

$$\begin{array}{ccc}
 \text{I.72} & & \text{I.73} & & \text{I.74} \\
 \begin{array}{c} \text{Diagram 1} \\ \text{I.72} \end{array} & - & \begin{array}{c} \text{Diagram 2} \\ \text{I.73} \end{array} & - & \begin{array}{c} \text{Diagram 3} \\ \text{I.74} \end{array} & = 0
 \end{array} \tag{52}$$

Figure 27. The first diagrammatic identity of the second family which relies on (40).

This diagrammatic identity follows directly from (40). Although we have given both (51,52) in un-nested form, it is clear that they both hold in appropriately nested cases. Indeed, we now combine the nested versions of these diagrammatic identities to give the final diagrammatic identity. This is shown in figure 28 and is, in some sense, the second family analogue of diagrammatic identity (47). Wherever a \star and $>$ bite the same thing, the \star is taken to act first, as in diagram I.72.

$$\begin{array}{c}
 \sum_{m'=0}^m \left[\begin{array}{c} \text{Diagram 4} \\ \text{I.72} \end{array} - \begin{array}{c} \text{Diagram 5} \\ \text{I.73} \end{array} \right] \\
 - \sum_{m'=0}^m m' C_{m''} \sum_{m''=0}^{m'} \left[\begin{array}{c} \text{Diagram 6} \\ \text{I.74} \end{array} - \begin{array}{c} \text{Diagram 7} \\ \text{I.74} \end{array} \right] = 0
 \end{array} \tag{53}$$

Figure 28. The final diagrammatic identity belonging to the second family.

3.3. Subtraction Techniques

3.3.1. *Introduction* As discussed in the introduction, and as we will see shortly, the n -loop β function is computed by evaluating a set of diagrams at $O(p^2)$:

$$\beta_n \square_{\mu\nu}(p) = \text{Diagrams}|_{p^2}.$$

A subset of the diagrams contributing to β_n possess a stub which is manifestly $O(p^2)$ and so we would like to Taylor expand the remaining components of these diagrams to zeroth order in p . The problem is that individual diagrams may possess components which are not Taylor expandable to $O(p^2)$. We could proceed simply by ignoring these components since we know that the sum of all diagrams contributing to β_n must be Taylor expandable to $O(p^2)$. However, for the purposes of this paper we adopt a higher level of rigour and so keep them. As an example, consider the first diagram of figure 29 where, in anticipation of what follows, we have added and subtracted a term.

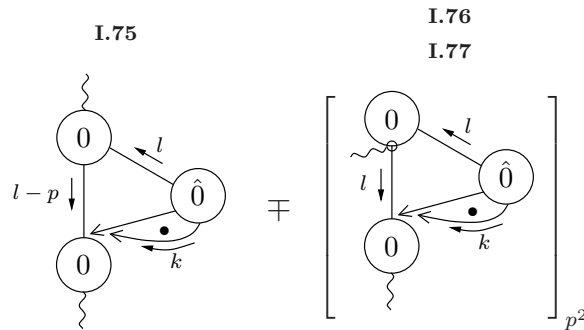


Figure 29. A two-loop diagram with an $O(p^2)$ stub, components of which cannot be Taylor expanded to $O(p^2)$, and a term constructed to isolate these components.

We begin by focusing on diagram I.75. Since we can always Taylor expand vertices in momenta, let us suppose that we take a power of l from the top-most vertex (we cannot take any powers of p , at $O(p^2)$) and let us choose to take a power of k from the other vertex. Using table 1 and (29), we see that the leading IR behaviour of the l -integral is given by

$$\int_l \frac{1}{l^2(l-p)^2},$$

which is not Taylor expandable to $O(p^2)$. Note that had we taken a power of l from the right-hand vertex, rather than a power of k , then the extra power of l in the integrand would render the diagram Taylor expandable in p (to the required order).

Next, let us consider the pair of diagrams I.76 and I.77, where the first of these—the subtraction—comes with the minus sign and the corresponding addition comes with the plus sign. The tag p^2 tells us that only the stub carries momentum p *i.e.* these diagrams are constructed by setting $p = 0$ in diagram I.75 everywhere but the stub.

The effect of the subtraction on the parent is to cancel all those components which are Taylor expandable to $O(p^2)$. This immediately tells us the following about any surviving contributions to diagram I.75:

- (i) all fields carrying momentum l must be in the A^1 -sector;
- (ii) we must take $\mathcal{O}(l^0)$ from the k -integral (note that the k -integral is Taylor expandable in l);
- (iii) we must discard any remaining contributions to the l integral which are Taylor expandable to $\mathcal{O}(p^0)$.

The contributions to diagram I.75 not removed by diagram I.76 are shown on the left-hand side of figure 30.

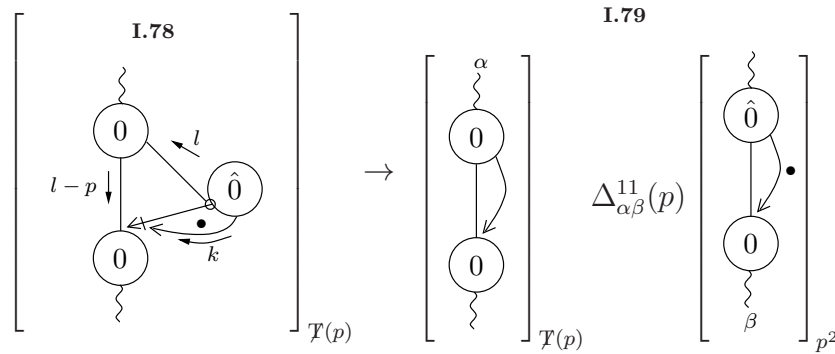


Figure 30. The contribution to diagram I.75 not removed by its subtraction.

Focusing first on diagram I.78, we see that, as required, we have taken the $\mathcal{O}(l^0)$ from the k -integral. The tag $\mathcal{T}(p)$ demands that we retain only the component of the diagram which, whilst possessing an overall $\mathcal{O}(p^2)$ contribution, is not Taylor expandable in p (in dimensional regularization, this contribution would go as $\mathcal{O}(p^2)p^{-2\epsilon}$, for this diagram). The bar sitting just before the $>$ which bites the classical, two-point vertex indicates a discontinuity in momenta: the $>$ which bites the classical, two-point vertex carries momentum l , but the loop to its right carries only momentum k along all lines. We can neaten this diagram up (getting rid of the momentum discontinuity) to obtain diagram I.79. To do this, we first notice that the sub-diagram of I.78 which is independent of l carries two indices, say ρ and τ . By Lorentz invariance, this sub-diagram must go as $\delta_{\rho\tau}$, which allows us to tie up the effective propagator attaching to the momentum derivative to the gauge remainder which follows the bar. This procedure yields the $\mathcal{T}(p)$ component of diagram I.79, but with indices μ and ν , rather than μ and α . We now re-express

$$\square_{\mu\nu}(p) = \square_{\mu\alpha}(p) \frac{\delta_{\alpha\beta}}{2p^2} 2\square_{\beta\nu}(p)$$

which allows us to re-write diagram I.78 in the form I.79, up to $\mathcal{O}(p^4)$ corrections (*cf.* (29)).

Before discussing the addition, we note that we define the subtraction to be the diagram which removes the components of the parent diagram which are Taylor expandable to $\mathcal{O}(p^2)$, not by its sign. We could always move the momentum derivatives in diagrams I.76 from one side of the vertex they strike to the other, at the expense

of a minus sign (this would amount to replacing ∂_ν^{-l} with ∂_ν^l); were we to do so, the subtraction would now come with a plus sign and the addition with a minus.

Additions like our example I.77 can be manipulated by using the effective propagator relation and diagrammatic identity (A.9). For the two structures, A and B we have:

$$\begin{array}{c} \text{---} A \\ | \\ \textcircled{0} \\ | \\ \text{---} B \end{array} = - \begin{array}{c} \text{---} A \\ | \\ \textcircled{\times} \\ | \\ \text{---} B \end{array} - \begin{array}{c} \text{---} \Delta \\ | \\ \textcircled{\times} \\ | \\ \text{---} B \end{array} - \begin{array}{c} \text{---} A \\ | \\ \textcircled{\times} \\ | \\ \text{---} \nabla \end{array} \quad (54)$$

where

$$\begin{array}{c} \Delta \\ | \\ \textcircled{\times} \\ | \\ \nabla \end{array} \equiv \begin{array}{c} \Delta \\ | \\ \textcircled{\uparrow} \\ | \\ \nabla \end{array} - \frac{1}{2} \begin{array}{c} \Delta \\ | \\ \textcircled{\times} \\ | \\ \nabla \end{array} \quad \text{and} \quad \begin{array}{c} \dots \\ | \\ \textcircled{\times} \\ | \\ \nabla \end{array} \equiv \begin{array}{c} | \\ | \\ \textcircled{\downarrow} \\ | \\ \nabla \end{array} - \frac{1}{2} \begin{array}{c} \Delta \\ | \\ \textcircled{\times} \\ | \\ \nabla \end{array} .$$

It is now apparent why the definition (50) is useful.

As a consequence of the decomposition (50), it is clear that diagrams I.81 and I.82 have components where an active gauge remainder strikes both structures A and B . However, in practical calculations, this turns out to be a red-herring: it is most efficient never to perform this decomposition and so we only ever process the explicitly drawn gauge remainders in (54).

It is useful to consider the special case where the realizations of A and B are summed over, as we can use charge conjugation invariance to combine terms, in this case. Specifically, can we identify the structure A (B) of diagram I.82 with the structure B (A) of diagram I.81. This is shown in figure 31 where, for the sake of generality, we suppose that the active gauge remainders in (54) can be arbitrarily nested.

$$\begin{array}{c} \text{I.83} \\ \text{---} \Delta \\ \{ \} >^m \\ \vdots \\ \textcircled{\times} \\ \text{---} \end{array} + \begin{array}{c} \text{I.84} \\ \text{---} \Delta \\ \{ \} >^m \\ \vdots \\ \textcircled{\times} \\ \text{---} \end{array}$$

Figure 31. Generalized versions of the second and third diagrams of (54), where A and B have been identified with each other.

Let us now consider a specific arrangement of bites to the left / right in diagrams I.83 and I.84. To be precise, we suppose that there are a total of G such operations, where $G = L + R = L' + R'$, the (un)primed variable corresponding to diagram (I.83) I.84. The signs of diagrams I.83 and I.84 are, according to the rules of section 3.1, $(-1)^R$ and $(-1)^{R'}$, respectively.

We now choose to focus on pairs of terms for which $R' = L$ and consider taking the charge conjugate of diagram I.83 which, we recall, amounts to reflecting it, picking up a

sign for each of the G performed gauge remainders and the momentum derivative. We remove this latter sign by reversing the direction of the momentum derivative symbol so that its sense is once again counterclockwise. By doing this, we have arranged for the reflected version of diagram I.83 to look exactly the same as diagram I.84. The associated sign of the reflected diagram is $(-1)^{G+R} = (-1)^{R'}$ which is, of course, just the sign associated with diagram I.84. Therefore diagrams I.83 and I.84 can be combined.

At the beginning of this section, we stated that the effect of subtractions is to isolate the components of the parent which are not Taylor expandable to $O(p^2)$ and that, by construction, the additions are Taylor expandable to the desired order. Strictly speaking, this latter statement requires a caveat. The point is that we can encounter diagrams like I.75 as a sub-diagram of some larger, factorizable diagram. By factorizable, we mean that the complete diagram has (at least one) internal line which carries just p . Thus, we could imagine the top-most external field of diagram I.75 instead being an effective propagator, carrying p , attaching to some other sub-diagram (which would be decorated by the spare external field). This latter sub-diagram, which we note cannot possess a kernel (only one is allowed per complete diagram), may contain components which are not Taylor expandable to $O(p^2)$. The strategy is to simply leave such sub-diagrams alone, but proceed as usual with the other part of the complete diagram *i.e.* the sub-diagram of the form I.75. The rule that we will effectively obey is that we only ever construct subtractions for (sub) diagrams which contain a kernel. The corresponding additions, whilst always possessing a sub-diagram which is Taylor expandable in p , may also possess a sub-diagram which is not. This does not worry us: we simply manipulate the Taylor expandable sub-diagram and effectively ignore the other one.

3.3.2. General Analysis In this section, we analyse the construction and effects of subtractions in complete generality. In section 5.3, we will discover that we only have to construct subtractions for diagrams with two basic templates, which are shown in figure 32.

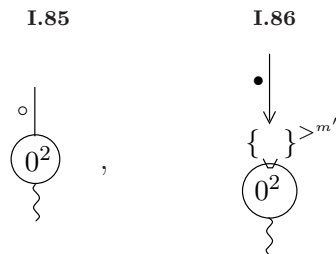


Figure 32. The template for diagrams for which we will construct subtractions.

Clearly, we have suppressed all other diagrammatic ingredients which can include vertices, effective propagators and $>$ s. Our aim now is to start fleshing out the sub-diagrams I.85 and I.86 to see if we can find any components which are not Taylor expandable to $O(p^2)$. To stand any chance of doing so, we must find effective propagators

or gauge remainders carrying $l - p$ (where l is a loop momentum) since we recall that, in the A^i sector, these objects go as $1/(l - p)^2$ and $(l - p)_\alpha/(l - p)^2$, respectively. To this end, consider decorating diagram I.85 with a single socket, and consider the complete set of momentum routings, as shown in figure 33.

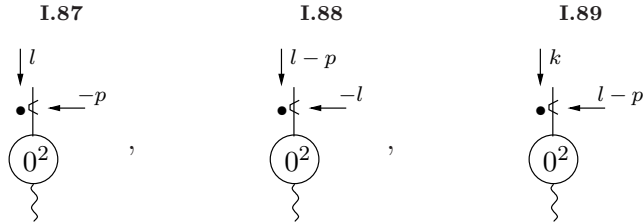


Figure 33. Momentum routings for diagram I.85.

First, consider diagram I.87. There is no possibility of having an effective propagator carrying $l - p$ and so the (sub) diagram derived from fully fleshing out I.87 is Taylor expandable to $O(p^2)$ (we re-iterate that the field carrying momentum p could attach to a factorizable sub-diagram which is not Taylor expandable to the desired order in p).

Now we move on to diagram I.88. Notice that there is no need to consider also a diagram with the momentum arguments interchanged because such a diagram identical, by momentum re-routing invariance. Since $l - p$ is carried by the kernel (rather than by an effective propagator), there is no chance of generating a factor of $1/(l - p)^2$ from the structures drawn. However, the p could, in principle, flow into an effective propagator or gauge remainder such that their arguments are *e.g.* $k - p$, as illustrated in figure 34.

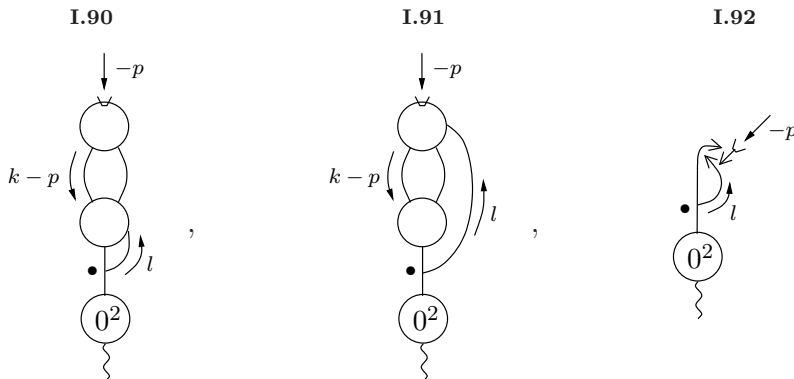


Figure 34. Fleshings out of diagram I.88 such that either an effective propagator or gauge remainder carries $k - p$.

At first sight, diagram I.90 seems to possess the momentum dependence we are looking for, so long as we put the k -dependent effective propagators in the A^i sector,

which we do for all that follows. (Group theory considerations in fact force them to be in the A^1 sector.) In this case, the k -dependent effective propagators

$$\sim \frac{1}{k^2(k-p)^2},$$

which is certainly not Taylor expandable to zeroth order in p . However, we must also consider the vertices. Specifically, by charge conjugation invariance, the field filling the socket of the topmost vertex must be in the A^1 sector. Taylor expanding this vertex to zeroth order in p (which we can always do) must yield at least one power of k by Lorentz invariance. Furthermore, Lorentz invariance and the requirement that (up to powers of $p^{-2\epsilon}$) the diagram is $O(p^2)$ forces us to pick up a second power of k from the four-point vertex. It is thus quite clear, despite first appearances, that the diagram is Taylor expandable to $O(p^2)$.

A similar analysis of diagrams I.91 and I.92 leads to the conclusion that the worst momentum dependence is

$$\frac{O(l^2, l.k)}{(k-p)^2(l-k)^2l^2},$$

in both cases. Consequently, both diagrams are Taylor expandable to $O(p^2)$.

We now attempt to worsen the behaviour of diagram I.90 by adding additional diagrammatic elements. Clearly, simply adding more effective propagators will do nothing. What we can try, however, is splitting open one of the existing effective propagators, as shown in figure 35.

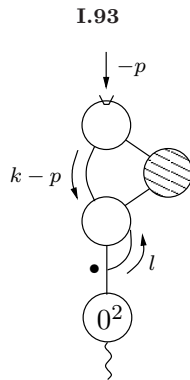


Figure 35. Attempting to worsen the IR behaviour of diagram I.90.

This seems to have done the trick: rather than having a single effective propagator giving a factor of $1/k^2$, we now have two (attached to an arbitrary structure), and the diagram appears not to be Taylor expandable to $O(p^2)$. However, in all the cases we encounter, we will find that when we sum over all possible diagrams which can be represented by the arbitrary structure, the arbitrary structure turns out to be transverse in its external momentum (when the legs are in the A^i sector). Once again we are thwarted: diagrams of the type I.93 are, in practise Taylor expandable to $O(p^2)$.

Similarly, we cannot modify diagrams I.91 and I.92 such that they are no longer Taylor expandable to $O(p^2)$.

We can repeat precisely the same arguments with diagram I.89 and are thus lead to the conclusion that all diagrams with I.85 as a template are Taylor expandable to $O(p^2)$. We can of course still construct subtractions, but they exactly cancel the parent (leaving over the additions).

Diagrams built up from the template I.86 are, however, a different kettle of fish. Indeed, the example with which we began section 3.3.1 is of this type. From diagram I.86, there are two ways in which we can construct diagrams which are not Taylor expandable to $O(p^2)$, as shown in figure 36.

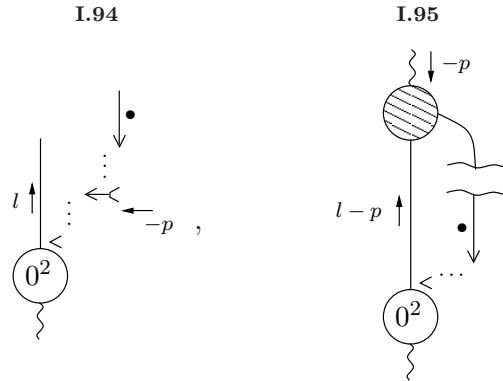


Figure 36. The two types of diagram derived from I.86 which are not Taylor expandable to $O(p^2)$.

Excluding those terms in which the loose ends of the effective propagator and kernel of diagram I.94 attach to something transverse in l (in the A^i sector), both diagrams have a component which goes as

$$\frac{1}{l^2(l-p)^2},$$

and so both diagrams possess a component which is not Taylor expandable to order p^2 . We know from the example at the beginning of section 3.3.1 that further progress can be made by combining such diagrams with their subtractions. To isolate the components which survive, the strategy is as follows:

- (i) identify all loop integrals over momenta other than l but which carry dependence on l ;
- (ii) determine which, if any, of these loop integrals are factorizable from the others;
- (iii) Focus on the loop integral / non-factorizable loop integrals for which the kernel is in the integrand and either
 - (a) Taylor expand to zeroth order in l , directly;
 - (b) construct subtractions if appropriate and iterate the procedure.

An example of this is shown in figure 37, where we recognize that the first diagram is a generalization of I.75.

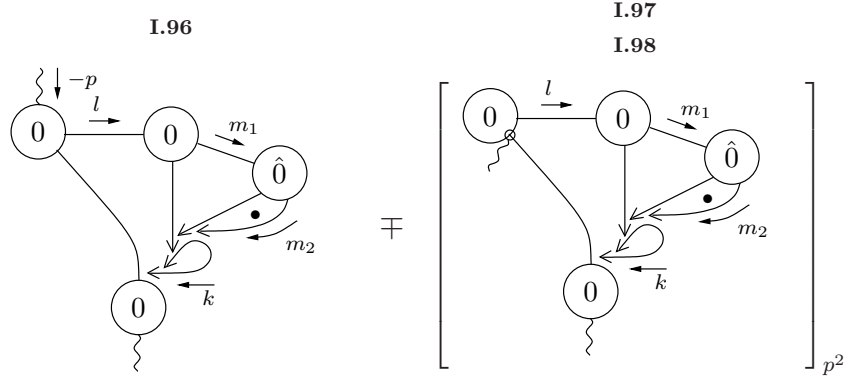


Figure 37. A diagram possessing a component which is not Taylor expandable to $O(p^2)$, together with its subtraction and addition.

Following the above recipe, we recognize that the integrals over k , m_1 and m_2 all contain dependence on l . Given that the m_2 integral contains the kernel and that the m_1 integral has dependence on m_2 but the k integral does not, we can factorize out the integral over k . The parent and subtraction combine to yield the first diagram of figure 38, for which we have constructed a subtraction designed to isolate the part of the m_1 , m_2 dependent sub-diagram which is not Taylor expandable in l .

Diagram I.99 combines with diagram I.100 to yield diagram I.102. Just as we have utilized Lorentz invariance to draw diagram I.102 in an appealing form, so too do we recognize that a similar thing can be done with the addition, I.101, yielding diagram I.103.

Returning to diagram I.102, notice that we must take the component of the m_1 integral which, up to the non-polynomial dependence on l goes as l^0 . Were we to take the l^2 component, instead, then we could not take the $\mathcal{T}(p)$ component of the diagram as a whole. The appearance of the tag $\mathcal{T}(l)$ is awkward, since it requires specification of a loop momentum, which is unnatural from our diagrammatic view point. However, with a little thought, we can replace this tag with something which refers only to the external momentum, p . Diagram I.102 obviously possesses three loop integrals. However, only two of them (the ones over l and m_1) are tagged such that we must take the $\mathcal{T}(\text{mom})$ component, where ‘mom’ refers to the momentum external with respect to the appropriate sub-diagram. There is a simple rule to determine the loops from which we must take the $\mathcal{T}(\text{mom})$ component (a similar rule can be derived for diagrams of type I.94). In all that follows, if there are any sub-diagrams which attach to just two effective propagators carrying equal momenta (*cf.* figure 35), we can ignore each sub-diagram and one of the effective propagators to which it attaches. Starting with a diagram of arbitrary loop order, the recipe is as follows:

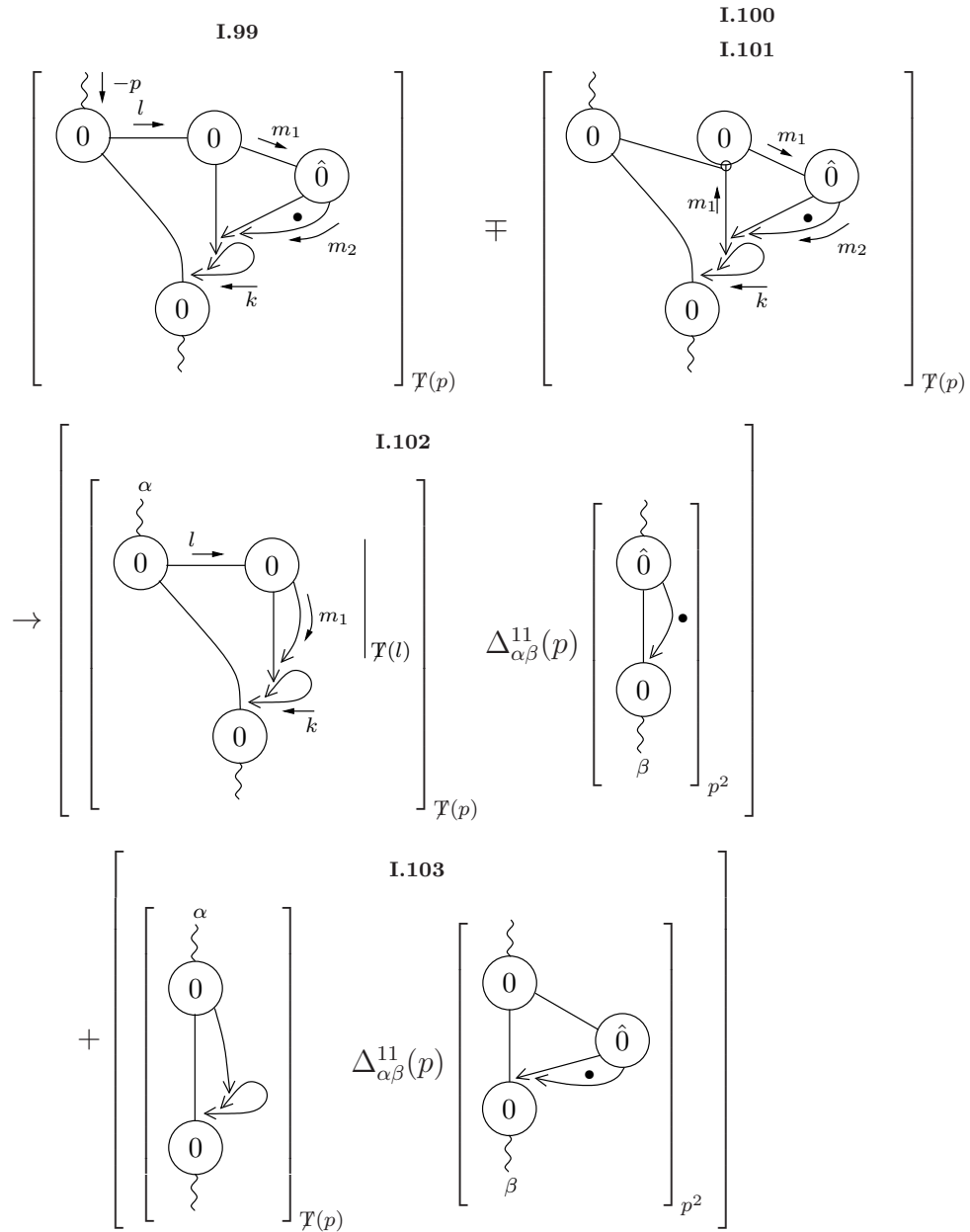


Figure 38. The result of combining diagrams I.96 and I.97.

- (i) Identify the loop momentum associated with the internal field which attaches to the classical, two-point vertex (in the above examples, this momentum has always been l) and route momenta such that
 - (a) the external field attaching to the classical, two-point vertex carries momentum $+p$;
 - (b) momentum $l + p$ flows into the vertex decorated by the other external field;
- (ii) Cut the diagram in every place that there is a gauge remainder carrying l and cut the effective propagator carrying l at the end out of which $+l$ flows.
- (iii) Discard the sub-diagrams for which there is a gauge remainder which carries just l

- (this includes the sub-diagram carrying p and l , which is supposed to have already been tagged with $\mathcal{T}(p)$);
- (iv) Identify the remaining sub-diagram as the one that must be tagged $\mathcal{T}(l)$;
 - (v) Iterate the procedure, if necessary, taking the sub-diagram tagged with $\mathcal{T}(l)$ as the starting point.

In figure 39 we apply this procedure to diagram I.102, with the red lines indicating the cuts. The above recipe tells us to tag the sub-diagram with loop momentum m_1 , but not the one with loop momentum k , since the latter sub-diagram includes a $>_l$ and so is excluded by iii, above.

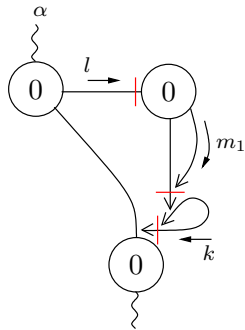


Figure 39. Algorithmic determination of which loop integrals are tagged with $\mathcal{T}()$.

Since this recipe works at any number of loops, there is no need to explicitly tag the appropriate loop integrals of some diagram already tagged by $\mathcal{T}(p)$; rather, we simply tag the diagram as a whole by $\mathcal{T}_M(p)$.

4. Preliminary Diagrammatics

4.1. Additional Notation

4.1.1. (Pseudo) Effective Propagators In section 3.1, we encountered a single effective propagator amongst the implicit decorations (see *e.g.* diagram I.3). We now generalize to consider an arbitrary number of such effective propagators. The rule for explicit decoration is defined as follows. If we wish to join two objects (say two vertices) together with j' out of a total of j effective propagators, then there are ${}^j C_{j'} 2^{j'}$ ways to do this. Intuitively, the first factor captures the notion that, so long as they are implicit decorations, the effective propagators are indistinguishable. The factor of $2^{j'}$ allows for the fact that we can interchange the two ends of an effective propagator. If these effective propagators were instead used to form j' loops on a single vertex, then the factor of $2^{j'}$ would disappear, since the vertices are defined such that all cyclically independent arrangement of their decorative fields are summed over.

Given that we have seen how fields and effective propagators can usefully appear as implicit decorations, it is not surprising that, in our calculation of β_n , gauge

remainder components and pseudo effective propagators also appear in this fashion. The combinatorics for pseudo effective propagators is exactly the same as for effective propagators. When we come to decorate with pseudo effective propagators, we can make life easy for ourselves by noting that, in practise, pseudo effective propagators can be arranged to appear only in one way and always in combination with another term, precisely as in (50). The combinatoric factor associated with partitioning j \star s into two sets of j' and $j - j'$ is just ${}^j C_{j'}$. However, unlike effective propagators, the ends of \star are not interchangeable.

4.1.2. Gauge Remainders We begin by giving the rules for converting a set of m gauge remainder components of type $>$ from implicit to explicit decorations. Thus, we are considering decorations of the form

$$[]^{>^m \dots}, \tag{55}$$

where the square brackets could enclose some diagrammatic structure, but need not. The ellipsis represents any additional implicit decorations, so long as they are not further instances of $>$. The superscript notation $>^m$ simply tells us, as before, that there are m instances of $>$.

There are only two structures we are allowed to form from implicit decorations containing $>$. The first of these is a ring, as in figure 11. Noting that, in some completely fleshed out diagram, the sockets of all the $>$ will be filled, this means that we can generate a diagram like I.25 from implicit decorations, but never a diagram like I.24. However, there is no restriction that we create a single ring structure from our m gauge remainders: we can create up to m independent structures. Furthermore, we need not promote all of the $>$ to explicit decorations at the same time. Thus, we can imagine partitioning the m gauge remainders into $q+1$ sets, with the first q of these sets forming an independent ring structure and the final set remaining as implicit decorations *viz.*

$$M \left[\left\{ \left\{ \right\}^{>^{m^1}} \left\{ \right\}^{>^{m^2}} \dots \left\{ \right\}^{>^{m^q}} \right\}^{>^{m^{q+1} \dots}} \right], \tag{56}$$

where M a combinatoric factor and the notation, $\left\{ \right\}^{>^{m^i}}$, tells us that these decorative gauge remainders must form a single ring *i.e.* they cannot be further partitioned, nor can this ring be added to by the remaining implicit decorations. The m^i are positive integers which sum up to m .

The combinatoric factor is easy to compute: if we partition m gauge remainders into two sets of m' and $m - m'$ gauge remainders, then the combinatoric factor is defined to be

$${}^m C_{m'} .$$

Therefore, we can rewrite (56) as:

$$\frac{m!}{m^{q+1}!} \left[\prod_{i=1}^q \frac{1}{m^i!} \left\{ \right\}^{>^{m^i}} \right]^{>^{m^{q+1} \dots}} .$$

The final gauge remainder structure we can construct out of implicit decorations containing $>$ s occurs only in diagrams possessing an $O(p^2)$ stub. The contexts in which this structure occurs are illustrated in figure 40.

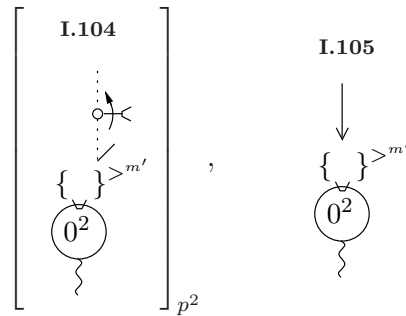


Figure 40. A gauge remainder structure which only occurs in diagrams possessing an $O(p^2)$ stub.

Diagrams I.104 and I.105 both possess a string (not a ring) of m' gauge remainders (*cf.* figure 10), the last of which bites the socket on the classical, two-point vertex (in either sense). In diagram I.104, the first of the m' gauge remainders is bitten by a \star whereas, in diagram I.105 it is bitten by a $>$ attached to an effective propagator. The loose end of the \star / effective propagator can attach to any of the $>$ s or to the socket on the classical, two-point vertex or to any (un-drawn) structures (the \star cannot attach to its own socket, though).

All diagrams possessing a string of gauge remainders bitten by a \star are tagged p^2 . This tells us that everything attaching to the $O(p^2)$ stub is independent of p (as in section 3.3). Diagrams tagged with p^2 can possess more than one instance of the structure which attaches to the stub in diagram I.104: although there is only one stub, structures involving a \star can attach to the momentum derivative symbol of another such structure, as illustrated in figure 41.

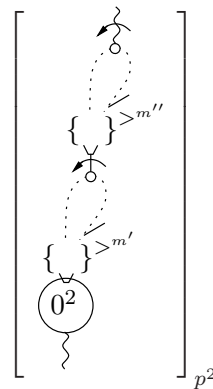


Figure 41. An example of a diagram possessing multiple \star s.

We note the following. First, it is not legal to join any of the m' gauge remainders to any of the m'' gauge remainders. In other words, no two \star s are permitted to carry a common loop momentum. Secondly, the \star s are always tied up such that the momentum derivative symbols are on the ‘outside’ of the diagram. In other words, we can draw a line from any momentum derivative symbol / external field to any other without crossing an internal line. Diagrams in which this is not the case vanish by a combination of group theory and charge conjugation invariance considerations [49, 51].

4.1.3. Vertices When deriving an expression for β_n , we will find it invaluable to compactly represent all vertices in a diagram which are yet to be explicitly decorated. To this end, we introduce a set of vertex arguments, v^j , where the upper roman index acts as a label. Thus, the v^j are integers, denoting the loop orders of some set of vertices. We denote the reduction of these vertices by $v^{j;R}$, where we recall that a reduced vertex lacks a classical, two-point component.

Next, we introduce the compact notation

$$\begin{aligned} v^{j;j+} &\equiv v^j - v^{j+1}, \\ v^{j;j+;R} &\equiv v^{j;R} - v^{j+1;R}. \end{aligned}$$

We use this notation to define

$$\left(n_s, j \right) \equiv \prod_{i=0}^j \sum_{v^{i+}=0}^{v^i} \left(v^{i,i+;R} \right), \quad (57)$$

where the first argument of the structure on the left-hand side, n_s , gives the value of v^0 . Notice that all other vertex arguments are summed over. The interpretation of the product symbol is as a generator of $j + 1$ vertices.

The structure shown in (57) always appears as a part of diagrams which possess an additional vertex, which carries the argument v^{j+} (this argument need not appear on its own—it could be part of something more complicated *e.g.* $v^{j+,k}$). An example, which will play an important role later, is

$$\left[\begin{array}{c} \left(v^{j+;R} \right) \\ \left(n_s, j \right) \end{array} \right] \equiv \prod_{i=0}^j \sum_{v^{i+}=0}^{v^i} \left[\begin{array}{c} \left(v^{j+;R} \right) \\ \left(v^{i,i+;R} \right) \end{array} \right]. \quad (58)$$

Notice that the sum over all vertex arguments is trivially n_s :

$$\sum_{i=0}^j v^{i,i+} + v^{j+} = \sum_{i=0}^j (v^i - v^{i+1}) + v^{j+1} = v^0 = n_s. \quad (59)$$

The interpretation that the structure defined by (57) possesses $j + 1$ vertices allows

us to usefully define (58) for $j = -1$:

$$\left[\begin{array}{c} \textcircled{v^{j+;R}} \\ \textcircled{n_s, j} \end{array} \right]_{j=-1} \equiv \textcircled{n_s^R}, \quad (60)$$

where n_s^R is, of course, just an $n - s$ loop, reduced vertex. (Note that this example illustrates the rule that v^{j+} is replaced by v^0 ; this holds irrespective of whether or not v^{j+} occurs only as part of some more complicated vertex argument.) We can even usefully define what we mean by (58) for $j = -2$:

$$\left[\begin{array}{c} \textcircled{v^{j+;R}} \\ \textcircled{n_s, j} \end{array} \right]_{j=-2} \equiv \delta(n - s). \quad (61)$$

Notice that (60) still makes sense if one and only one of the vertices is decorated (in practise, we will always take this to be the top vertex): if more than one vertex is decorated then this implies that the number of vertices is at least two, which leads to a contradiction. On the other hand, (61) makes sense only as is, and not if any of the vertices are decorated. In the computation of β_n , we will find structures like (58), where we sum over j . The lower value of this sum will start out at -2 . However, as we perform explicit decorations of the vertices, so we will need to raise the lower limit on j , such that the diagrams still make sense.

4.1.4. Decoration of Kernels etc. It will prove useful to isolate the decorated components of a kernel from the undecorated parts. To facilitate this separation, we introduce the symbol \odot to indicate an undecorated kernel and \circ to indicate a decorated kernel, such that

$$\text{---}\bullet\text{---} = \text{---}\odot\text{---} + \text{---}\circ\text{---}. \quad (62)$$

Noting that decoration is not defined for either \star s or pseudo effective propagators (or gauge remainder components) we define

$$\text{---}\circ\text{---} \equiv \text{---}\odot\text{---} + \text{---}\bullet\text{---} - \frac{1}{2} \text{---}\circ\text{---}, \quad (63)$$

where we have used (A.2,50).

4.2. Diagrammatic Functions

In this section we introduce a set of diagrammatic functions, $\mathcal{D}_{n\mu\nu}^{i11}(p)$, which will prove crucial in our treatment of β_n (recall that the 1s are shorthand for A^1 s). By analysing

their various properties, we will be able to illustrate the use of many of the diagrammatic techniques, in their natural setting. We will ultimately be interested in the $O(p^2)$ parts of these diagrams (up to functions not polynomial in p).

4.2.1. The Function $\mathcal{D}_{n\mu\nu}^{a11}(p)$ We introduce the function

$$\mathcal{D}_{n\mu\nu}^{a11}(p) \equiv 2 \sum_{s=1}^n \sum_{m=0}^{2s} \sum_{j=-2}^{n+s-m-2} \frac{\Upsilon_{j+s+1,j+2}}{m!} \left[\begin{array}{c} \textcircled{\psi^{j+1;R}} \\ \textcircled{n_s, j} \end{array} \right]^{11\Delta^{j+s+1} > m}, \quad (64)$$

where, for the non-negative integers a and b , we define

$$\Upsilon_{a,b} = \frac{(-1)^{b+1}}{a!b!} \left(\frac{1}{2}\right)^{a+1}, \quad (65)$$

which we see obeys the following relationships:

$$2a\Upsilon_{a,b} = \Upsilon_{a-1,b}, \quad (66a)$$

$$b\Upsilon_{a,b} = -\Upsilon_{a,b-1}. \quad (66b)$$

In the case that either a or b are negative, $\Upsilon_{a,b}$ is null. The overall combinatoric factor, $\Upsilon_{j+s+1,j+2}/m!$, is said to be canonical, since the three arguments, $j + s + 1$, $j + 2$ and m match, respectively, the number of effective propagators, the number of vertices and the number of $>s$.

There is a simple, intuitive explanation for the relationship between the number of vertices, the number of effective propagators and the sum over the vertex arguments. Consider the components of $\mathcal{D}_{n\mu\nu}^{a11}(p)$ for which there is at least one vertex *i.e.* for which $j > -2$ and for which $m = 0$. We know from (59) that the sum of the vertex arguments is $n - s$. Now, given $j + 2$ vertices, exactly $j + 1$ effective propagators are required to create a connected diagram. This leaves over s effective propagators, each of which must create a loop. Therefore, the loop order of the diagram is $n - s + s = n$, as must be the case. Now we relax the restriction that $m = 0$ and suppose that we create m' gauge remainder rings (*cf.* figure 11). To ensure that each of these rings is connected to some other part of the diagram, we must use up m' of our s ‘spare’ effective propagators. However, this is precisely counteracted by the contribution of each of the rings to the loop order of the diagram. Next, consider the component of the diagram for which $j = -2$:

$$2 \sum_{m=0}^{2n} \frac{\Upsilon_{n-1,0}}{m!} [\]^{11\Delta^{n-1} > m}. \quad (67)$$

To ensure that the diagram is fully connected, m must take the value $2n$ since, for any smaller value, there are not enough $>s$ for the $2(n - 1) + 2$ fields which require a socket in which to reside. The loop order of all diagrams generated by (67) is clearly n .

Having discussed how the various diagrammatic elements conspire to yield a diagram of loop order n , we now discuss the ranges on the various sums. The maximum

value of s clearly follows from the requirement that the loop order of the diagram is ≥ 0 . The maximum values of the sums over m and j and the minimum value of s follow from the constraint that all fully fleshed out diagrams must be connected and must have an $O(p^2)$ contribution. Suppose that there were a term contributing to $\mathcal{D}_{n\mu\nu}^{a11}(p)$ with $s = 0$. In this case, we would no longer have any decorative gauge remainder components, being left with just $j + 2$ reduced, Wilsonian effective action vertices, $j + 1$ effective propagators and two external fields. Recalling that effective propagators are two-ended objects, we see that there are $2j + 4$ available decorations. Now, from section 2.1 we know that it is imposed as a constraint that all one-point, Wilsonian effective action vertices vanish (though one-point, *seed* action vertices do exist, beyond tree level), in order that the vacuum expectation value of the superscalar which breaks the $SU(N|N)$ symmetry is not shifted by quantum corrections. We can thus insist that all Wilsonian effective action vertices are at least two-point. This requires $2(j + 2)$ decorations, which is precisely equal to the number of available decorations for the diagram as a whole to be connected. Consequently, each vertex must be precisely two-point. Immediately, this precludes the existence of any classical vertices, since reduced vertices do not possess such a component. Thus we have a line of vertices with a loop order of at least one apiece. At each end of the line is a vertex decorated by one external field and by one end of an effective propagator; all other vertices are joined to two other vertices, in each case by a single effective propagator. Now, since none of these vertices is classical, they must each, by (26), contribute $O(p^4)$. Although the effective propagators each contain a $1/p^2$ component this is insufficient to prevent the diagram as a whole vanishing at $O(p^2)$.

In similar fashion, we can understand the maximum values of the sums over m and j . Of the $j + 2$ vertices, suppose that T are classical vertices. Since the vertices are reduced, a minimum of $3T$ decorations are required for the classical vertices and so, if there are m gauge remainders, a minimum of

$$2(j + 2 - T) + 3T + m = 2j + T + m + 4 \tag{68}$$

decorations are required. Noting that the number of available decorations is $2(j + s + 1) + 2$, it is clear that

$$T + m \leq 2s. \tag{69}$$

It therefore follows that

$$m \leq 2s. \tag{70}$$

Next, let us deduce the maximum number of vertices *i.e.* the maximum number taken by $j + 2$ for some values of s and m . From (59), we know that the sum over vertex arguments is $n - s$. Therefore, we can have at most $n - s$ vertices which are not tree level and so a total of at most $n - s + T$ vertices. Hence,

$$j + 2 \leq n + s - m,$$

where we have used (69). Before moving on, let us return to the conclusion (70). In fact, there may be a tighter constraint than this since, if there are more than $n - s$

vertices, then T is compelled to be greater than zero. However, we stick with the limit given by (70), discarding any diagrams which turn out to be disconnected and adopting the prescription that terms for which the maximum value of the sum over j is less than its minimum value do not exist.

This completes our discussion of the form of $\mathcal{D}_{n\mu\nu}^{a11}(p)$ and we will now discuss some of its properties. However, rather than working with $\mathcal{D}_{n\mu\nu}^{a11}(p)$ directly, we introduce the auxiliary function

$$\mathcal{E}_{n\mu\nu}^{a11}(p) \equiv 2 \sum_{s=0}^n \sum_{m=0}^{2s+1} \sum_{j=-2}^{n+s-m-1} \frac{\Upsilon_{j+s+1, j+2}}{m!} \left[\begin{array}{c} \textcircled{\nu^{j+;R}} \\ \textcircled{n_s, j} \end{array} \right]^{11\Delta^{j+s+1} > m}. \quad (71)$$

Comparing $\mathcal{E}_{n\mu\nu}^{a11}(p)$ with $\mathcal{D}_{n\mu\nu}^{a11}(p)$, we notice that the ranges on the sums over s , m and j differ between the two expressions. Thus, we know from our previous arguments that there are diagrams contained in $\mathcal{E}_{n\mu\nu}^{a11}(p)$ which vanish at $O(p^2)$ and / or contain one-point, Wilsonian effective action vertices. The point is that, in our computation of β_n , we will consider $[\mathcal{E}_{n\mu\nu}^{a11}(p)]^\bullet$. To process this expression, we will use the weak coupling flow equations. However, when we do so, there are generically elements of the resulting set of terms which, though not generated by $[\mathcal{D}_{n\mu\nu}^{a11}(p)]^\bullet$, do not *individually* vanish. We will find that some of these terms cancel against terms generated by the flow of other diagrams and so we can view $\mathcal{E}_{n\mu\nu}^{a11}(p)$ as being the same as $\mathcal{D}_{n\mu\nu}^{a11}(p)$, at $O(p^2)$, up to a useful re-expression of zero.

We now demonstrate that

$$\mathcal{E}_{n\mu\nu}^{a11}(p) \sim \square_{\mu\nu}(p) + O(p^4). \quad (72)$$

To do this, we first show that $\mathcal{E}_{n\mu\nu}^{a11}(p)$ is transverse in p . This is done by contracting $\mathcal{E}_{n\mu\nu}^{a11}(p)$ with the momenta p_μ and $(-p)_\nu$ of the external fields.‡ Since we are not computing the flow of any of the vertices, we can discard all one-point vertices, and so decrease the upper limits on the sums over m and j by one each. Explicitly decorating with one of the external fields but leaving the other as an implicit decoration yields the diagrams of figure 42.

Diagram I.106 comes with a factor of $j - 2$, compared to the parent (which have have absorbed into Υ , using (66b)), recognizing the indistinguishability of the $j + 2$ vertices, prior to explicit decoration. Furthermore, the lower limit on the sum over j is -1 and not -2 , since diagram I.106 must possess at least one vertex. The combinatorics for diagram I.107 follows from section 4.1.2; we have recognized that for the diagram as a whole to be connected (or, alternatively, on account of diagrammatic identity (A.10)), the explicit gauge remainder structure must possess a minimum of two $>s$.

‡ To prove the transversality of $\mathcal{E}_{n\mu\nu}^{a11}(p)$ it is necessary only to contract $\mathcal{E}_{n\mu\nu}^{a11}(p)$ with one of the external momenta, but it technically easier to do it with both.

$$\begin{array}{c}
 \left[\begin{array}{c}
 \sum_{s=0}^n \sum_{m=0}^{2s-1} \sum_{j=-1}^{n+s-m-3} \frac{\Upsilon_{j+s+1, j+1}}{m!} \\
 \text{I.108} \\
 \left[\begin{array}{c}
 \text{wavy line} \\
 \{ \} \\
 \text{circle } \nu^{j+;R} \\
 \text{circle } (n_s, j)
 \end{array} \right] \\
 \rightsquigarrow \Delta^{j+s+1} > m
 \end{array} \right]
 \end{array}
 \quad -2 \quad
 \begin{array}{c}
 \left[\begin{array}{c}
 \sum_{s=0}^n \sum_{m=0}^{2s-1} \sum_{j=-2}^{n+s-m-3} \frac{\Upsilon_{j+s+2, j+2}}{m!} \\
 \text{I.109} \\
 \left[\begin{array}{c}
 \text{wavy line} \\
 \{ \} \\
 \text{circle } 0^2 \\
 \text{circle } \nu^{j+;R} \\
 \text{circle } (n_s, j)
 \end{array} \right] \\
 \rightsquigarrow \Delta^{j+s+2} > m
 \end{array} \right]
 \end{array}
 \quad -2
 \end{array}$$

Figure 43. The result of processing diagram I.106.

$j \rightarrow j + 1$.

The next step is to decorate the classical, two-point vertex of diagram I.109, just as we did with diagram I.11 (see figures 8 and 9). If we attach the remaining \rightsquigarrow , the diagram dies, courtesy of diagrammatic identity (A.7). Thus, all we can do is attach an effective propagator, the loose end of which joins either to a reduced Wilsonian effective action vertex or to a gauge remainder structure (recall that if the both ends of the effective propagator attach to the classical, two-point vertex then the diagram dies as a consequence of charge conjugation invariance). In each case, the combinatoric factor associated with choosing one effective propagator, either end of which can attach to the classical, two-point vertex, is $2(j + s + 2)$. In the case that the other end attaches to one of the $j + 2$ reduced vertex, there is an additional factor of $j + 2$.

Illustrative Cancellation 4 *The component of diagram I.109 in which the classical, two-point vertex is attached to a reduced, Wilsonian effective action vertex cancels diagram I.108, up to a gauge remainder contribution.*

Crucially, the surviving gauge remainder contribution is a nested version of diagram I.106. Thus, processing the nested gauge remainder just repeats the above cancellations, generating successively more nested diagrams. The process terminates when there are insufficient decorations for the gauge remainder to strike a reduced vertex. What, then, remains? At each level of nesting (including the un-nested case, as discussed already), we can attach the classical, two-point vertex to a gauge remainder structure. Additionally, from the first level of nesting onwards, we can attach the classical, two-point vertex to one of the gauge remainders which is nested with respect to the gauge remainder which bites the vertex. The complete set of surviving diagrams is collected together in figure 44.

Notice that, in diagram I.111, the sum over m' starts from two, as the $m' = 1$ case vanishes on account of diagrammatic identity (A.11). There is a very important point

$$\begin{aligned}
 & \left[\sum_{s=0}^n \sum_{m'=1}^{2s-1} \sum_{m=0}^{2s-1-m'} \sum_{j=-1}^{n+s-m-m'-3} \frac{\Upsilon_{j+s+1,j+2}}{m!} \right] \\
 & \quad \left[\begin{array}{c} \text{I.110} \\ \text{Diagram I.110} \\ \text{Diagram I.110} \\ \text{Diagram I.110} \end{array} \right] \rightsquigarrow \Delta^{j+s+1} > m \\
 & \quad -2 \\
 & \left[\sum_{s=0}^n \sum_{m''=0}^{2s-3} \sum_{m=2}^{2s-1-m''} \sum_{j=-1}^{n+s-m-m''-3} \frac{\Upsilon_{j+s+1,j+2}}{m!m''!} \sum_{m'=2}^m \right] \\
 & \quad \left[\begin{array}{c} \text{I.111} \\ \text{Diagram I.111} \\ \text{Diagram I.111} \\ \text{Diagram I.111} \end{array} \right] \rightsquigarrow \Delta^{j+s+1} > m-m' \\
 & \quad -2 \\
 & \quad m C_{m'}
 \end{aligned}$$

Figure 44. All surviving terms generated by the diagrams of figure 43.

to make about diagrams I.110 and I.111. Recall that, in section 4.1.2, we stated strings of gauge remainders formed by implicit decorations can only occur in diagrams with $O(p^2)$ stubs, yet here we appear to have a counter-example. However, the strings of gauge remainders in diagrams I.110 and I.111 are formed by the action of nested gauge remainders and *not* by the original set of implicit decorations. With these structures formed, it is useful to sum over nestings, in the usual way, using the notation $\{ \}^{>q}$, as indicated (remembering to compensate with a combinatoric factor of $1/q!$). However, we can not further promote these gauge remainders to join the implicit decorations of the diagram as a whole.

We now find a wonderful cancellation.

Illustrative Cancellation 5 *Diagrams I.107, I.110 and I.111 cancel, courtesy of diagrammatic identity (A.12). This is seen most clearly by making the following changes*

of variables:

Diagram I.107 $m \rightarrow m + 1, m' \rightarrow m' + 1;$

Diagram I.110 $m \rightarrow m - m',$ and recognising that

$$\sum_{m'=1}^{2s-1} \sum_{m=m'}^{2s-1} = \sum_{m=1}^{2s-1} \sum_{m'=1}^m;$$

Diagram I.111 $m \rightarrow m - m'', m' \rightarrow m' - m''$ and recognising that

$$\sum_{m''=0}^{2s-3} \sum_{m=m''+2}^{2s-1} \sum_{m'=2+m''}^m = \sum_{m=2}^{2s-1} \sum_{m'=2}^m \sum_{m''=0}^{m'-2}.$$

We have thus demonstrated that

$$p_\mu(-p)_\nu \mathcal{E}_{n\mu\nu}^{a11}(p) = 0, \quad (73)$$

as we set out to. The patterns of cancellations involved are the template for all cancellations we will encounter when we deal with gauge remainders henceforth.

At first sight, (72) follows directly from (73). However, consider the components of $\mathcal{E}_{n\mu\nu}^{a11}(p)$ which are factorizable. The worry is that such diagrams necessarily contain at least one effective propagator carrying just the external momentum, which contributes a factor of $1/p^2 + O(p^0)$. The resolution to this problem comes from breaking all such contributions down into non-factorizable sub-diagrams and recognizing that these sub-diagrams are transverse, thereby providing the necessary powers of p to cancel those coming from the effective propagators.

To see this explicitly, we consider the component of $\mathcal{E}_{n\mu\nu}^{a11}(p)$ which possesses two non-factorizable sub-diagrams. To this end, we split up

- (i) the two external fields;
- (ii) the $j + s + 1$ effective propagators into three sets of $j + s - s'$, s' and 1 effective propagator(s) with the single effective propagator required to join together the two factorizable sub-diagrams;
- (iii) the $j + 2$ vertices into two sets of $j - j'$ and $j' + 2$ vertices;
- (iv) the m gauge remainders into two sets of $m - m'$ and m' gauge remainders;

Noting that we sum over j' , m' and s' , the combinatoric factor is

$$2(j + s + 1) {}^{j+s}C_{j+s-s'} {}^{j+2}C_{j'+2} {}^m C_{m'}. \quad (74)$$

Including this with (74) and combining the result with $\Upsilon_{j+s+1, j+2}/m!$ yields

$$-2 \frac{\Upsilon_{j+s-s', j-j'}}{(m - m')!} \frac{\Upsilon_{s', j'+2}}{m!}.$$

It is now convenient to shift $j \rightarrow j + j' + 2$, $s' \rightarrow s' + j' + 1$ and $m \rightarrow m + m'$, which yields the contribution shown in figure 45. It is understood that the repeated vertex argument v^{j+2} is summed over.

$$\begin{aligned}
 & -4 \sum_{s=0}^n \sum_{m=0}^{2s+1} \sum_{m'=0}^{2s+1-m} \sum_{j=-2}^{n+s-m-m'-1} \sum_{j'=-2}^{n+s-m-m'-j-3} \sum_{s'=-j'-1}^{j+s+1} \\
 & \left[\begin{array}{c} \frac{\Upsilon_{j'+s'+1, j'+2}}{m!} \\ \\ \\ \\ \frac{\Upsilon_{j+s+1-s', j+2}}{m!} \end{array} \left[\begin{array}{c} \text{---} \\ \left[\begin{array}{c} \textcircled{v^{j+j'+3}; R} \\ \textcircled{v^{j+2}, j'} \end{array} \right] \\ \text{---} \\ \left[\begin{array}{c} \textcircled{v^{j+, j+2}; R} \\ \textcircled{n_s, j} \end{array} \right] \\ \text{---} \end{array} \right] \begin{array}{l} 1\Delta^{j'+s'+1} > m' \\ \\ \\ \\ 1\Delta^{j+s+1-s'} > m \end{array} \end{array} \right]
 \end{aligned}$$

Figure 45. A factorizable contribution to $\mathcal{E}_{n\mu\nu}^{a11}(p)$. The two sub-diagrams are understood to be non-factorizable.

The crucial point to recognize is that the combinatoric factor for each of the sub-diagrams is the canonical one. Immediately we see that each of these sub-diagrams is transverse. It is trivial to generalize this analysis to the case where there are an arbitrary number of non-factorizable sub-diagrams, from which (72) follows. In view of this, it is hardly surprising that we can split $\mathcal{E}_{n\mu\nu}^{a11}(p)$ into Non-Factorizable (NF) components in an enlightening way. Indeed, shifting $s \rightarrow s + s'$ and $v^{i \leq j+2} \rightarrow v^i - s'$ it is apparent that

$$\mathcal{E}_{n\mu\nu}^{a11}(p) = \bar{\mathcal{E}}_{n\mu\nu}^{a11}(p) - \sum_{n'=1}^{n-1} \bar{\mathcal{E}}_{n-n'\mu\rho}^a{}^{11}(p) \Delta_{\rho\sigma}^{11}(p) \bar{\mathcal{E}}_{n'\sigma\nu}^a{}^{11}(p) + \dots, \quad (75)$$

where $\bar{\mathcal{E}}_{n\mu\nu}^{a11}(p) \equiv \mathcal{E}_{n\mu\nu}^{a11}(p)|_{\text{NF}}$, and the ellipsis builds up a full geometric series.

4.2.2. The Function $\mathcal{D}_{n\mu\nu}^{b11}(p)$ We define the function $\mathcal{D}_{n\mu\nu}^{b11}(p)$ and two auxiliary functions as shown in figure 46. Notice that the range for s is the same for all three functions; only the upper limits on m and j differ.

In the case of $\mathcal{E}_{n\mu\nu}^{b'11}(p)$, we must be careful to define precisely what it is we mean by $[\]_{p^2}$, in this context. The basic notion is that for all diagrammatic components enclosed by $[\]_{p^2}$, all p dependence comes from the $O(p^2)$ stub, alone; those components not explicitly enclosed by $[\]_{p^2}$ can either be brought under its influence or not, as we begin to flesh out the diagrams. Thus, for the non-factorizable components of $\mathcal{E}_{n\mu\nu}^{b'11}(p)$, all diagrammatic elements can be brought under the influence of $[\]_{p^2}$, whereas this is

$$\begin{aligned}
 \mathcal{D}_{n\mu\nu}^{b11}(p) &\equiv \left[\begin{array}{c} 4 \sum_{s=1}^n \sum_{r=1}^s \sum_{m=0}^{2(s-r)} \sum_{j=-2}^{n+s-2r-m-2} \frac{\Upsilon_{j+s+2-r,j+2}}{m!r!} \\ \left[\begin{array}{c} \textcircled{0^2} \\ \textcircled{\psi^{j+;R}} \\ \textcircled{n_s, j} \end{array} \right]_{p^2} \\ \left. \vphantom{\sum_{j=-2}^{n+s-2r-m-2}} \right]_{1\Delta^{j+s+2-r} \star^r > m}
 \end{array} \right] \\
 \mathcal{E}_{n\mu\nu}^{b11}(p) &\equiv \left[\begin{array}{c} 4 \sum_{s=1}^n \sum_{r=1}^s \sum_{m=0}^{2(s-r)+1} \sum_{j=-2}^{n+s-2r-m-1} \frac{\Upsilon_{j+s+2-r,j+2}}{m!r!} \\ \times \left[\begin{array}{c} \textcircled{0^2} \\ \textcircled{\psi^{j+;R}} \\ \textcircled{n_s, j} \end{array} \right]_{p^2} \\ \left. \vphantom{\sum_{j=-2}^{n+s-2r-m-1}} \right]_{1\Delta^{j+s+2-r} \star^r > m}
 \end{array} \right] \\
 \mathcal{E}_{n\mu\nu}^{b'11}(p) &\equiv \left[\begin{array}{c} 4 \sum_{s=1}^n \sum_{r=1}^s \sum_{m=0}^{2(s-r)+1} \sum_{j=-2}^{n+s-2r-m-1} \frac{\Upsilon_{j+s+2-r,j+2}}{m!r!} \\ \left[\left[\begin{array}{c} \textcircled{0^2} \\ \textcircled{\psi^{j+;R}} \\ \textcircled{n_s, j} \end{array} \right]_{p^2} \right]^{\star^r} \\ \left. \vphantom{\sum_{j=-2}^{n+s-2r-m-1}} \right]_{1\Delta^{j+s+2-r} > m}
 \end{array} \right]
 \end{aligned}$$

Figure 46. The definition of $\mathcal{D}_{n\mu\nu}^{b11}(p)$ and two auxiliary functions.

not the case for the factorizable components. Notice, though, that all \star s must decorate the part of the diagram under the influence of $[\]_{p^2}$. With these points in mind, we can write

$$\mathcal{E}_{n\mu\nu}^{b'11}(p) = \mathcal{E}_{n\mu\nu}^{b11}(p) - \sum_{n'=1}^{n-1} \mathcal{E}_{n-n'\mu\rho}^b{}^{11}(p) \Delta_{\rho\sigma}^{11}(p) \mathcal{E}_{n'\sigma\nu}^{a11}(p). \quad (76)$$

4.2.3. *The Function $\mathcal{D}_{n\mu\nu}^{c11}(p)$* We define the function $\mathcal{D}_{n\mu\nu}^{c11}(p)$, together with an auxiliary function, as follows:

$$\mathcal{D}_{n\mu\nu}^{c11}(p) \equiv \sum_{s=1}^n \sum_{m=1}^{2s} \sum_{j=-2}^{n+s-m-2} \frac{\Upsilon_{j+s+2,j+2}}{m!} \left[\begin{array}{c} \textcircled{0^2} \\ \textcircled{v^{j+;R}} \\ \textcircled{n_s, j} \end{array} \right]^{1\Delta^{j+s+2} > m} \quad (77)$$

$$\mathcal{E}_{n\mu\nu}^{c11}(p) \equiv \sum_{s=1}^n \sum_{m=1}^{2s+1} \sum_{j=-2}^{n+s-m-1} \frac{\Upsilon_{j+s+2,j+2}}{m!} \left[\begin{array}{c} \textcircled{0^2} \\ \textcircled{v^{j+;R}} \\ \textcircled{n_s, j} \end{array} \right]^{1\Delta^{j+s+2} > m}. \quad (78)$$

As with \mathcal{E}^a , it is useful to isolate the non-factorizable components of \mathcal{E}^c :

$$\mathcal{E}_{n\mu\nu}^{c11}(p) = \bar{\mathcal{E}}_{n\mu\nu}^{c11}(p) - \sum_{n'=1}^{n-1} \bar{\mathcal{E}}_{n-n'\mu\rho}^c{}^{11}(p) \Delta_{\rho\sigma}^{11}(p) \mathcal{E}_{n'\sigma\nu}^{a11}(p). \quad (79)$$

We now demonstrate that

$$2 \left[\bar{\mathcal{E}}_{n\mu\nu}^{c11}(p) \right]_{p^2} = \mathcal{E}_{n\mu\nu}^{b11}(p) + \text{remainders}. \quad (80)$$

The presence of the $[\]_{p^2}$ allows us to Taylor expand all diagrammatic components of $\bar{\mathcal{E}}_{n\mu\nu}^{c11}(p)$, besides the $O(p^2)$ stub, to $O(p^0)$. The result of this procedure is shown in figure 47.

There are a number of comments to make about the diagrams of figure 47. First, each diagram has a socket that we demand is filled by the external field (we will see shortly why we do not fill the socket). In diagram I.114 it is understood that, given that the final gauge remainder in the string is the one that bites the vertex, the first gauge remainder in the string cannot be filled by the external field, as this generates an illegal diagram (see section 4.1.2).

Secondly, the factor of two that diagrams I.112 and I.113 have acquired relative to the parent diagram comes from using charge conjugation to combine the pull back like

$$\begin{aligned}
 & -4 \left[\sum_{s=1}^n \sum_{m=1}^{2s} \sum_{j=-1}^{n+s-m-2} \frac{\Upsilon_{j+s+2,j+1}}{m!} \right]_{1\Delta^{j+s+2}>m} \left[\begin{array}{c} \text{I.112} \\ \text{Diagram: } \textcircled{v^{j+;R}} \text{ with } \textcircled{0^2} \text{ and } \textcircled{n_s, j} \end{array} \right]_{p^2} \\
 & -4 \left[\sum_{s=1}^n \sum_{m=1}^{2s} \sum_{j=-2}^{n+s-m-2} \frac{\Upsilon_{j+s+3,j+2}}{m!} \right]_{1\Delta^{j+s+3}>m} \left[\begin{array}{c} \text{I.113} \\ \text{Diagram: } \textcircled{v^{j+;R}} \text{ with } \textcircled{0^2} \text{ and } \textcircled{n_s, j} \end{array} \right]_{p^2} \\
 & +2 \left[\sum_{s=1}^n \sum_{m=2}^{2s} \sum_{j=-2}^{n+s-m-2} \frac{\Upsilon_{j+s+2,j+2}}{m!} \sum_{m'=2}^m m' C_{m'} \right]_{1\Delta^{j+s+2}>m-m'} \left[\begin{array}{c} \text{I.114} \\ \text{Diagram: } \textcircled{v^{j+;R}} \text{ with } \textcircled{n_s, j} \text{ and } \textcircled{0^2} \text{ with } \sqcup_{>m'} \end{array} \right]_{p^2} \\
 & +2 \left[\sum_{s=1}^n \sum_{m=4}^{2s} \sum_{j=-2}^{n+s-m-2} \frac{\Upsilon_{j+s+2,j+2}}{m!} \sum_{m'=3}^{m-1} m' C_{m'} \right]_{1\Delta^{j+s+2}>m-m'} \left[\begin{array}{c} \text{I.115} \\ \text{Diagram: } \textcircled{v^{j+;R}} \text{ with } \textcircled{n_s, j} \text{ and } \textcircled{0^2} \text{ with } \sqcup_{>m'} \end{array} \right]_{p^2}
 \end{aligned}$$

Figure 47. The diagrams contributing to $2 \left[\overline{\mathcal{E}}_{n\mu\nu}^{c11}(p) \right]_{p^2}$.

momentum derivative with the push forward like derivative momentum. There is no such factor of two in diagrams I.114 and I.115 since are no momentum derivatives.

Thirdly, the fact that the diagrams are under the influence of $[]_{p^2}$ leads to some novelties. Notice that in diagram I.115, the explicitly drawn gauge remainder structure is required to have at least three gauge remainders. If there were only a single gauge remainder, whose socket is necessarily filled by an A^1 sector field, then the diagram would vanish as a consequence of charge conjugation invariance—nothing unusual there. But why is it not possible for there to be only two gauge remainders? The reason is that such a structure which, crucially, is decorated by a \sqcup , would be compelled to be attached to the rest of the diagram by an effective propagator carrying just p . Such a term is forbidden by the influence of $[]_{p^2}$.

To make progress, we attach two effective propagators to the classical, two-point vertex of diagram I.113. As a consequence of the $[]_{p^2}$, these two effective propagators must carry the same (loop) momentum and so we can utilise (54). Processing the gauge remainders, we arrive at the diagrams of figure 48, where we have used charge conjugation invariance to collect terms together, as described under (54).

Diagrams I.119 and I.120 are related, arising from isolating particular components of a single diagram. In the parent diagram from which I.119 and I.120 are derived, the classical, two-point vertex is decorated by $m' >s$. The \triangleright at the end of the \star can be contracted into any of these $>s$ or the socket on the classical, two-point vertex. However, it is useful to isolate the component in which the \triangleright is contracted into the $>$ at the top of the string *i.e.* diagram I.120. In this case alone, we can use diagrammatic identity (A.8). We recognize the resulting term as the $r = 1$ component of $\mathcal{E}_{n\mu\nu}^{b11}(p)$, demonstrating that we are well on the way to proving (80).

In anticipation of what is to follow, we note that diagrams I.112 and I.116 naturally form part of a set in which all diagrammatic elements are struck by a momentum derivative. To find a further member of the set, we process diagram I.117 by isolating the component possessing a classical, two-point vertex and proceeding as usual. The reason we have held back with this step, rather than using our experience of dealing with such terms to jump straight to the result of iterating the diagrammatic procedure until exhaustion, is because of the presence of $[]_{p^2}$.

The loose end of the \star can attach to any available socket in the diagram, besides its own. Suppose that it attaches to the vertex with argument v^{j+} , such that the \star bites its own base. In this case, the vertex does not possess a (classical) two-point component due to the influence of $[]_{p^2}$. Given that the vertex with argument v^{j+} must be at least three point, how do we proceed? The point is that, since the \star bites itself, the field on the vertex to which the \star attaches carries zero momentum. Furthermore, charge conjugation invariance forces this field to be in the A^i sector (group theory considerations then force it to be in the A^1 sector). Thus, we *effectively* have a vertex which has been Taylor expanded to zeroth order in the momentum of a decorative A^1 field, and so we can repeat the above analysis! The difference is that, rather than the socket associated with

$$\begin{aligned}
 & \left[\sum_{s=1}^n \sum_{m=1}^{2s} \sum_{j=-2}^{n+s-m-2} \frac{\Upsilon_{j+s+1,j+2}}{m!} \right]_{p^2} \quad \left[\sum_{s=1}^n \sum_{m=1}^{2s-1} \sum_{j=-1}^{n+s-m-2} \frac{\Upsilon_{j+s+1,j+1}}{m!} \right]_{p^2} \\
 & \left[\begin{array}{c} \text{I.116} \\ \text{Diagram 1} \\ v^{j+;R} \\ n_s, j \\ 0^2 \end{array} \right]_{p^2} \quad -4 \quad \left[\begin{array}{c} \text{I.117} \\ \text{Diagram 2} \\ v^{j+} \\ n_s, j \\ 0^2 \end{array} \right]_{p^2} \\
 & \left[\sum_{s=1}^n \sum_{m=3}^{2s} \sum_{j=-2}^{n+s-m-2} \frac{\Upsilon_{j+s+1,j+2}}{m!} \sum_{m'=2}^{m-1} {}^m C_{m'} \right]_{p^2} \\
 & \left[\begin{array}{c} \text{I.118} \\ \text{Diagram 3} \\ 0^2 \\ v^{j+;R} \\ n_s, j \end{array} \right]_{p^2} \\
 & \left[\sum_{s=1}^n \sum_{m=1}^{2s} \sum_{j=-2}^{n+s-m-2} \frac{\Upsilon_{j+s+1,j+2}}{m!} \sum_{m'=1}^m {}^m C_{m'} m' \right]_{p^2} \\
 & \left[\begin{array}{c} \text{I.119} + \text{I.120} \\ \text{Diagram 4} \\ 0^2 \\ v^{j+;R} \\ n_s, j \end{array} \right]_{p^2}
 \end{aligned}$$

Figure 48. Diagrams spanned by I.113.

$$\begin{aligned}
 & 4 \left[\left[\sum_{s=1}^n \sum_{m=1}^{2s} \sum_{j=-2}^{n+s-m-2} \frac{\Upsilon_{j+s+2,j+2}}{m!} \right] \left[\begin{array}{c} \text{I.122} \\ \text{Diagram with } 0^2, \psi^{j+;R}, n_s, j \text{ and a socket} \end{array} \right] \right]_{p^2}^{1\Delta^{j+s+2}>m} \\
 & -4 \left[\left[\sum_{s=1}^n \sum_{m=1}^{2s} \sum_{j=-2}^{n+s-m-2} \frac{\Upsilon_{j+s+2,j+2}}{m!} \sum_{m'=1}^m m C_{m'} \right] \left[\begin{array}{c} \text{I.123} \\ \text{Diagram with } 0^2, \psi^{j+;R}, n_s, j \text{ and a socket with } \{ \} >^{m'} \end{array} \right] \right]_{p^2}^{1\Delta^{j+s+2}>m-m'} \\
 & -4 \left[\left[\sum_{s=1}^n \sum_{m=4}^{2s-1} \sum_{j=-2}^{n+s-m-3} \frac{\Upsilon_{j+s+2,j+2}}{m!} \sum_{m'=3}^{m-1} m C_{m'} m'(m'-1) \right] \left[\begin{array}{c} \text{I.124} \\ \text{Diagram with } 0^2, \psi^{j+;R}, n_s, j \text{ and a socket with } \{ \} >^{m'-2} \end{array} \right] \right]_{p^2}^{1\Delta^{j+s+2}>m-m'}
 \end{aligned}$$

Figure 50. The result of combining diagrams I.112 and I.116 with the surviving components of diagram I.121.

momentum derivative of diagram I.124 to be transferred from the $>$ to the \triangleright , at the expense of a minus sign.

Next, consider the diagrams of item ii, above. From the earlier comments about the un-nested diagram I.117 it is clear that the diagrams of item ii simply yield versions of diagram I.112 and I.113 but where the socket associated with the momentum derivative is filled by an external field of a sub-diagram containing a \star (this is why we left the socket unfilled in the first place, rather than decorating it with the external field). The similar generalization of diagram I.115 arises from the diagrams of item iii, above. We

can manipulate the new version of diagram I.113 just as we manipulated the original version and precisely the same pattern of terms and cancellations will be generated. In particular, we will generate versions of diagram I.120. We recognise these as the $r > 1$ components of $\mathcal{E}_{n\mu\nu}^{b11}(p)$. Therefore, we have succeeded in demonstrating (80); now we find an explicit expression for the remainders.

The remainders can be thought of as a set of primitive diagrams, together with their analogues possessing implicit \star s. The primitive diagrams are: the diagrams of item iv and diagrams I.114, I.119 and I.123.

Diagrams of item iv can be redrawn via diagrammatic identities (A.14), upon which one of the resultant diagrams exactly cancels diagram I.119. Diagram I.114 can be redrawn using diagrammatic identity (A.13). The resultant diagram naturally combines with diagram I.123 upon recognizing that

$$\textcircled{0^2} \cdots \textcircled{\text{Y}} \cdots = \textcircled{0^2} \textcircled{\text{Y}} = \textcircled{\text{Y}} + \textcircled{\text{Y}} . \quad (81)$$

We thus find that

$$2 \left[\overline{\mathcal{E}}_{n\mu\nu}^{c11}(p) \right]_{p^2} = \mathcal{E}_{n\mu\nu}^{b11}(p) + 2\mathcal{E}_{n\mu\nu}^{c'11}(p), \quad (82)$$

where $\mathcal{E}_{n\mu\nu}^{c'11}(p)$ is given in figure 51.

5. An Expression for β_n

5.1. Initial Manipulations

In this section, we will derive a compact expression for β_n which has no explicit dependence on either the seed action or the details of the covariantization of the cutoff. Our starting point is to consider

$$\left[\mathcal{E}_{n\mu\nu}^{a11}(p) + \mathcal{E}_{n\mu\nu}^{b11}(p) \right]^\bullet .$$

(We work with these auxiliary function because it is technically easier to do so than to work directly with $\mathcal{D}^{a,b}$. At the end of the calculation, will be able to conveniently trade \mathcal{E} s for \mathcal{D} s.)

As a precursor to computing the flow of these functions, it is clear that we will need to understand how to compute the flow of a reduced vertex. Recall that a reduced vertex lacks a classical, two-point component. Consequently, the flow of a reduced vertex lacks a component given by the flow of a classical, two-point vertex, which we can read off from figure 5. Now, the classical flow equation involves only the a_0 term; there are no β , α or a_1 terms. Hence, we need only take care with the dumbbell term generated by the flow of a reduced vertex, which we will tag with an R . It is straightforward to check that a dumbbell term tagged in this way must either possess at least one reduced vertex or must have a decorated kernel.

We begin by focusing on the terms generated by $\left[\mathcal{E}_{n\mu\nu}^{a11}(p) \right]^\bullet$ and adjust the ranges the sums over s , m and j to remove diagrams which vanish even after the action of

$-\Lambda\partial_\Lambda|_\alpha$. This is trivial in the case where $-\Lambda\partial_\Lambda|_\alpha$ strikes an effective propagator: the limits of the sums just reduce to those of $\mathcal{D}_{n\mu\nu}^{a11}(p)$. If $-\Lambda\partial_\Lambda|_\alpha$ strikes a $>$ things are much the same only now the sum over m must, of course, start from one and not zero.

However, things are more subtle in the case that $-\Lambda\partial_\Lambda|_\alpha$ strikes a vertex. Immediately, since we must have at least one vertex, the lower limit of the sum over j increases from -2 to -1 . Consider now the resulting α and β terms. Compared to the parent vertex, the loop order of the daughter vertex is changed, but the number of legs remains the same. Thus, if the parent diagram vanishes at $O(p^2)$, it is not necessarily the case that the daughter α and β -terms also vanish $\dagger\dagger$: it is clear from (25,26) that a change to the loop order of a two-point vertex carrying momentum p can change the order of its leading contribution in p . However, if the parent diagram vanishes because it possesses a one-point vertex, then the daughter α and β -terms will vanish for this reason also. Consequently, for the α and β -terms the minimum value of s stays the same, but the maximum values of both m and j are reduced by one.

With these points in mind, it is worth considering the α and β -terms in more detail and so, to this end, we explicitly give them in figure 52. The combinatoric factor follows from recognizing that the $-\Lambda\partial_\Lambda|_\alpha$ can strike any of the $j + 2$ vertices and using (66b).

$$-2 \left[\sum_u^{n-1} \sum_{s=0}^{2s} \sum_{m=0}^{n+s-m-1-u} \sum_{j=-1}^{n+s-1-j+1} \frac{\Upsilon_{j+s+1,j+1}}{m!} \sum_{v^k=1}^{v^{j+1}} \delta(v^k - u) \right]^{11\Delta^{j+s+1}>m} \left[\begin{array}{c} \left[2(v^{j+,k} - 1) \beta_{v^k} + \gamma_{v^k} \frac{\partial}{\partial \alpha} \right] \textcircled{v^{j+,k}} \\ \textcircled{n_s, j} \end{array} \right]$$

Figure 52. The α and β terms produced by $[\mathcal{E}_{n\mu\nu}^{a11}(p)]^\bullet$.

There are a number of important points to make. First, it is understood that the sum over the vertex argument v^k —which is identified with v^{j+2} —is performed *after* the sums over $v^1 \dots v^{j+1}$ buried in the diagrammatics (*cf.* (58)). Secondly, we notice a sum over the new variable, u , and a δ -function $\delta(v^k - u)$. This is to ensure that the upper limit on the sum over j is given correctly, given that the sum over vertex arguments is now $n - s - v^k$. Finally, the upper limit on the sum over s has been reduced by unity. This follows from the minimum value of v^k being unity (β_0 does not exist) which, in turn, forces $n - s$ to take a minimum value of unity. The expression for the β and α terms is quite ugly in its current form, but it can be neatened up by a change of variables:

$$v^{i>0} \rightarrow v^i + v^k,$$

$\dagger\dagger$ Of course, it must be the case that the sum over all daughters, including those generated by a_0 and a_1 , does vanish at $O(p^2)$.

to give the diagrams of figure 53. Notice that we have changed the dummy variable k to n' which now appears as the outer sum and also as the label for both α and β .

$$-2 \left[\sum_{n'=1}^n \sum_{s=0}^{n-n'} \sum_{m=0}^{2s} \sum_{j=-1}^{n-n'+s-m-1} \frac{\Upsilon_{j+s+1,j+1}}{m!} \right]^{11\Delta^{j+s+1}>m} \left[\begin{array}{c} \left[2(v^{j+} - 1) \beta_{n'} + \gamma_{n'} \frac{\partial}{\partial \alpha} \right] \textcircled{v^{j+}} \\ \textcircled{n_{n'+s}, j} \end{array} \right]$$

Figure 53. A re-expression of the α and β -terms.

We now focus on the $s = 0$ components of these diagrams. Demanding that the resulting terms are connected, we discard all diagrams possessing one-point (Wilsonian effective action) vertices. Utilizing (25,26) it is straightforward to demonstrate that the sole contribution which survives at $O(p^2)$ is:

$$\begin{aligned} & -2\Upsilon_{0,0} \left(-2\beta_n + \gamma_n \frac{\partial}{\partial \alpha} \right) \textcircled{0^2} \\ & = -4\beta_n \square_{\mu\nu}(p) + O(p^4), \end{aligned}$$

where we have used (65).

Returning to our consideration of $[\mathcal{E}_{n\mu\nu}^{a11}(p)]^\bullet$, we note that terms generated by the action of a_0 are particularly simple to deal with: the ranges of the sums over s , m and j just stay the same. This follows because a_0 converts a Wilsonian effective action vertex into a dumbbell structure, components of which possess seed action vertices; seed action vertices, unlike their Wilsonian effective action counterparts, exist at the one-point level. Suppose that the parent diagram vanishes at $O(p^2)$, on account of an $S_{n'\mu\nu}^{11}(p)$ vertex. This can be converted into (amongst other terms) a dumbbell possessing a one-point, n' -loop seed action vertex, joined to a classical, three-point vertex. This term no longer vanishes at $O(p^2)$. If the parent diagram vanishes on account of a one-point Wilsonian effective action vertex, the daughter can survive since the vanishing vertex of the parent can be converted into a dumbbell structure possessing a one-point, seed action vertex joined to a two-point vertex.

Finally, consider the effect of the action of a_1 . Due to the equivalence of each of the vertices in a given term, we can take the a_1 to strike the vertex with argument $v^{j+;R}$ (so long as we multiply by $j+2$), causing the argument to become $\Sigma_{v^{j+}-1}$. The R has been dropped, since a quantum term is necessarily formed from a vertex whose argument is greater than zero. The lower limit on the sum over v^{j+} should be now changed from zero

to one, in recognition of the fact that a_1 does not act on tree level terms. Furthermore, the sum over all vertex arguments is now $n + s - 1$, rather than $n + s$, and so we should reduce the upper limit of the sum over s by one. It is convenient to change variables:

$$v^{i>0} \rightarrow v^i + 1$$

and then to let $s \rightarrow s - 1$. This affects the ranges of all three sums.

The diagrams formed by $[\mathcal{E}_{n\mu\nu}^{a11}(p)]^\bullet$ are shown in figure 54. It is understood here, and in all that follows, that the vertex argument v^k is to be identified with v^{j+2} . If this vertex argument appears in more than one vertex (as will always be the case) it is understood to be summed over, in the usual manner.

It is worth considering the diagrams arising from explicitly decorating D.6 with the differentiated effective propagator in more detail. For convenience, these diagrams are collected together in figure B1. Explicit decoration with the differentiated effective propagator has the capacity to further change the limits on the various sums. For example, if we attach both ends to the same vertex, then this will reduce the maximum value of m by one since, in order to form a connected diagram, the vertex decorated by the differentiated effective propagator must be at least three-point. This effectively uses up a decoration which could otherwise have filled a $>$.

In the case that each end of the differentiated effective propagator attaches to a different vertex, we note that such a diagram can only exist for $j > -1$. Our strategy here is to shift $j \rightarrow j + 1$, so that the sum over j starts from -1 , identifying v^{j+2} with v^k as usual.

We now isolate all classical, two-point vertices in diagrams D.3–D.5. This step is crucial to the entire diagrammatic procedure: if a classical, two-point vertex is attached to an effective propagator, we can employ the effective propagator relation, whereas if it is attached to an external field, we can perform manipulations at $O(p^2)$. Although the classical, two-point vertices of diagram D.4 are fully decorated, it will nonetheless prove useful to isolate them, as this will help elucidate the structure of the forthcoming cancellations.

Let us consider isolating the classical, two-point vertices of diagram D.3 in more detail. First, let us take both vertices of the dumbbell structure to be reduced vertices. This immediately allows us to reduce the maximum value of the sum over j by one, since the formation of the dumbbell term causes the total number of vertices to increase from $j + 2$ to $j + 3$ (and the maximum number of reduced vertices we can decorate in the formation of a connected diagram remains the same). Of the terms which remain, consider those possessing exclusively Wilsonian effective action vertices. Since we discard one-point, Wilsonian effective action vertices in all diagrams in which $\Lambda\partial_\Lambda|_\alpha$ has acted, we can reduce the maximum values of j and m and increase the minimum value of s by one. The component of the resulting diagram in which the kernel is undecorated is exactly cancelled by the component of diagram D.6 in which the differentiated effective propagator joins two different vertices (see diagram D.99). Since

$$\begin{aligned}
 & [\mathcal{E}_{n\mu\nu}^{a11}(p)]^\bullet + O(p^4) = -4\beta_n \square_{\mu\nu}(p) \\
 & -2 \left[\sum_{n'=1}^{n-1} \sum_{s=1}^{n-n'} \sum_{m=0}^{2s} \sum_{j=-1}^{n-n'+s-m-1} \frac{\Upsilon_{j+s+1,j+1}}{m!} \right]^{11\Delta^{j+s+1}>m} \\
 & \left[\begin{array}{c} \text{D.1} \quad \text{D.2} \\ \left[2(v^{j+} - 1)\beta_{n'} + \gamma_{n'} \frac{\partial}{\partial \alpha} \right] \circlearrowleft^{j+} \\ \circlearrowleft^{n_{n'+s}, j} \end{array} \right] \\
 & - \sum_{s=0}^n \sum_{m=0}^{2s+1} \sum_{j=-1}^{n+s-m-1} \frac{\Upsilon_{j+s+1,j+1}}{m!} \left[\begin{array}{c} \text{D.3} \\ \circlearrowleft^k \\ \bullet \\ \circlearrowleft^{j+,k} \\ \circlearrowleft^{n_s, j} \end{array} \right]_R^{11\Delta^{j+s+1}>m} \\
 & + \sum_{s=1}^n \sum_{m=0}^{2s-1} \sum_{j=-1}^{n+s-m-2} \frac{\Upsilon_{j+s,j+1}}{m!} \left[\begin{array}{c} \text{D.4} \quad \text{D.5} \\ \circlearrowleft^{\bullet} + \circlearrowleft^{\bullet} \\ \circlearrowleft^{\Sigma_{v^{j+}}} \\ \circlearrowleft^{n_s, j} \end{array} \right]^{11\Delta^{j+s}>m} \\
 & + \left[\sum_{s=1}^n \sum_{m=0}^{2s} \sum_{j=-2}^{n+s-m-2} \frac{\Upsilon_{j+s,j+2}}{m!} \right]^{11\Delta^{j+s} \overset{\circ}{\Delta} > m} \left[\begin{array}{c} \text{D.6} \\ \circlearrowleft^{j+;R} \\ \circlearrowleft^{n_s, j} \end{array} \right] \\
 & + \left[2 \sum_{s=1}^n \sum_{m=1}^{2s} \sum_{j=-2}^{n+s-m-2} \frac{\Upsilon_{j+s+1,j+2}}{(m-1)!} \right]^{11\Delta^{j+s+1} > m-1 \overset{\bullet}{>}} \left[\begin{array}{c} \text{D.7} \\ \circlearrowleft^{j+;R} \\ \circlearrowleft^{n_s, j} \end{array} \right]
 \end{aligned}$$

Figure 54. An expression for $[\mathcal{E}_{n\mu\nu}^{a11}(p)]^\bullet$.

the surviving component has a decorated kernel, the maximum values of both m and j are reduced by one, again.

Isolating a single classical, two-point vertex in diagram D.3 is straightforward: taking the argument of the top or bottom vertex of the dumbbell structure to be a classical, two-point vertex amounts to the same thing; hence we will choose to isolate the classical, two-point part of \bar{v}^k and multiply by two. When taking the classical part of \bar{v}^k , the other vertex argument, $\bar{v}^{j+k;R} \equiv \bar{v}^{j+;R} - \bar{v}^{k;R}$, reduces to simply $\bar{v}^{j+;R}$. We now expanded out the barred vertices, according to (24), noting that certain terms cancel on account of us having set the classical, two-point seed action vertices equal to their Wilsonian effective action counterparts. There is no need to change the limits on any of the sums: compared to the parent diagram, we have an extra two-point vertex, but also an extra two decorative fields, corresponding to the two ends of the kernel.

Taking two classical, two-point vertices in diagram D.3 requires some thought. First, we note that the resulting dumbbell structure cannot have been formed by the flow of a one-point vertex. Since we are interested only in one-point Wilsonian effective action vertices if they have been processed, we can reduce the maximum values of m and j and increase the minimum value of s to remove any unwanted diagrams. If $j = -1$, then there are only two vertices in total, and so this case should be treated differently from $j \geq 0$. In the latter case, it will prove useful to shift variables $j \rightarrow j + 1$, so that the sum over j starts, once again, from -1 . We can then recombine terms into a diagram with a sum that starts from $j = -2$. The isolation of the classical, two-point vertices of diagram D.3 is shown in figure 55.

It is now easy to isolate the classical, two-point vertices of diagrams D.4 and D.5, though we note the following. First, on account of the equality of the Wilsonian effective action, classical, two-point vertices and their seed action counterparts, $\Sigma_{0RS}^{XX}(k) = -S_{0RS}^{XX}(k)$; in other words, the classical, two-point component of Σ has a minus sign, relative to the reduced part. Secondly, the kernel attaching to the classical, two-point vertex contained in diagram D.4 must be decorated, in order that a connected diagram can be formed. Finally, the component of diagram D.4 in which all vertices are Wilsonian effective action vertices and the kernel is undecorated is cancelled by the component of diagram D.6 in which the differentiated effective propagator attaches at both ends to the same vertex (see diagram D.100). The isolation of the classical, two-point vertices of diagrams D.4 and D.5 is shown in figure 56.

The next step of the diagrammatic procedure is to decorate the classical, two-point vertices of diagrams D.10, D.11 and D.17 with either an external field or an end of an effective propagator. In the latter case we must then attach the loose end of the effective propagator to an available structure. We refer to the primary part of a diagram as the component left over after applying the effective propagator relation as many times as possible but, each time, retaining only the Kronecker- δ contribution.

Assuming that the necessary structures exist, we can do the following with a diagram possessing a single classical, two-point vertex:

$$\begin{aligned}
 & - \left[\sum_{s=1}^n \sum_{m=0}^{2s-1} \sum_{j=-1}^{n+s-m-4} \frac{\Upsilon_{j+s+1,j+1}}{m!} \right]_{11\Delta^{j+s+1} > m} \\
 & \quad \left[\text{D.8} \right] \\
 & \quad \begin{array}{c} \text{D.8} \\ \circlearrowleft \psi^{k;R} \\ | \\ \circ \\ \circlearrowleft \psi^{j+,k;R} \end{array} \quad \circlearrowleft n_s, j
 \end{aligned}$$

$$\begin{aligned}
 & + 2 \left[\sum_{s=0}^n \sum_{m=0}^{2s+1} \sum_{j=-1}^{n+s-m-2} \frac{\Upsilon_{j+s+1,j+1}}{m!} \right]_{11\Delta^{j+s+1} > m} \\
 & \quad \left[\text{D.9} \right] \\
 & \quad \begin{array}{c} \text{D.9} \\ \circlearrowleft \hat{\psi}^{k;R} \\ | \\ \bullet \\ \circlearrowleft \psi^{j+,k;R} \end{array} \quad \circlearrowleft n_s, j
 \end{aligned}$$

$$\begin{aligned}
 & + \left[\sum_{s=1}^n \sum_{m=0}^{2s-1} \sum_{j=-2}^{n+s-m-3} \frac{\Upsilon_{j+s+2,j+2}}{m!} \right]_{11\Delta^{j+s+2} > m} \\
 & \quad \left[\text{D.10} \right] \\
 & \quad \begin{array}{c} \text{D.10} \\ \circlearrowleft 0^2 \\ | \\ \circ \\ \circlearrowleft 0^2 \\ | \\ \circlearrowleft \psi^{j+;R} \\ | \\ \circlearrowleft n_s, j \end{array}
 \end{aligned}$$

$$\begin{aligned}
 & + 2 \left[\sum_{s=0}^n \sum_{m=0}^{2s+1} \sum_{j=-1}^{n+s-m-1} \frac{\Upsilon_{j+s+1,j+1}}{m!} \right]_{11\Delta^{j+s+1} > m} \\
 & \quad \left[\text{D.11} \right] \\
 & \quad \begin{array}{c} \text{D.11} \\ \circlearrowleft 0^2 \\ | \\ \bullet \\ \circlearrowleft \hat{\psi}^{j+;R} \\ | \\ \circlearrowleft n_s, j \end{array}
 \end{aligned}$$

Figure 55. Isolation of the classical, two-point vertices of diagram D.3 plus diagram D.99.

$$\begin{aligned}
 & \left[\sum_{s=1}^n \sum_{m=0}^{2s-1} \sum_{j=-1}^{n+s-m-2} \frac{\Upsilon_{j+s,j+1}}{m!} \right]_{11\Delta^{j+s} > m} \\
 & \left[\begin{array}{c} \text{D.12} \\ -2 \begin{array}{c} \circ \\ \hat{v}^{j+;R} \end{array} \\ \begin{array}{c} \circ \\ n_s, j \end{array} \end{array} \right]_{11\Delta^{j+s} > m} - \left[\begin{array}{c} \text{D.13} \\ \begin{array}{c} \circ \\ 0^2 \end{array} \\ \begin{array}{c} \circ \\ v^{j+;R} \end{array} \\ \begin{array}{c} \circ \\ n_s, j \end{array} \end{array} \right]_{11\Delta^{j+s} > m} \\
 & + \left[\sum_{s=1}^n \sum_{m=0}^{2s-1} \sum_{j=-1}^{n+s-m-3} \frac{\Upsilon_{j+s,j+1}}{m!} \right]_{11\Delta^{j+s} > m} \\
 & \left[\begin{array}{c} \text{D.14} \quad \text{D.15} \quad \text{D.16} \\ \begin{array}{c} \circ \\ v^{j+;R} \end{array} + \begin{array}{c} \bullet \\ v^{j+;R} \end{array} - 2 \begin{array}{c} \bullet \\ \hat{v}^{j+;R} \end{array} \\ \begin{array}{c} \circ \\ n_s, j \end{array} \end{array} \right]_{11\Delta^{j+s} > m} \\
 & - \left[\sum_{s=1}^n \sum_{m=0}^{2s-1} \sum_{j=-2}^{n+s-m-3} \frac{\Upsilon_{j+s+1,j+2}}{m!} \right]_{11\Delta^{j+s+1} > m} \\
 & \left[\begin{array}{c} \text{D.17} \\ \begin{array}{c} \bullet \\ 0^2 \end{array} \\ \begin{array}{c} \circ \\ v^{j+;R} \end{array} \\ \begin{array}{c} \circ \\ n_s, j \end{array} \end{array} \right]_{11\Delta^{j+s+1} > m}
 \end{aligned}$$

Figure 56. Isolation of the classical, two-point vertices of diagrams D.4 and D.5 plus diagram D.100.

- (i) attach an external field;
- (ii) attach one end of an effective propagator, with the other end attaching to:
 - (a) the seed action vertex to which the kernel attaches;
 - (b) one of the Wilsonian effective action vertices;
 - (c) the kernel;
 - (d) a gauge remainder.

In each of (ii)a–(ii)d the effective propagator relation can be applied. For the time being, we will concern ourselves with just the primary parts of (ii)a–(ii)c, which yield a series of cancellations, returning to both the gauge remainder contributions and other diagrams later. First, we analyse the result of decorating the classical, two-point vertex of diagram D.11.

Cancellation 1 (Diagram D.9) *Consider the primary part of diagram D.11 corresponding to (ii)b, above, which we note exists only for $j > -1$. For comparison with diagram D.9, it is convenient to change variables $j \rightarrow j + 1$, so that the sum over j once again starts from -1 and to identify \hat{v}^{j+2} with \hat{v}^k . Thus, the two-point, tree level vertex of diagram D.11 can be joined to any of $j + 2$ identical Wilsonian effective action vertices, using any of $j + s + 2$ effective propagators. Noting that this effective propagator can attach either way round, the combinatoric factor is*

$$2(j + s + 2)(j + 2),$$

which, from (66a,66b), combines with $\Upsilon_{j+s+2,j+2}$ to give $-\Upsilon_{j+s+1,j+1}$. Thus, the primary part of diagram D.11 corresponding to (ii)b, above, precisely cancels diagram D.9.

Cancellation 2 (Diagram D.12) *Consider the primary part of diagram D.11 corresponding to (ii)a, above, which we might hope cancels diagram D.12. At first sight, though, it does not look like the cancellation will quite work since, although the combinatorics are fine, the limits on the sums over s , m and j differ between diagrams D.11 and D.12. However, the formation of a loop in diagram D.11 allows us to restrict the ranges over these sums (just as we did for diagram D.100), and so the two diagrams do exactly cancel.*

Cancellation 3 (Diagram D.16) *Consider the primary part of diagram D.11 corresponding to (ii)c, above. Following through similar arguments to those invoked in cancellation 2, it can be shown that the primary part of diagram D.11 corresponding to (ii)c exactly cancels diagram D.16.*

This concludes our initial discussion of diagram D.11. Rather than immediately analysing diagram D.17, which also possesses a single classical, two-point vertex, it is useful to first consider the decoration of diagram D.10 which possesses two such vertices. At $O(p^2)$, we can discard the case in which an external field attaches to each of the classical, two-point vertices. If one of the vertices is decorated by an external field, then we can attach an effective propagator to the other according to (ii)b–(ii)d above. If both vertices are decorated by an end of an effective propagator, then we can tie up the associated loose ends in the following independent ways:

- (i) Join one classical, two-point vertex to a Wilsonian effective action vertex and the other to:
 - (a) the same vertex;
 - (b) a different vertex;
 - (c) the kernel;
 - (d) a gauge remainder;
- (ii) Join one classical, two-point vertex to the kernel and the other to:
 - (a) the kernel;
 - (b) a gauge remainder;
- (iii) Join one classical, two-point vertex to a gauge remainder and the other to a gauge remainder
 - (a) in the same gauge remainder structure;
 - (b) in a different gauge remainder structure;
- (iv) Join the classical, two-point vertices together.

We now consider the results of decorating diagram D.10 according to (i)a–iv.

Cancellation 4 (Diagram D.14) *The primary part of D.10 corresponding to (i)a, above, exactly cancels diagram D.14.*

Cancellation 5 (Diagram D.13) *Diagram D.13 is exactly cancelled by the primary part of diagram D.10 corresponding to iv, above.*

Cancellation 6 (Diagram D.8) *The primary part of diagram D.10 corresponding to (i)b, above, exactly cancels diagram D.8.*

Cancellation 7 (Components of diagram D.17) *The primary part of diagram D.10 corresponding to (ii)a, above, exactly cancels the primary part of diagram D.17 in which the classical, two-point vertex attaches to the kernel.*

Looking at cancellation 7, it is tempting to say that the primary parts of diagram D.17 are all exactly cancelled by a subset of the primary parts of diagram D.10. However, this is not true: consider the primary part of diagram D.10 corresponding to (ii)b, above. In this case, because each of the classical, two-point vertices attaches to something different, we pick up a factor of two, in recognition of the fact that either of the vertices could attach to the kernel / gauge remainder. However, the primary part of diagram D.17 in which the classical, two-point vertex attaches to a gauge remainder can only be formed in one way; hence the cancellation is only partially realized. The key to cancellation 7 is that both classical, two-point vertices of diagram D.10 attach to the same structure, and so there is no factor of two picked up.

A diagram generated by the partial cancellation of a component of diagram D.17 against a component of diagram D.10 is immediately involved in a cancellation.

Cancellation 8 (Diagram D.15) *The primary part of diagram D.10 corresponding to (i)c above and the primary part of diagram D.17 in which the classical, two-point attaches to a vertex combine to exactly cancel diagram D.15.*

Using cancellations 1–8 and partial cancellations of the type just discussed, we can rewrite $\mathcal{E}_{n\mu\nu}^{a11}(p)$ as shown in figure 57. $\mathcal{G}_{n\mu\nu}^{a11}(p)$ and $\mathcal{H}_{n\mu\nu}^{a11}(p)$ are disjoint sets whose elements are all spawned by a_0 and a_1 : all such diagrams which possess an $O(p^2)$ stub belong to $\mathcal{H}_{n\mu\nu}^{a11}(p)$; all elements of $\mathcal{G}_{n\mu\nu}^{a11}(p)$ possess a full gauge remainder (arising from the application of the effective propagator relation).

The formation of diagram D.18 deserves further comment. This diagram is a combination of the following terms:

- (i) the primary part of D.10 in which both classical, two-point vertices attaches to a different gauge remainder structure
- (ii) the component of diagram D.6 in which both ends of the differentiated effective propagator attaches to a different gauge remainder structure (see diagram D.102).

Notice that the limits on the sums over m and j , in diagram D.18 are the same as in diagram D.6 and not D.10. Diagram D.10 supplements diagram D.6, converting a differentiated effective propagator into a full kernel in all cases where there are sufficiently few gauge remainders and vertices to permit decoration of the kernel. The values of m and j for which diagram D.6 exists but diagram D.10 does not are those for which the differentiated effective propagator of D.6 can be trivially replaced by a full kernel, since this kernel can effectively never be decorated.

Similar considerations apply to diagrams D.19 and D.23. In the latter case, to save space, we have put this diagram under the same summations as diagram D.22. Whereas diagram D.22 exists for the maximum values of m and j , diagram D.23 possesses a Wilsonian effective action, one-point vertex in these cases and so has no support: the maximum values of m and j for which diagram D.23 exists are $2s$ and $n + s - m - 2$, respectively. In the same fashion, diagram D.20 does not in fact exist for the maximum values of m indicated. Having taken great care, up until now, to restrict the ranges on the sums as much as possible for each diagram, we will now often put diagrams under the same summation sign to save space, mindful that not all diagrams necessarily exist for all values of s , m and j .

5.2. Gauge Remainders

The terms of $\mathcal{G}_{n\mu\nu}^{a11}(p)$ can be usefully decomposed into five sets comprising:

- (I) diagrams possessing a single full gauge remainder, the $>$ part of which attaches to a kernel, the other end of which attaches to:
 - (a) itself;
 - (b) a reduced seed action vertex;
 - (c) a reduced Wilsonian effective action vertex;

(iii) a socket, which can be filled by one of the decorations.

Summing over diagrams of the first item yields zero: because the kernel bites itself, its top end can be struck in two independent ways. First, the active gauge remainder can push forward (pull back) onto the field on the kernel which the kernel bites; this field is identified with the top end of the kernel. Secondly, the active gauge remainder can pull back (push forward) unhindered to the top. These two independent cases exactly cancel each other (see also the discussion around diagrams I.21–I.23).

Now we consider processing the active gauge remainder of diagram D.24 and splitting off the classical, two-point component from the reduced component. Compared to diagram I.109, the classical, two-point vertex can, in addition to being attached to a reduced Wilsonian effective action vertex or gauge remainder structure, be attached to the kernel or decorated with an external field. If it attaches to the kernel, this just cancels the component of diagram D.25 where the gauge remainder bites a socket on the kernel, up to a gauge remainder contribution. This cancellation, together with the analogue of illustrative cancellation 4 occurs at each level of nesting. Of those diagrams which survive, two cancel against diagram D.26 via diagrammatic identity (A.12).

Up to those diagrams with an $O(p^2)$ stub, the only diagrams which survive are those spawned by diagram D.25 and its nested partners in which the gauge remainder strikes the bottom end of the kernel, as shown in figure 59.

$$\left[\begin{array}{c} \sum_{s=1}^n \sum_{m'=1}^{2s-1} \sum_{m=0}^{2s-1-m'} \sum_{j=-2}^{n+s-m-m'-3} \\ \frac{\Upsilon_{j+s,j+2}}{m!m'!} \left[\begin{array}{c} \text{D.27} \\ \text{Diagram: } \begin{array}{c} \text{Socket with dot} \\ \text{Bracket } \{ \}^{>m'} \\ \text{Circle } (\varrho^{j+;R}) \\ \text{Circle } (n_s, j) \end{array} \end{array} \right]^{11\Delta^{j+s}>m} \end{array} \right]$$

Figure 59. Surviving terms generated by the diagrams of figure 58, up to terms with an $O(p^2)$ stub.

The sign and combinatoric factor of diagram D.27 follow from the discussion around figure 11.

Cancellation 9 (Diagram D.20) *Diagram D.27 exactly cancels diagram D.20. This follows from first letting $m \rightarrow m - m'$ in D.27 and recognizing that*

$$\sum_{m'=1}^{2s-1} \sum_{m=m'}^{2s-1} = \sum_{m=1}^{2s-1} \sum_{m'=1}^m,$$

and secondly recalling that the upper limits on the sums over m and j in diagram D.20 can be reduced by one apiece.

We have thus demonstrated how all diagrams spawned by the type (I)a gauge remainders, up to those with an $O(p^2)$ stub, cancel. In preparation for our treatment of the other gauge remainders, it is worth reviewing this how this happens. If an active gauge remainder strikes a socket on a reduced vertex or on a kernel, this diagram will be cancelled by a diagram in which the gauge remainder instead strikes a socket on a classical, two-point vertex, which is subsequently attached to either a reduced vertex or a kernel with an effective propagator. Such cancellations leave over diagrams of exactly the same basic form as the parent diagrams, but where the gauge remainder is nested. Allowing the nested gauge remainder to act then just repeats the cancellations just described. We are left with following:

- (i) Diagrams possessing a classical, two-point vertex attached to
 - (a) an $O(p^2)$ stub;
 - (b) a gauge remainder nested with respect to to the original, active gauge remainder;
 - (c) a gauge remainder structure.
- (ii) The original type (I)a diagram possessing a trapped gauge remainder;
- (iii) Diagrams in which a kernel is bitten at its end by a (nested) gauge remainder.

Diagrams of type (i)b, (i)c and ii cancel, courtesy of diagrammatic identity A.12. Diagrams of type iii cancel against terms generated elsewhere in the calculation.

We thus see that most of the diagrams spawned by the type (I)a gauge remainders cancel amongst themselves. The wonderful thing is that this basic pattern of cancellations is repeated for all the other types of gauge remainders. The differences come with the types of terms generated which cancel against terms generated elsewhere in the calculation. With this in mind, we now treat the gauge remainders of types (I)b and (I)c, which are collected together in figures 60 and 61, respectively.

It is apparent that the gauge remainders of types (I)b and (I)c are almost exactly the same, which is why we choose to treat them together. The differences are first that the gauge remainders of type (I)b possess a seed action vertex and secondly that the kernels of all type (I)c diagrams must be decorated. In diagrams D.28 and D.31, we note that we can reduce the maximum values of the sums over m and j by one more than expected: if the seed action vertex is one-point, then the kernel must be decorated, else the full gauge remainder is forced to be in the C^i sector—where of course it is null—by charge conjugation invariance.

Processing the gauge remainders, it is obvious what will happen. Diagram D.28 (D.32) has two components: one in which the gauge remainder strikes a socket on a reduced vertex and one in which the gauge remainder strikes a socket on a classical, two-point vertex. The former case is cancelled, up to a nested gauge remainder by the

$$\begin{aligned}
 & +2 \left[\begin{array}{c} \sum_{s=0}^n \sum_{m=0}^{2s} \sum_{j=-1}^{n+s-m-3} \frac{\Upsilon_{j+s+1,j+1}}{m!} \\ \left[\begin{array}{c} \text{D.28} \\ \begin{array}{c} \hat{v}^{k;R} \\ \bullet \\ \downarrow \\ v^{j_+,k;R} \end{array} \\ \text{---} \\ \begin{array}{c} \text{---} \\ \bullet \\ \text{---} \\ n_s, j \end{array} \end{array} \right]^{11\Delta^{j+s+1} > m} \end{array} \right] \\
 & -2 \left[\begin{array}{c} \sum_{s=1}^n \sum_{m=0}^{2s-1} \sum_{j=-1}^{n+s-m-2} \frac{\Upsilon_{j+s,j+1}}{m!} \\ \left[\begin{array}{c} \text{D.29} \quad \text{D.30} \\ \begin{array}{c} \hat{v}^{j_+;R} \\ \bullet \\ \text{---} \\ \hat{v}^{j_+;R} \end{array} \quad + \quad \begin{array}{c} \hat{v}^{j_+;R} \\ \bullet \\ \text{---} \\ \hat{v}^{j_+;R} \end{array} \\ \text{---} \\ \begin{array}{c} \text{---} \\ \bullet \\ \text{---} \\ n_s, j \end{array} \end{array} \right]^{11\Delta^{j+s} > m} \end{array} \right] \\
 & -2 \left[\begin{array}{c} \sum_{s=0}^n \sum_{m=2}^{2s} \sum_{m'=2}^m \sum_{j=-1}^{n+s-m-2} \frac{\Upsilon_{j+s,j+1}}{m!} \\ \left[\begin{array}{c} \text{D.31} \\ \begin{array}{c} \{ \} >^{m'} \\ \bullet \\ \uparrow \\ \hat{v}^{j_+;R} \end{array} \\ \text{---} \\ \begin{array}{c} \text{---} \\ \bullet \\ \text{---} \\ n_s, j \end{array} \end{array} \right]^{11\Delta^{j+s} > m-m'} \end{array} \right] \\
 & \quad \quad \quad {}^m C_{m'}
 \end{aligned}$$

Figure 60. Gauge remainders of type (I)b.

contribution in which the classical, two-point vertex is joined to one of the Wilsonian effective action vertices. If, instead, the classical, two-point vertex is attached to a socket on either the seed action vertex or kernel then, up to a nested gauge remainder, this cancels the contributions from diagrams D.29 (D.33) and D.30 (D.34) in which, respectively, the gauge strikes a socket on the reduced component of the seed action vertex and a socket on the kernel. Up to terms with an $O(p^2)$ stub, the final type of diagram spawned by D.28 (D.32) is one in which the classical, two-point vertex formed by the action of the gauge remainder is attached to a gauge remainder structure. Putting this to one side for the moment, we note that processing the nested gauge remainders repeats this pattern of cancellations.

At the first level of nesting we get, as usual, a new type of diagram: one in which the classical, two-point vertex generated by D.28 (D.32) attaches to the nested gauge remainder. Iterating the diagrammatic procedure, diagrams of this type, together with diagrams of the type temporarily put aside, exactly cancel diagram D.31 (D.35), courtesy of diagrammatic identity (A.12).

Of the diagrams that remain, two are immediately involved in cancellations.

Cancellation 10 (Diagrams D.22 and D.23) *Diagram D.22 (D.23) is exactly cancelled by the component of diagrams D.30 (D.34) and its nested partners in which the gauge remainder strikes the top end of the kernel.*

Up to $O(p^2)$ terms, the diagrams which survive are the following terms and their nested partners.

- (i) The component of diagram D.29 in which the gauge remainder strikes
 - (a) a socket on a classical, two-point vertex;
 - (b) the field which attaches to the base of the kernel, and for which the seed action vertex is:
 1. a reduced vertex;
 2. a classical, two-point vertex;
- (ii) The component of diagram D.30 in which the gauge remainder strikes the bottom end of the kernel;
- (iii) The component of diagram D.33 in which the gauge remainder strikes
 - (a) a socket on a classical, two-point vertex;
 - (b) the field which attaches to the base of the kernel, and for which the seed action vertex is:
 1. a reduced vertex;
 2. a classical, two-point vertex;
- (iv) The component of diagram D.34 in which the gauge remainder strikes the bottom end of the kernel;

Now, (i.b)1 and ii exactly cancel (*cf.* illustrative cancellation 1). However, (iii.b)1 and iv do not: in the former case, the kernel must be decorated whereas, in the latter

$$\begin{aligned}
 & \left[\sum_{s=1}^n \sum_{m=0}^{2s-1} \sum_{j=-1}^{n+s-m-3} \frac{\Upsilon_{j+s,j+1}}{m!} \sum_{m'=0}^m \right. \\
 & \quad \left. \left[\begin{array}{c} \text{D.36} \\ \circlearrowleft \\ \{ \} \succ m' \\ \psi^{j+;R} \\ \circlearrowleft \\ (n_s, j) \end{array} \right] \right]^{11\Delta^{j+s} > m-m'} \\
 & -2 \left[\sum_{s=1}^n \sum_{m=0}^{2s-1} \sum_{j=-2}^{n+s-m-3} \frac{\Upsilon_{j+s+1,j+2}}{m!} \sum_{m'=0}^m m C_{m'} \right. \\
 & \quad \left. \left[\begin{array}{c} \text{D.37} \quad \text{D.38} \\ \circlearrowleft \quad \circlearrowright \\ \{ \} \succ m' \quad \{ \} \succ m' \\ \circlearrowleft \quad \circlearrowright \\ 0^2 \quad 0^2 \\ \psi^{j+;R} \\ \circlearrowleft \\ (n_s, j) \end{array} \right] \right]^{11\Delta^{j+s+1} > m-m'}
 \end{aligned}$$

Figure 62. Surviving terms from the type (I)b and (I)c gauge remainders, up to those with an $O(p^2)$ stub.

case, there is no such restriction. Thus, a diagram possessing a differentiated effective propagator is left behind. The component of diagram (i)a ((i.b)2) in which the kernel is decorated is exactly cancelled by diagram (iii)a ((iii.b)2). Thus, we are left with a whole set of diagrams, collected together in figure 62, possessing differentiated effective propagators.

Diagram D.38 can be simplified by utilizing the primary diagrammatic identities and the classical flow equation. We illustrate this by considering the un-nested version; identical manipulations can be performed in the nested case.

$$\begin{aligned}
 \circlearrowleft \circlearrowleft \quad \circlearrowleft &= \left[\circlearrowleft \circlearrowleft \quad \circlearrowleft \right]^\bullet - \bullet \circlearrowleft \circlearrowleft - \circlearrowleft \bullet \\
 &= \left[\circlearrowleft \circlearrowleft \quad \circlearrowleft \right]^\bullet - \bullet \circlearrowleft \circlearrowleft - \mathcal{A} \bullet + \mathcal{A} \bullet
 \end{aligned}$$

$$= - \text{hook} \bullet \tag{83}$$

To go from the first line to the second, we have employed diagrammatic identity (A.9) and the effective propagator relation. On the second line, the first term vanishes courtesy of diagrammatic identity (A.7); similarly, the second term, if we employ (A.2). The final term on the second line vanishes on account of diagrammatic identities (A.8) and (A.2):

$$[\triangleright \triangleright]^\bullet = 0 = \overset{\bullet}{\triangleright} \triangleright + \triangleright \overset{\bullet}{\triangleright} = \triangleright \overset{\bullet}{\triangleright} .$$

Thus, the structure in diagram D.38 comprising a classical, two-point vertex, differentiated effective propagator and \triangleright reduces to just a differentiated \triangleright . We now promote the $\overset{\bullet}{\triangleright}$ to an implicit decoration noting that, according to the rules for converting implicit decorations to explicit decorations, this comes with a minus sign (see the discussion around figure 11). Finally, the decorations $\{ \}^{\triangleright m' \overset{\bullet}{\triangleright}}$ can be combined with the overall decorations \triangleright^m . Upon shifting $m \rightarrow m' - 1$ we find that:

Cancellation 11 (Diagram D.21) *Diagram D.38 exactly cancels diagram D.21.*

We now proceed to decorate the classical, two-point vertex of diagram D.37. In the case that we join this vertex to a Wilsonian effective action vertex, we just cancel diagram D.36, up to a gauge remainder. Processing this gauge remainder, we can think of the resultant diagram as versions of D.36 and D.37 but where the end of the differentiated effective propagator which attaches to the two-point vertex now attaches to one of the nested gauge remainders, instead. Thus, this version of diagram D.36 is cancelled also. Up to diagrams with an $O(p^2)$ stub, the only terms that remain are those of the form D.37 (but where the differentiated effective propagator can attach to nested gauge remainders, in addition to the classical, two-point vertex) where the classical, two-point vertex is attached to one of the nested gauge remainders or to a gauge remainder structure. These terms can be combined, courtesy of diagrammatic identity (A.12), to yield the diagrams of figure 63.

It is worth expanding on the origin of diagrams D.39 and D.40 a little further, which is most readily done by returning to (A.12). Essentially, we have combined the following terms:

- (i) a version of the first term in which a differentiated effective propagator attaches at one end to the explicitly drawn \triangleright and at the other end to either the socket decorating the classical, two-point vertex or to one of the implicit decorations;
- (ii) a version of the final term in which a differentiated effective propagator attaches at one end to the explicitly drawn \triangleright and at the other end to either the socket decorating the classical, two-point vertex or to one of the implicit decorations which forms the string of gauge remainders biting this socket.

Clearly, we can re-express these diagrams in terms of:

$$\begin{aligned}
 & -2 \left[\sum_{s=1}^n \sum_{m=1}^{2s-1} \sum_{j=-2}^{n+s-m-3} \sum_{m'=1}^m \frac{\Upsilon_{j+s,j+2}}{(m-m')!(m'+1)!} \right. \\
 & \quad \left[\begin{array}{c} \text{D.39} \\ \circlearrowleft \left\{ \right\}^{> m'+1} \\ \circlearrowleft (\nu^{j+;R}) \\ \circlearrowleft (n_s, j) \end{array} \right] \right. \\
 & \quad \left. \left. \right]^{11\Delta^{j+s+1} > m-m'} \right. \\
 & +2 \left[\sum_{s=1}^n \sum_{m=1}^{2s-1} \sum_{j=-2}^{n+s-m-3} \frac{\Upsilon_{j+s,j+2}}{m!} \sum_{m'=2}^m m C_{m'} \right. \\
 & \quad \left[\begin{array}{c} \text{D.40} \\ \circlearrowleft \left\{ \right\}^{> m''} \\ \circlearrowleft (0^2) \\ \circlearrowleft \left\{ \right\}^{> m'-m''} \\ \circlearrowleft (\nu^{j+;R}) \\ \circlearrowleft (n_s, j) \end{array} \right] \right. \\
 & \quad \left. \left. \right]^{11\Delta^{j+s} > m-m'} \right. \\
 & \quad \left. \left. \sum_{m''=0}^{m'-2} m' C_{m''} \right. \right.
 \end{aligned}$$

Figure 63. The surviving diagrams spawned by the gauge remainders of types (I)b and (I)c, up to those with an $O(p^2)$ stub.

- (i) the second diagram of (A.12) in which a differentiated effective propagator attaches at one end to the full gauge remainder and at the other end to one of the implicit decorations;
- (ii) a version of the final term in which a differentiated effective propagator attaches at one end to the explicitly drawn $>$ and at the other end to the gauge remainder components which decorate the top of the diagram.

Having completed the analysis of the type (I)b and (I)c gauge remainders, we now move on to gauge remainders of type (I)d, which we collect together in figure 64.

Allowing the gauge remainder to act in diagrams D.41 and D.44, we uncover the by now familiar pattern of cancellations. Up to terms with an $O(p^2)$ stub, we are left with:

$$\begin{aligned}
 & 2 \left[\sum_{s=1}^n \sum_{m=1}^{2s-1} \sum_{j=-1}^{n+s-m-3} \frac{\Upsilon_{j+s,j+1}}{m!} \sum_{m'=1}^m m C_{m'} \right] \\
 & \left[\begin{array}{c} \text{D.41} \\ \{ \}^{> m'} \\ \circ \\ \downarrow \\ \text{kernel } \gamma^{j+;R} \\ \text{kernel } (n_s, j) \end{array} \right]^{11\Delta^{j+s} > m-m'} \\
 \\
 & -2 \left[\sum_{s=1}^n \sum_{m=1}^{2s-1} \sum_{j=-2}^{n+s-m-3} \frac{\Upsilon_{j+s,j+2}}{m!} \sum_{m'=1}^m m C_{m'} \right] \\
 & \left[\begin{array}{c} \sum_{m''=1}^{m'-1} m' C_{m''} \\ \text{D.42} \\ \{ \}^{> m'-m''} \\ \circ \\ \downarrow \\ \{ \}^{> m''} \\ \text{D.43} \\ \{ \}^{> m'} \\ \circ \\ \text{D.44} \\ \{ \}^{> m'} \\ \text{kernel } \gamma^{j+;R} \\ \text{kernel } (n_s, j) \end{array} \right]^{11\Delta^{j+s} > m-m'}
 \end{aligned}$$

Figure 64. Gauge remainders of type (I)d.

- (i) diagram D.43, which we notice combines with diagram D.39;
- (ii) diagrams in which the (nested) gauge remainder of (the nested version of) D.44 strikes:
 - (a) the top end of the kernel;
 - (b) the bottom end of the kernel;
- (iii) diagrams in which the classical, two-point vertex of D.41 and its nested partners is attached to one of the m' gauge remainders, at the top of the diagram.

With a little thought, we see that diagrams of the last item are of the same structure as diagram D.40. Indeed, these diagrams combine, to yield a single term with a full kernel. The resultant term is shown in figure 65, together with the other surviving diagrams spawned by the gauge remainders of type (I)d, up to those with an $O(p^2)$ stub.

We note the following about the diagram of figure 65. First, we should explain the sign of diagram D.47, since the parent diagram comes with a minus sign. Consider

$$\begin{aligned}
 & \left[\sum_{s=0}^n \sum_{m=0}^{2s-1} \sum_{j=-1}^{n+s-m-4} \frac{\Upsilon_{j+s+1, j+1}}{m!} \right]_{11\Delta^{j+s+1} > m} + \left[\sum_{s=1}^n \sum_{m=0}^{2s-3} \sum_{j=-2}^{n+s-m-5} \frac{\Upsilon_{j+s, j+2}}{m!} \right]_{11\Delta^{j+s} > m} \\
 & \left[\begin{array}{c} \text{D.49} \\ \begin{array}{c} \textcircled{\psi^{k;R}} \\ \uparrow \\ \textcircled{\psi^{j+,k;R}} \end{array} \\ \textcircled{n_s, j} \end{array} \right] + \left[\begin{array}{c} \text{D.50} \\ \begin{array}{c} \textcircled{\psi^{j+,R}} \\ \uparrow \\ \textcircled{n_s, j} \end{array} \end{array} \right] \\
 - & \left[\sum_{s=1}^n \sum_{m=0}^{2s-1} \sum_{j=-1}^{n+s-m-3} \frac{\Upsilon_{j+s, j+1}}{m!} \right]_{11\Delta^{j+s} > m} \\
 & \left[\begin{array}{c} \text{D.51} \quad \text{D.52} \\ \begin{array}{c} \textcircled{\psi^{j+,R}} \\ \uparrow \\ \textcircled{n_s, j} \end{array} + 2 \begin{array}{c} \textcircled{\psi^{j+,R}} \\ \uparrow \\ \textcircled{n_s, j} \end{array} \end{array} \right]
 \end{aligned}$$

Figure 66. Gauge remainders of type II, part 1.

Secondly, notice that diagram D.45 is exactly the same as diagram D.18 (the difference between the lower limits on the sums over m and m' is just an artefact of putting diagram D.45 under the same summation signs as diagram D.20—which does exist for $m, m' = 1$), up to a relative factor of -2 . Thus, these two diagrams do not exactly cancel; to find the missing term that completes the cancellation—and also to understand the roles of diagrams D.47–D.48—we must conclude our discussion of the gauge remainders by analysing the gauge remainders of type II, which are collected together in figures 66 and 67.

The first thing to note about the gauge remainders of type II is that we are guaranteed to generate trapped gauge remainders in diagrams D.50 and D.51 (*cf.* figures 12 and 13). In each of these cases, we can choose to act with either gauge remainder first, and one of the things it will do is bite the field on the structure to which the tip of the other gauge remainder is attached. If, on the other hand, the first action of one of the gauge remainders is to bite a socket or the end of a kernel, then we are free to perform the other gauge remainder as well. However, it is inefficient to allow the second gauge remainder to act immediately, as we can identify cancellations prior to this; we employ this strategy with diagrams D.49 and D.52, also. Note, though, that

$$\begin{aligned}
 & -2 \left[\sum_{s=0}^n \sum_{m=2}^{2s-1} \sum_{m'=2}^m \sum_{j=-1}^{n+s-m-3} \frac{\Upsilon_{j+s,j+1}}{m!} \right. \\
 & \quad \left. \begin{array}{c} \text{D.53} \\ \left. \begin{array}{c} \{ \} >^{m'} \\ \circ \\ \downarrow \\ \textcircled{\psi^{j+};R} \\ \textcircled{n_s, j} \end{array} \right] \end{array} \right]^{11\Delta^{j+s} > m-m'} \\
 & + \left[\sum_{s=1}^n \sum_{m=1}^{2s-1} \sum_{j=-2}^{n+s-m-3} \frac{\Upsilon_{j+s,j+2}}{m!} \sum_{m'=1}^m {}^m C_{m'} \right. \\
 & \quad \left. \begin{array}{c} \text{D.54} \quad \text{D.55} \quad \text{D.56} \\ \left. \begin{array}{c} \sum_{m''=1}^{m'-1} {}^{m'} C_{m''} \left[\begin{array}{c} \{ \} >^{m'-m''} \\ \circ \\ \downarrow \\ \{ \} >^{m''} \end{array} \right] + \left[\begin{array}{c} \{ \} >^{m'} \\ \circ \\ \downarrow \\ \textcircled{\psi^{j+};R} \\ \textcircled{n_s, j} \end{array} \right] + 2 \left[\begin{array}{c} \bullet \\ \downarrow \\ \{ \} >^{m'} \end{array} \right] \end{array} \right] \end{array} \right]^{11\Delta^{j+s} > m-m'}
 \end{aligned}$$

Figure 67. Gauge remainders of type II, part 2.

diagram D.52 is not symmetrical with respect to the action of its two gauge remainders; the most efficient way to proceed is to be diplomatic: we take one instance of this diagram where one gauge remainder acts first and one instance where the other acts first, dividing by two to avoid over-counting.

Amongst the diagrams generated by processing one of the gauge remainders of diagrams D.49–D.52 are versions of the parents, nested with respect to the gauge remainder which acted. The strategy for dealing with these terms is to process only the nested gauge remainder, for the time being.

We delay processing diagrams D.53 and D.56, which have only a single active gauge remainder, until after one of the gauge remainders in each of diagrams D.49 and D.52, and their nested partners, has acted. It is easy to see why we do this. Consider the component of diagram D.49, and its nested partners, in which a classical, two-point vertex, created by the action of one of the gauge remainders, is joined to either a nested gauge remainder or a gauge remainder structure. This diagram partially cancels D.53, courtesy of diagrammatic identity (A.12) and without the need to process any further

gauge remainders. Similarly, we process the gauge remainders of diagram D.52 according to the strategy outlined above, and diagram D.56 is also partially cancelled. Treating the partially cancelled diagrams together (and using also diagram D.54), it is evident that diagrams in which the active gauge remainder strikes a socket cancel in the usual way. Up to $O(p^2)$ terms, the only survivors from this chain of cancellations are the partially cancelled components of

- (i) diagram D.53 and its nested partners in which a classical, two-point vertex, created by the action of the gauge remainder, is attached to the explicitly specified gauge remainder structure;
- (ii) diagram D.56 and its nested partners in which the active gauge remainder strikes either end of the kernel.

Returning to diagrams D.50 and D.52 and their nested partners, if the first gauge remainder strikes the end of a kernel, we then have no choice but to go ahead and process the second gauge remainder. Diagrams in which this second gauge remainder strikes a socket, combined with diagrams of item ii, above, cancel, in the usual manner.

Thus, up to diagrams with an $O(p^2)$ stub, all surviving terms possess either a trapped gauge remainder, or a kernel which is bitten at one or both of its ends or a classical, two-point vertex attached to an explicitly specified gauge remainder structure (*i.e.* i, above).

The terms with a trapped gauge remainder, which are collected together in figure B2, can be simplified. Notice that the trapped gauge remainder diagrams spawned by D.51 (see diagrams D.104 and D.105) are very similar to diagrams D.36 and D.37. (There is no analogue of diagram D.38: if one of the gauge remainders of diagram D.51 were to strike a socket on a classical, two-point vertex then this vertex would be killed by the other gauge remainder, courtesy of diagrammatic identity (A.7).) The essential difference is the decoration of the kernel and the trapped gauge remainder. Now, we know that diagrams D.36 and D.37 can be processed to yield diagrams D.39 and D.40. Clearly, processing the diagrams with trapped gauge remainders will generate analogues of these diagrams, but with the differentiated effective propagator replaced by a decorated kernel, ending in a trapped gauge remainder. Noting that the overall factor of these diagrams is half of diagrams D.39 and D.40 we see that both the diagrams corresponding to item i, above, and diagram D.55 are exactly cancelled.

However, there are some new diagrams left over as a consequence of the kernel admitting decorations. First, the classical, two-point vertex of diagram D.105, can be attached to the kernel. The corresponding primary part is simply cancelled by diagram D.106. The secondary part yields a version of diagram D.106 with an active gauge remainder inserted between the end of the vertical line emanating from the trapped gauge remainder and the kernel. If this gauge remainder strikes a socket, then we can think of the resulting diagram as a version of diagram D.106 but where the trapped gauge remainder is contracted into the gauge remainder which bites the kernel, rather than the kernel itself. This diagram is cancelled by a term generated in the

following way. Attach the classical, two-point vertex of diagram D.105 to a vertex and apply the effective propagator relation. Focusing on the gauge remainder part, allow the gauge remainder to act and attach the resulting classical, two-point vertex to the kernel. The primary part yields the term we require for our cancellation. Iterating the diagrammatic procedure, the only terms that survive are those in which an active gauge remainder bites one of the ends of the kernel (or which possess an $O(p^2)$ stub).

We collect together all surviving diagrams spawned by the gauge remainders of type (I)d, up to those with an $O(p^2)$ stub, in figure 68.

The sign of diagram D.58 requires comment. This diagram is formed from diagram D.50 and its nested partners; however, we can understand the sign from the un-nested term, alone. In this case, the gauge remainder structure is formed as follows. The first gauge remainder bites the end of the kernel, just above the second (active) gauge remainder. This active gauge remainder then bites the kernel at the end to which the $>$ corresponding to the first gauge remainder attaches. The point is that each of the gauge remainders bites the end of a kernel and so, for this pair of gauge remainders—which form part of the same gauge remainder structure—bites to the left (right) must be interpreted as pulls back (pushes forward). Thus, the sign of the diagram is given by $(-1)^{R-2}$. Promoting these gauge remainders to an explicitly specified structure, $\{ \}^{>2}$, we see from the discussion around figure 11 that we must compensate with minus sign. For *e.g.* diagram D.57 there is no such sign, since the gauge remainders of diagram D.50 and its nested partners have formed separate structures.

Finally, we comment on diagram D.63. The loose end of the kernel can attach to any of the $m' >$ s or to the socket on the classical, two-point vertex. The primary part of the component of the diagram in which the loose end of the kernel attaches to the socket is spawned by diagram D.50 and its nested partners. Indeed, the $m' = 1$ case corresponds to the illustrative diagram I.25 of figure 15. The corresponding secondary part is spawned by a version of diagram D.106 with a (nested) gauge remainder inserted between the end of the vertical line emanating from the trapped gauge remainder and the kernel. Both the primary and secondary parts of the component of diagram D.63 in which the loose end of the kernel attaches to a gauge remainder are spawned by diagram D.52 and its nested partners.

Cancellation 12 (Diagram D.19) *Diagram D.58 exactly cancels diagram D.19.*

Cancellation 13 (Diagram D.18) *Diagrams D.57 and D.45 exactly cancel diagram D.18.*

Finally, we conclude our treatment of the gauge remainders with the following elaborate cancellation.

Cancellation 14 (Diagram D.46) *Diagrams D.47 and D.48 combine with diagrams D.60 and D.62, reversing their signs. The resultant diagrams, when combined with diagrams D.61 and D.63, can be redrawn, courtesy of diagrammatic identity (A.12), to*

yield an exact copy of diagram D.59. Thus the overall factor of diagram D.59 is doubled, providing precisely the necessary contribution to exactly cancel diagram D.46.

Referring back to figure 54, we have therefore demonstrated that

$$\left[\mathcal{E}_{n\mu\nu}^{a11}(p)\right]^\bullet + \mathcal{O}(p^4) = -4\beta_n \square_{\mu\nu}(p) + \text{D.1} + \text{D.2} + \dots,$$

where the ellipsis stands for terms with an $\mathcal{O}(p^2)$ stub, to which we now turn.

5.3. Terms with an $\mathcal{O}(p^2)$ Stub

Every time a classical, two-point vertex was generated in the computation of $\left[\mathcal{E}_{n\mu\nu}^{a11}(p)\right]^\bullet$, we had the option of decorating it with an external field. In figures 69 and 70 we collect together the set of terms spawned by a_0 and a_1 which remain after all active gauge remainders have been processed, all cancellations have been identified and all diagrams which manifestly vanish at $\mathcal{O}(p^2)$ have been discarded. The treatment of gauge remainders in diagrams with an $\mathcal{O}(p^2)$ stub is identical to the analysis just performed, and the same patterns of cancellations are observed. Wherever possible, we have combined terms possessing a seed action vertex with their counterparts possessing just Wilsonian effective action vertices by introducing the notation

$$\Pi = S - \hat{S}.$$

Notice, though, that since the terms possessing exclusively Wilsonian effective action vertices necessarily possess a decorated kernel, we are left over with terms possessing a seed action vertex attached to a differentiated effective propagator.

Before processing diagrams D.64–D.72, we emphasise a very important observation. Consider the set of diagrams obtained by promoting the explicitly drawn external field to an implicit decoration. This set of diagrams is, of course, nothing other than the complete set of terms generated by $\left[\mathcal{E}_{n\mu\nu}^{a11}(p)\right]^\bullet$ which possess a single, classical, two-point vertex (with a free socket) *after* all gauge remainders have acted. We can use this to immediately deduce the set of diagrams left over after taking $\left[\mathcal{E}_{n\mu\nu}^{b11}(p)\right]^\bullet$ (see figure 46) and iterating the diagrammatic procedure until exhaustion. First, there will be the α and β terms. Secondly, there will be diagrams in which $-\Lambda\partial_\Lambda|_\alpha$ strikes either one of the \star s or one of the elements of a string of $>$ s. Finally, there are those diagrams arising from attaching all classical, two-point vertices generated at each stage of the calculation either to a \star or to one of the elements of a string of $>$ s. In the case that there is just a single, classical, two-point vertex to play with, the resulting set of diagrams can be directly deduced from diagrams D.64–D.72. In the case that there are two classical, two-point vertices to play with, the resultant diagrams will arise from an analogue of diagram D.10. (Note that the two classical, two-point vertices must be attached to elements of the same structure comprising a single \star plus string of $>$ s plus vertices plus $>$ s, as follows from section 4.1.2.)

$$\begin{aligned}
 & \left[\sum_{s=1}^n \sum_{m=0}^{2s} \sum_{j=-1}^{n+s-m-2} \frac{\Upsilon_{j+s+1, j+1}}{m!} \right] \\
 & \left[\begin{array}{c} \text{D.64} \quad \text{D.65} \\ \begin{array}{c} \textcircled{\hat{\nu}^{j+;R}} \\ \circ \\ \textcircled{0^2} \\ \text{~} \end{array} \quad - \quad \begin{array}{c} \textcircled{\Pi^{j+;R}} \\ \circ \\ \textcircled{0^2} \\ \text{~} \end{array} \\ \textcircled{n_s, j} \end{array} \right]^{1\Delta^{j+s+1} > m} \\
 + \\
 & \left[\sum_{s=1}^n \sum_{m=0}^{2s-2} \sum_{j=-2}^{n+s-m-4} \frac{\Upsilon_{j+s+1, j+2}}{m!} \right] \\
 & \left[\begin{array}{c} \text{D.66} \\ \begin{array}{c} \bullet \\ \textcircled{0^2} \\ \text{~} \end{array} \\ \textcircled{\nu^{j+;R}} \\ \textcircled{n_s, j} \end{array} \right]^{1\Delta^{j+s+1} > m}
 \end{aligned}$$

Figure 69. $O(p^2)$ terms generated by $[\mathcal{E}_{n\mu\nu}^{a11}(p)]^\bullet$, part 1.

Diagram D.64 is simple to deal with. First, notice that the differentiated effective propagator must be in the A^1 sector (which, incidentally, means that the seed action vertex, to which it attaches at one end, cannot be a one-point vertex). Now we redraw this diagram by detaching the differentiated effective propagator from the seed action vertex and decorating the seed action vertex with an A^1 which carries the same index as the loose end of the effective propagator, say α . Next, we decorate the diagram with the remaining external field, which we suppose carries index ν . Putting the $O(p^2)$ stub and differentiated effective propagator to one side, consider contracting the remaining part of the diagram with $(-p)_\nu p_\alpha$. It is straightforward to demonstrate that the final outcome is zero. Therefore, by Lorentz invariance, the diagram to which the $O(p^2)$ stub attaches via the differentiated effective propagator is transverse in p and, just like $\mathcal{E}_{n\mu\nu}^{a11}(p)$, in fact goes as $\square_{\mu\nu}(p) + O(p^4)$. Consequently, diagram D.64 as a whole is $O(p^4)$ and so does not contribute to $[\mathcal{E}_{n\mu\nu}^{a11}(p)]^\bullet$ at $O(p^2)$.

$$\begin{aligned}
 & \left[\sum_{s=1}^n \sum_{m=0}^{2s-1} \sum_{j=-1}^{n+s-m-3} \frac{\Upsilon_{j+s+1,j+1}}{m!} \sum_{m'=0}^m {}^m C_{m'} \right] \\
 & \left[\begin{array}{c} \text{D.67} \quad \text{D.68} \\ \begin{array}{c} \textcircled{\hat{\nu}^{j+;R}} \\ \downarrow \ominus \\ \{ \}^{> m'} \\ \textcircled{0^2} \end{array} \quad - \quad \begin{array}{c} \textcircled{\Pi^{j+;R}} \\ \downarrow \circ \\ \{ \}^{> m'} \\ \textcircled{0^2} \end{array} \\ \textcircled{n_s, j} \end{array} \right] \Big|_{1\Delta^{j+s+1} > m-m'} \\
 & + \left[\sum_{m'=0}^m {}^m C_{m'} \right] \left[\begin{array}{c} \text{D.69} \quad \text{D.70} \quad \text{D.71} \\ \begin{array}{c} \bullet \\ \downarrow \\ \{ \}^{> m'} \\ \textcircled{0^2} \end{array} \quad - \quad \begin{array}{c} \circ \\ \downarrow \\ \{ \}^{> m'} \\ \textcircled{0^2} \end{array} \quad + \quad 2 \quad \begin{array}{c} \circ \\ \downarrow \\ \{ \}^{> m'} \\ \textcircled{0^2} \end{array} \\ \textcircled{\nu^{j+;R}} \quad \textcircled{n_s, j} \end{array} \right] \Big|_{1\Delta^{j+s+1} > m-m'} \\
 & - 2 \left[\sum_{m'=2}^m {}^m C_{m'} \sum_{m''=2}^{m'} {}^{m'} C_{m''} \right] \left[\begin{array}{c} \text{D.72} \\ \{ \}^{> m''} \\ \downarrow \ominus \\ \{ \}^{> m'-m''} \\ \textcircled{0^2} \\ \textcircled{\nu^{j+;R}} \quad \textcircled{n_s, j} \end{array} \right] \Big|_{1\Delta^{j+s+1} > m-m'}
 \end{aligned}$$

Figure 70. $O(p^2)$ terms generated by $[\mathcal{E}_{\mu\nu}^{a11}(p)]^\bullet$, part 2.

To process diagrams D.65–D.71 we construct subtractions. We begin with diagram D.66 for which, as we know from section 3.3.2, the subtractions completely kill the parents. This leaves behind only the additions, which are collected together in figure 71.

The first thing to notice about the diagrams of figure 71 is that they are very similar to the diagrams of figure 47 (which we recall arose from considering $[\bar{\mathcal{E}}_{n\mu\nu}^{c11}(p)]_{p^2}$). Consequently, they will be very easy to manipulate. The differences are essentially three-fold. First, we must be careful to properly take account of the effects of $[\]_{p^2}$, since it does not necessarily apply to all elements of a fully fleshed out diagram. Consider first the non-factorizable components of diagrams D.73–D.75. In this case, the socket of each diagram is filled by the external field; there can be no effective propagators carrying just p and all diagrammatic elements can be brought under the influence of $[\]_{p^2}$. In other words, each of the additions can be thought of as arising from Taylor expanding the corresponding components of the parent diagram to $O(p^2)$. In the factorizable case, however, p dependence comes not only from the $O(p^2)$ stub, but also from the effective propagators carrying just p and the sub-diagrams to which they attach. These sub-diagrams may possess components which are not Taylor expandable in p and so we leave them alone. Only those diagrammatic components which are not part of a p dependent sub-diagrams can be brought under the influence of $[\]_{p^2}$, in this case.

The second difference between the diagrams of figures 47 and 71 is that the latter diagrams do not possess a string of gauge remainders decorating their classical, two-point vertex decorated by the external field. This makes life easier and means that we will never generate the analogue of the diagrams of figure 51. The third difference, however, makes our life slightly harder: the presence of a kernel in the diagrams of figure 71 means there is an additional structure to which effective propagators can attach. As usual, this ultimately generates a set of surviving diagrams in which gauge remainders which bite the kernel slide down to its base. Immediately, then, we can deduce the single diagram left over from iterating the diagrammatic procedure until exhaustion, which is shown in figure 72.

What is to be the fate of diagram D.77? As we will demonstrate shortly, it will be exactly cancelled by terms arising from processing

$$[\mathcal{E}_{n\mu\nu}^{b11}(p)]^\bullet - \sum_{n'=1}^{n-1} [\mathcal{E}_{n-n'\mu\rho}^{b11}(p)]^\bullet \Delta_{\rho\sigma}^{11}(p) \mathcal{E}_{n'\sigma\nu}^{a11}(p) \quad (84)$$

(see figure 46 and equation (76)). Before seeing this explicitly, we will deal with the remaining diagrams of figures 69 and 70. First, we deal with diagram D.65, the only term other than D.66 that is completely killed by its subtractions. Inspired by the analysis of D.66, it is obvious that the final result of processing diagram D.65 is the diagram of figure 73.

$$\begin{aligned}
 & 2 \left[\left[\left[\sum_{s=1}^n \sum_{m=0}^{2s-3} \sum_{j=-2}^{n+s-m-5} \frac{\Upsilon_{j+s+1,j+2}}{m!} \right] \right] \right. \\
 & \quad \left. \left[\begin{array}{c} \text{D.73} \\ \text{Diagram: } \textcircled{0^2} \text{ with a loop and a wavy line} \\ \text{Diagram: } \textcircled{\psi^{j+;R}} \\ \text{Diagram: } \textcircled{n_s, j} \end{array} \right] \right]_{p^2} \Big|_{1\Delta^{j+s+1} > m} \\
 & -2 \left[\left[\left[\sum_{s=1}^n \sum_{m=0}^{2s-3} \sum_{j=-1}^{n+s-m-5} \frac{\Upsilon_{j+s+1,j+1}}{m!} \right] \right] \right. \\
 & \quad \left. \left[\begin{array}{c} \text{D.74} \\ \text{Diagram: } \textcircled{0^2} \text{ with a loop and a wavy line} \\ \text{Diagram: } \textcircled{\hat{\psi}^{j+;R}} \\ \text{Diagram: } \textcircled{n_s, j} \end{array} \right] \right]_{p^2} \Big|_{1\Delta^{j+s+1} > m} \\
 & -2 \left[\left[\left[\sum_{s=1}^n \sum_{m=0}^{2s-3} \sum_{j=-2}^{n+s-m-5} \frac{\Upsilon_{j+s+2,j+2}}{m!} \right] \right] \right. \\
 & \quad \left. \left[\begin{array}{c} \text{D.75} \\ \text{Diagram: } \textcircled{0^2} \text{ with a loop and a wavy line} \\ \text{Diagram: } \textcircled{0^2} \text{ with a loop and a wavy line} \\ \text{Diagram: } \textcircled{\psi^{j+;R}} \\ \text{Diagram: } \textcircled{n_s, j} \end{array} \right] \right]_{p^2} \Big|_{1\Delta^{j+s+2} > m} \\
 & + \left[\left[\left[\sum_{s=1}^n \sum_{m=3}^{2s-2} \sum_{j=-2}^{n+s-m-4} \frac{\Upsilon_{j+s+1,j+1}}{m!} \sum_{m'=3}^m m C_{m'} \right] \right] \right. \\
 & \quad \left. \left[\begin{array}{c} \text{D.76} \\ \text{Diagram: } \textcircled{0^2} \text{ with a loop and a wavy line} \\ \text{Diagram: } \textcircled{\psi^{j+;R}} \\ \text{Diagram: } \textcircled{n_s, j} \\ \text{Diagram: } \{ \} \sqcup > m' \end{array} \right] \right]_{p^2} \Big|_{1\Delta^{j+s+1} > m-m'}
 \end{aligned}$$

Figure 71. Additions for diagram D.66.

$$-2 \left[\left[\left[\begin{array}{c} \text{D.77} \\ \text{Diagram: a circle with a dot and a wavy line below it} \end{array} \right]_{p^2} \right]^{\star^r} \left[\begin{array}{c} \text{Diagram: a circle with } v^{j+;R} \\ \text{Diagram: a circle with } n_s, j \end{array} \right]_{1\Delta^{j+s+1-r} > m} \right] \sum_{s=2}^n \sum_{r=1}^{s-1} \sum_{m=0}^{2(s-r)-1} \sum_{j=-2}^{n+s-2r-m-3} \frac{\Upsilon_{j+s+1-r, j+2}}{m!r!}$$

Figure 72. The only diagram left from the full treatment of the additions of figure 71.

$$4 \left[\left[\left[\begin{array}{c} \text{D.78} \\ \text{Diagram: a circle with } \Pi^{j+;R} \\ \text{Diagram: a circle with } 0^2 \text{ and a wavy line below it} \end{array} \right]_{p^2} \right]^{\star^r} \left[\begin{array}{c} \text{Diagram: a circle with } n_s, j \end{array} \right]_{1\Delta^{j+s+1-r} > m} \right] \sum_{s=2}^n \sum_{r=1}^{s-1} \sum_{m=0}^{2(s-r)-1} \sum_{j=-2}^{n+s-2r-m-3} \frac{\Upsilon_{j+s+1-r, j+1}}{m!r!}$$

Figure 73. The final result of processing diagram D.65.

We must now bite the bullet and deal with those diagrams which are not completely cancelled by their subtractions, starting with diagram D.69—whose subtractions and additions are collected together in figure 74.

We proceed as before by isolating the classical, two-point component of the differentiated vertex of diagram D.82, decorating it with two effective propagators and utilizing (54). However, compared to the treatment of diagram D.66, we will encounter four novelties, all associated with the $m' >$ s which bite the classical, two-point vertex decorated by an external field. First, the active gauge remainders associated with (54) can be contracted into one of these $m' >$ s or the socket which they bite. Secondly, classical two-point vertices generated by the action of (arbitrarily) nested gauge remainders can be similarly attached. Thirdly, we can no longer exactly combine terms into total momentum derivatives since, at this stage of the calculation, those terms involving momentum derivatives of any of the $m' >$ s or the $>$ which bites them are missing. However, it proves convenient to express the sum of momentum derivative terms that we do have as a total momentum derivative (which we throw away) minus the missing terms. Lastly, we have not yet encountered an analogue of diagram D.86, and so we put this to one side for a moment.

$$\begin{array}{c}
 \mp 2 \\
 \left[\begin{array}{c} \sum_{s=1}^n \sum_{m=0}^{2s-2} \sum_{j=-2}^{n+s-m-4} \frac{\Upsilon_{j+s+1,j+2}}{m!} \sum_{m'=0}^m m C_{m'} \\ \left[\begin{array}{c} \text{D.79} \\ \text{D.80} \\ \text{Diagram: } \left[\begin{array}{c} \bullet \\ \downarrow \\ \{ \} \xrightarrow{m'} \\ \text{O}^2 \end{array} \right] \end{array} \right]_{p^2} \\ \left[\begin{array}{c} \text{Diagram: } \left[\begin{array}{c} \text{O}^{j+;R} \\ \text{O}^{n_s, j} \end{array} \right] \end{array} \right]_{1\Delta^{j+s+1} > m-m'} \end{array} \right]
 \end{array}
 \end{array}$$

$$\begin{array}{c}
 \pm 2 \\
 \left[\begin{array}{c} \sum_{s=1}^n \sum_{m=0}^{2s-1} \sum_{j=-1}^{n+s-m-3} \frac{\Upsilon_{j+s+1,j+1}}{m!} \sum_{m'=0}^m m C_{m'} \\ \left[\begin{array}{c} \text{D.81} \\ \text{D.82} \\ \text{Diagram: } \left[\begin{array}{c} \bullet \\ \downarrow \\ \{ \} \xrightarrow{m'} \\ \text{O}^2 \end{array} \right] \end{array} \right]_{p^2} \\ \left[\begin{array}{c} \text{Diagram: } \left[\begin{array}{c} \text{O}^{j+} \\ \text{O}^{n_s, j} \end{array} \right] \end{array} \right]_{1\Delta^{j+s+1} > m-m'} \end{array} \right]
 \end{array}
 \end{array}$$

$$\begin{array}{c}
 \mp \\
 \left[\begin{array}{c} \sum_{s=1}^n \sum_{m=2}^{2s-1} \sum_{j=-1}^{n+s-m-3} \frac{\Upsilon_{j+s+1,j+2}}{m!} \sum_{m'=2}^m m C_{m'} \sum_{m''=2}^{m'} m' C_{m''} \\ \left[\begin{array}{c} \text{D.83} \\ \text{D.84} \\ \text{Diagram: } \left[\begin{array}{c} \bullet \\ \downarrow \\ \{ \} \xrightarrow{m'-m''} \\ \text{O}^2 \end{array} \right] \end{array} \right]_{p^2} \\ \left[\begin{array}{c} \text{Diagram: } \left[\begin{array}{c} \text{O}^{j+;R} \\ \text{O}^{n_s, j} \end{array} \right] \end{array} \right]_{1\Delta^{j+s+1} > m-m'} \end{array} \right]
 \end{array}
 \end{array}$$

$$\begin{array}{c}
 \mp \\
 \left[\begin{array}{c} \sum_{s=1}^n \sum_{m=1}^{2s-1} \sum_{j=-1}^{n+s-m-3} \frac{\Upsilon_{j+s+1,j+2}}{m!} \sum_{m'=1}^m m C_{m'} \\ \left[\begin{array}{c} \text{D.85} \\ \text{D.86} \\ \text{Diagram: } \left[\begin{array}{c} \bullet \\ \downarrow \\ \{ \} \xrightarrow{m'} \\ \text{O}^2 \end{array} \right] \end{array} \right]_{p^2} \\ \left[\begin{array}{c} \text{Diagram: } \left[\begin{array}{c} \text{O}^{j+;R} \\ \text{O}^{n_s, j} \end{array} \right] \end{array} \right]_{1\Delta^{j+s+1} > m-m'} \end{array} \right]
 \end{array}
 \end{array}$$

Figure 74. Subtractions and additions for diagram D.69.

$$\begin{aligned}
 & +2 \left[\sum_{s=2}^n \sum_{r=1}^{s-1} \sum_{m=0}^{2(s-r)-1} \sum_{j=-2}^{n+s-2r-m-3} \frac{\Upsilon_{j+s+1-r, j+2}}{m!(r-1)!} \sum_{m'=0}^m m C_{m'} \right. \\
 & \left. \left[\left[\begin{array}{c} \text{D.89} \\ \text{Diagram: A loop with a dot, a wavy line, and a curly brace labeled } m' \text{ above it, connected to a circle labeled } 0^2 \text{ with a wavy line below it.} \end{array} \right]_{p^2} \right]^{*r-1} \left[\begin{array}{c} \psi^{j+;R} \\ n_s, j \end{array} \right]^{1\Delta^{j+s+1-r} > m-m'} \right] \\
 & -2 \left[\sum_{s=2}^n \sum_{r=1}^{s-1} \sum_{m=0}^{2(s-r)-1} \sum_{j=-2}^{n+s-2r-m-3} \frac{\Upsilon_{j+s-r, j+1}}{m!(r-1)!} \sum_{m'=0}^m m C_{m'} \sum_{m''=0}^{m'} m' C_{m''} \right. \\
 & \left. \left[\left[\begin{array}{c} \text{D.90} \\ \text{Diagram: A loop with a dot, a wavy line, and a curly brace labeled } m'-m'' \text{ above it, connected to a circle labeled } 0^2 \text{ with a wavy line below it. Above this is another curly brace labeled } m'' \text{ above a circle labeled } 0^2 \text{ with a wavy line below it.} \end{array} \right]_{p^2} \right]^{*r-1} \left[\begin{array}{c} \psi^{j+;R} \\ n_s, j \end{array} \right]^{1\Delta^{j+s-r} > m-m'} \right]
 \end{aligned}$$

Figure 76. The final result of processing diagrams D.80, D.82 and D.84 plus diagram D.77, part 2.

Cancellation 16 (Diagram D.88) *Diagram D.112 exactly cancels diagram D.88.*

Cancellation 17 (Diagram D.86) *Diagrams D.108 and D.110 exactly cancel diagram D.86, courtesy of diagrammatic identity (A.13).*

Cancellation 18 (Diagrams D.89 and D.90) *Diagrams D.113 and D.111 exactly cancel diagrams D.89 and D.90, courtesy of diagrammatic identity (A.14).*

This completes the analysis of the additions of diagram D.69. Note that the only diagrams remaining in which a kernel bites its own tail are diagram D.69, itself, and its subtractions. It should therefore not come as a surprise that we can now reduce

$$\left[\mathcal{E}_{n\mu\nu}^{a11}(p) + \mathcal{E}_{n\mu\nu}^{b11}(p) \right]^\bullet - \sum_{n'=1}^{n-1} \left[\mathcal{E}_{n-n'\mu\rho}^{b11}(p) \right]^\bullet \Delta_{\rho\sigma}^{11}(p) \mathcal{E}_{n'\sigma\nu}^{a11}(p) \quad (86)$$

to just α -terms, β -terms and the diagrams of figure 70 and their subtractions. To see this, we must explicitly construct subtractions for diagrams D.67, D.68, D.70, D.71 and D.72, which are shown in figures B5–B10.

Examining these diagrams, and recalling the expressions for the \mathcal{E}^i , we see that we have succeeded in deriving an expression for β_n which has no explicit dependence on either the seed action or the details of the covariantization!

5.4. The α and β Terms

We can simplify the diagrams of figure 78 and do so by starting with the α terms. This is done by using the diagrammatic relationship:

$$\begin{array}{c} \text{---} A \\ | \\ \textcircled{0} \textcircled{\alpha} \\ | \\ \text{---} B \end{array} = - \begin{array}{c} \text{---} A \\ | \\ \textcircled{\alpha} \\ | \\ \text{---} B \end{array} - \frac{1}{2} \begin{array}{c} \text{---} A \\ \triangle \\ \vdots \\ \textcircled{\alpha} \\ \vdots \\ \text{---} B \end{array} - \frac{1}{2} \begin{array}{c} \text{---} A \\ \nabla \\ \vdots \\ \textcircled{\alpha} \\ \vdots \\ \text{---} B \end{array}, \quad (89)$$

where

$$\begin{array}{c} \vdots \\ \textcircled{\alpha} \\ \nabla \end{array} \equiv \begin{array}{c} \downarrow \\ \textcircled{\alpha} \\ \nabla \end{array} - \frac{1}{2} \begin{array}{c} \uparrow \\ \textcircled{\alpha} \\ \nabla \end{array}$$

(and we recall that $\textcircled{\alpha} \equiv \partial/\partial\alpha$). Comparing (89) with (54) it is clear that the analysis of the α terms is very similar to the analysis of diagrams with momentum derivatives. Indeed, it is straightforward to show that the α terms yield a contribution to $-4\beta_n \square_{\mu\nu}(p)$ such that for every appearance of $[X_n]^\bullet$, there is a partner term which can be generated by making the substitution

$$[X_n]^\bullet \rightarrow - \sum_{n'=1}^{n-1} \gamma_{n'} \frac{\partial}{\partial\alpha} X_{n-n'}.$$

Equivalently, we can explicitly include the α -terms in (88) by inserting $\sum_n g^{2n+1}$ at the beginning of both sides of the equation and then making the replacement

$$-\Lambda \partial_\Lambda |_\alpha \rightarrow -\Lambda \partial_\Lambda. \quad (90)$$

The β terms are more subtle than one might expect. Let us begin with diagram D.91. Clearly, the way to proceed is to isolate any diagrams which possess a classical, two-point vertex and then decorate this vertex. There are two possible decorations: either we can attach one external field and one effective propagator, or we can attach two effective propagators; either way, we can apply the effective propagator relation. In the former case, the primary part simply yields

$$-4 \sum_{n'=1}^{n-1} \beta_{n'} \mathcal{E}_{n-n'\mu\nu}^{a11}(p). \quad (91)$$

The secondary part vanishes, since the associated gauge remainder strikes \mathcal{E}^a , which we know to be transverse. With this in mind, we re-express diagram D.91 in figure 79.

We can now see that there are some novelties associated with the β terms. First, diagram D.96 does not have a canonical normalization factor: there are $j + 2$ identical vertices, but the normalization factor $\sim 1/(j + 1)!$. Secondly, the presence of the

$$\begin{aligned}
 & -4 \sum_{n'=1}^{n-1} \beta_{n'} \mathcal{E}_{n-n'}^{a \ 11}(p) \\
 & +4 \left[\sum_{n'=1}^{n-1} \sum_{s=1}^{n-n'} \sum_{m=0}^{2s} \sum_{j=-1}^{n-n'+s-m-2} \frac{\Upsilon_{j+s+1, j+1}}{m!} \beta_{n'} \right. \\
 & \left. \left(\begin{array}{cc} \text{D.95} & \text{D.96} \\ v^{j+} & - \quad 1 \end{array} \right) \left[\begin{array}{c} \textcircled{v^{j+}; R} \\ \textcircled{n_{n'+s}, j} \end{array} \right] \right]^{11\Delta^{j+s+1} > m} \\
 & -2 \left[\sum_{n'=1}^{n-1} \sum_{s=1}^{n-n'} \sum_{m=0}^{2s} \sum_{j=-2}^{n-n'+s-m-2} \frac{\Upsilon_{j+s, j+2}}{m!} \beta_{n'} \right. \\
 & \left. \left[\begin{array}{cc} \text{D.97} & \text{D.98} \\ \downarrow & \downarrow \\ \textcircled{v^{j+}; R} \\ \textcircled{n_{n'+s}, j} \end{array} \right] \right]^{11\Delta^{j+s} > m}
 \end{aligned}$$

Figure 79. A re-expression of diagram D.91.

multiplicative factor v^{j+} in diagram D.95 makes this term different from any we have encountered so far. Note, though, that the combinatoric factor is effectively canonical, since the factor of v^{j+} singles out one of the vertices, leaving behind only $j + 1$ identical vertices. Thirdly, just as diagram D.95 has a special vertex, so diagram D.97 has a special effective propagator. This effective propagator cannot be promoted to an implicit decoration in the usual way, since then the combinatorics will be wrong. To put it another way, if we decorate a vertex with a total of $q + 1$ effective propagators, comprising the special one and q others, the combinatoric factor associated with choosing the effective propagators in this way will be $j^{+s}C_q$ and *not* $j^{+s+1}C_q$.

Nevertheless, diagrams D.95, D.96 and D.97 combine in a miraculous way. Starting with diagram D.95, we exploit the indistinguishability of the $j + 2$ vertices by replacing v^{j+} with

$$\frac{1}{j+2} \left[\sum_{i=0}^j v^{i, i+} + v^{j+} \right] = \frac{n_{n'} - s}{j+2},$$

where we have used (59) (but with $v^0 = n_{n'} - s$).

Next, consider creating some fully fleshed out diagram from D.97. The total of $j + s + 1$ effective propagators are to be divided into q sets, each containing L_i effective propagators. Since the special effective propagator can reside in any of these sets, there are q different ways to make the sets. The overall combinatoric factor associated with this partitioning is, therefore,

$$\frac{(j + s)!}{\prod_i L_i!} \sum_i L_i = \frac{(j + s + 1)!}{\prod_i L_i!},$$

which is just the combinatoric factor expected from partitioning $j + s + 1$ effective propagators into q sets. Therefore, we can now promote the special effective propagator of diagram D.97 to an implicit decorations but, counterintuitively, the combinatoric factor of the diagram, $\Upsilon_{j+s,j+2}$, *stays the same!*

With these points in mind, it is a trivial matter to show that

$$\text{D.95} + \text{D.96} + \text{D.97} = -2 \sum_{n'=1}^{n-1} \beta_{n'} (n_{n'} - 1) \mathcal{E}_{n-n'\mu\nu}^{a,11}(p) \tag{92}$$

Diagram D.98 can be processed, yielding:

$$-2 \sum_{n'=1}^{n-1} \beta_{n'} \mathcal{E}_{n-n'\mu\nu}^{c,11}(p) \tag{93}$$

Putting together (91), (92) and (93), diagram D.91 ultimately reduces to

$$-2 \sum_{n'=1}^{n-1} \beta_{n'} \left[(n_{n'} + 1) \mathcal{E}_{n-n'\mu\nu}^{a,11}(p) + \mathcal{E}_{n-n'\mu\nu}^{c,11}(p) \right]. \tag{94}$$

The treatment of diagram D.93 follows in similar fashion. Now, however, our options for decorating the classical, two-point vertex are to attach either two effective propagators or one effective propagator and one \star (it is illegal to attach two \star s—see section 4.1.2). In the latter case we proceed by expressing

$$\text{---} \bigcirc^{0^2} \text{---} \begin{array}{c} \diagup \\ \diagdown \end{array} \begin{array}{c} \star \\ \star \end{array} \text{---} = \frac{1}{2} \left[\text{---} \begin{array}{c} \diagup \\ \diagdown \end{array} \begin{array}{c} \star \\ \star \end{array} \text{---} - \begin{array}{c} \star \\ \star \end{array} \begin{array}{c} \diagup \\ \diagdown \end{array} \text{---} + \text{---} \begin{array}{c} \star \\ \star \end{array} \begin{array}{c} \circlearrowleft \\ \circlearrowright \end{array} - \text{---} \begin{array}{c} \star \\ \star \end{array} \begin{array}{c} \circlearrowright \\ \circlearrowleft \end{array} \right].$$

In this way, we can reduce diagram D.93 to

$$\sum_{n'=1}^{n-1} \beta_{n'} \left[2\mathcal{E}_{n-n'\mu\nu}^{c',11}(p) - (2n_{n'} + 1) \mathcal{E}_{n-n'\mu\nu}^{b,11}(p) + 2\tilde{\mathcal{E}}_{n-n'\mu\nu}^{b,11}(p) \right], \tag{95}$$

where

$$\tilde{\mathcal{E}}_{n\mu\nu}^{b,11}(p) \equiv \left[\begin{array}{c} 4 \sum_{s=1}^n \sum_{r=1}^s \sum_{m=0}^{2(s-r)+1} \sum_{j=-2}^{n+s-2r-m-1} \frac{\Upsilon_{j+s+2-r,j+2}}{m!(r-1)!} \\ \left[\begin{array}{c} \bigcirc^{0^2} \\ \text{---} \\ \bigcirc^{j+;R} \\ \text{---} \\ \bigcirc^{n_s, j} \end{array} \right]_{p^2} \end{array} \right]^{1\Delta^{j+s+2-r} \star^r > m}$$

Notice that the $r = 1$ contribution is the same as for $\mathcal{E}_{n\mu\nu}^{b11}(p)$.

By combining (88) with (94,95) and utilizing (90) we can write down the complete expression for β_n :

$$\begin{aligned}
 & -4 \sum_n g^{2n+1} \beta_n \square_{\mu\nu}(p) + \mathcal{O}(p^4) = \\
 & \qquad \sum_n g^{2n+1} \\
 & \left[\begin{aligned}
 & -\Lambda \partial_\Lambda \left[\mathcal{D}_{n\mu\nu}^{a11}(p) + \mathcal{D}_{n\mu\nu}^{b11}(p) \right] \\
 & -2 \sum_{n'=1}^{n-1} \beta_{n'} \\
 & \quad \times \left\{ \begin{aligned}
 & (n_{n'} + 1) \mathcal{D}_{n-n'\mu\nu}^a(p) + \mathcal{D}_{n-n'\mu\nu}^c(p) - \overline{\mathcal{D}}_{n-n'\mu\nu}^c(p) \Big|_{p^2} \\
 & + (n_{n'} + 1) \mathcal{D}_{n-n'\mu\nu}^b(p) - \tilde{\mathcal{D}}_{n-n'\mu\nu}^b(p)
 \end{aligned} \right\} \\
 & + \sum_{n'=1}^{n-1} \left[\mathcal{D}_{n'\mu\rho}^a(p) + \overline{\mathcal{D}}_{n'\mu\rho}^c(p) \Big|_{\mathcal{T}_M(p)} \right] \Delta_{\rho\sigma}^{11}(p) \\
 & \quad \times \left\{ \begin{aligned}
 & \Lambda \partial_\Lambda \left[\mathcal{D}_{n-n'\sigma\nu}^b(p) \right] \\
 & -2 \sum_{n''=1}^{n'-1} \beta_{n''} \left[\begin{aligned}
 & \overline{\mathcal{D}}_{n-n'-n''\sigma\nu}^c(p) \Big|_{p^2} \\
 & -(n_{n'}+n''+1) \mathcal{D}_{n-n'-n''\sigma\nu}^b(p) \\
 & + \tilde{\mathcal{D}}_{n-n'-n''\sigma\nu}^b(p)
 \end{aligned} \right]
 \end{aligned} \right\} \\
 & - \sum_{n'=1}^{n-1} \sum_{n''=1}^{n'-1} \overline{\mathcal{D}}_{n'\mu\rho}^c(p) \Big|_{\mathcal{T}_M(p)} \Delta_{\rho\tau}^{11}(p) \mathcal{D}_{n''\tau\kappa}^a(p) \Delta_{\kappa\sigma}^{11}(p) \\
 & \quad \times \left\{ \begin{aligned}
 & \Lambda \partial_\Lambda \left[\mathcal{D}_{n-n'-n''\sigma\nu}^b(p) \right] \\
 & -2 \sum_{n'''=1}^{n''-1} \beta_{n'''} \left[\begin{aligned}
 & \overline{\mathcal{D}}_{n-n'-n''-n'''\sigma\nu}^c(p) \Big|_{p^2} \\
 & -(n_{n'}+n''+n'''+1) \mathcal{D}_{n-n'-n''\sigma\nu}^b(p) \\
 & + \tilde{\mathcal{D}}_{n-n'-n''\sigma\nu}^b(p)
 \end{aligned} \right]
 \end{aligned} \right\}
 \end{aligned} \right] \tag{96}
 \end{aligned}$$

Notice that we have substituted for $\mathcal{E}^{c'}$ via (82) and have traded the \mathcal{E}^i for the \mathcal{D}^i , as this is the correct time to discard all diagrams which vanish at $\mathcal{O}(p^2)$ and / or contain a Wilsonian effective action one-point vertex.

Up until now, we have been very careful not to Taylor expand individual diagrams to $\mathcal{O}(p^2)$ unless we are certain that this step is valid. However, we know that the *sum* of diagrams contributing to β_n is Taylor expandable to $\mathcal{O}(p^2)$. It must therefore be the case that all contributions which include non-polynomial dependence on p , at $\mathcal{O}(p^2)$, cancel out of (96). At two loops it has already been demonstrated that a subset of such contributions cancel out diagrammatically [50, 51]. It is very likely that this analysis can be extended to any number of loops, but we leave the investigation of this for the future. In the meantime, we note that we can considerably simplify (96) if we focus just

on the $O(p^2)$ component of each diagram, which yields the following equation (we have used (79)).

$$\begin{aligned}
 & -4 \sum_n g^{2n+1} \beta_n \square_{\mu\nu}(p) + O(p^4) = \\
 & \sum_n g^{2n+1} \left[\begin{aligned}
 & -\Lambda \partial_\Lambda \left[\mathcal{D}_{n\mu\nu}^{a11}(p) + \mathcal{D}_{n\mu\nu}^{b11}(p) \right] + \sum_{n'=1}^{n-1} \mathcal{D}_{n'\mu\rho}^{a11}(p) \Delta_{\rho\sigma}^{11}(p) \Lambda \partial_\Lambda \left[\mathcal{D}_{n-n'\sigma\nu}^{b11}(p) \right] \\
 & - 2 \sum_{n'=1}^{n-1} \beta_{n'} \left\{ (n_{n'} + 1) \left[\mathcal{D}_{n-n'\mu\nu}^{a11}(p) + \mathcal{D}_{n-n'\mu\nu}^{b11}(p) \right] - \tilde{\mathcal{D}}_{n-n'\mu\nu}^{b11}(p) \right. \\
 & \left. + \sum_{n''=1}^{n'-1} \mathcal{D}_{n''\mu\rho}^{a11}(p) \Delta_{\rho\sigma}^{11}(p) \left[\tilde{\mathcal{D}}_{n-n'-n''\sigma\nu}^{b11}(p) - (n_{n'} + n'' + 1) \mathcal{D}_{n-n'-n''\sigma\nu}^{b11}(p) \right] \right\} \right]_{p^2}
 \end{aligned} \tag{97}
 \end{aligned}$$

Equation (97) reduces to particularly simple forms at one and two loops:

$$-4\beta_1 \square_{\mu\nu}(p) = \left[\overline{\mathcal{D}}_{1\mu\nu}^{a11}(p) + \overline{\mathcal{D}}_{1\mu\nu}^{b11}(p) \right]_{p^2}^\bullet \tag{98}$$

$$\begin{aligned}
 -4\beta_2 \square_{\mu\nu}(p) &= \left[\overline{\mathcal{D}}_{2\mu\nu}^{a11}(p) + \overline{\mathcal{D}}_{1\mu\rho}^{a11}(p) \Delta_{\rho\sigma}^{11}(p) \overline{\mathcal{D}}_{1\sigma\nu}^{b11}(p) + \overline{\mathcal{D}}_{2\mu\nu}^{b11}(p) \right]_{p^2}^\bullet \\
 &+ \gamma_1 \frac{\partial}{\partial \alpha} \left[\overline{\mathcal{D}}_{1\mu\nu}^{a11}(p) + \overline{\mathcal{D}}_{1\mu\nu}^{b11}(p) \right]_{p^2}, \tag{99}
 \end{aligned}$$

where we have used (29,75) and have defined

$$\overline{\mathcal{D}}_{n\mu\nu}^{b11}(p) \equiv \mathcal{D}_{n\mu\nu}^{b11}(p) + \frac{1}{2} \sum_{n'=1}^{n-1} \mathcal{D}_{n-n'\mu\rho}^{b11}(p) \Delta_{\rho\sigma}^{11}(p) \mathcal{D}_{n'\sigma\nu}^{b11}(p).$$

Equations (98,99) reproduce the results of [49–51], but written in a remarkably compact form.

6. Conclusion

We have constructed a manifestly gauge invariant calculus for $SU(N)$ Yang-Mills, which can be applied at any number of loops. The calculus, which is entirely diagrammatic in nature, has been comprehensively illustrated by demonstrating that the β -function is independent of both the seed action and the details of the covariantization of the cutoff, to all orders in perturbation theory.

The inspiration for this methodology, the first elements of which were developed in [45], is the immense freedom in the construction of ERGs. Given that we specialize not only to those ERGs that are manifestly gauge invariant but to those which also allow convenient renormalization to any loop order, there are still an infinite number with which we can work. The differences between these ERGs amount to non-universal details which need never be exactly specified, instead satisfying general constraints. In the computation of universal quantities, these non-universal details must cancel out; by leaving them unspecified, we are thus guided towards a very constrained calculational

procedure. However, as recognized in [51–53], such cancellations are embedded within the formalism at a particularly deep level: at least some of them occur in the calculation of quantities which are not universal, such as β -function coefficients beyond two loops. This observation formed the basis for developing the diagrammatic calculus to the level described in this paper.

Given a diagrammatic representation of the flow equation, the calculus comprises an operator which implements the flow *i.e.* $-\Lambda\partial_\Lambda$, a rule for implementing the effects of charge conjugation invariance, a set of primary and secondary diagrammatic identities and the subtraction techniques.

There are three types of primary diagrammatic identities (see section 2). Those of the first type make no reference to perturbation theory and reflect general properties of the exact flow equation and underlying theory. The single identity of the second type is the effective propagator relation, which arises as a solution to the classical flow equation, given a convenient choice of seed action we are free to make. The effective propagator relation states that for each classical two-point vertex (which cannot be consistently set to zero) there exists an effective propagator, which is the inverse of this vertex, up to a gauge remainder. The primary diagrammatic identities of the third type follow directly from those of the first and second types; they are stated, nonetheless, due to the central role they play in perturbative calculations.

The secondary diagrammatic identities, of which there are two types, encode the equivalence of distinct diagrammatic representations of structures comprising particular arrangements of components of gauge remainders. Those of the second type (see section 3.2.2) are applied only when we focus on the component of a diagram which has been Taylor expanded to zeroth order in its external momentum (in this paper we have dealt only with diagrams carrying a single external momentum); those of the first type (see section 3.2.1) are more generally applicable.

The final element of the calculus is the subtraction techniques. Working to some order in the external momentum of a diagram, these techniques are used to isolate those components which are of precisely the desired order from those which have an additional, non-polynomial contribution.

A crucial step which facilitates the practical application of the calculus is the notation introduced in section 4.1. As with perturbative methods in general, the number of diagrams contributing to some function grows very rapidly with loop order, n . However, rather than explicitly drawing each of these diagrams, it was realized that we can construct a function of both n and the various diagrammatic *components* which can be used to generate the correct set of diagrams, at any loop order. Such expressions are very compact, with a beautifully intuitive structure.

For the treatment of β_n , we constructed a set of diagrammatic functions $\mathcal{E}_{n\mu\nu}^{a11}(p)$, $\mathcal{E}_{n\mu\nu}^{b11}(p)$ and $\mathcal{E}_{n\mu\nu}^{c11}(p)$ (see section 4.2) which each include two external A_μ^1 s, carrying momenta p_μ and $-p_\nu$. We proceeded by focusing on the $O(p^2)$ components of these diagrammatic functions (up to additional non-polynomial dependence on p) and computed the flow of $\mathcal{E}_{n\mu\nu}^{a11}(p)$. Amongst the terms generated is a single instance of β_n ,

multiplied by a universal coefficient. Of the remaining terms, those involving either lower order β -function coefficients or α -derivatives were put to one side. The remaining diagrams were manipulated, wherever possible, using the following scheme.

The first stage was to isolate any classical, two-point vertices formed by the flow equation and, wherever possible, to attach either an external field or an effective propagator. In the former case, the diagram possesses a manifestly $O(p^2)$ stub; these $O(p^2)$ terms were put to one side. In the latter case, the effective propagator relation was applied. This relation collapses all classical, two-point vertices which are contracted into an effective propagator down into a Kronecker δ and a gauge remainder. The gauge remainders were either be processed using the primary diagrammatic identities or re-expressed using the secondary diagrammatic identities. In the former case, the whole procedure was repeated: classical, two-point vertices were isolated and decorated and the effective propagator relation was applied *etc.* The set of remaining diagrams now cancelled amongst themselves, up to the $O(p^2)$ terms.

To process the $O(p^2)$ terms, the subtraction techniques were employed, allowing the $O(p^2)$ terms to be effectively split into those which have additional non-polynomial dependence on p and those which do not. The latter terms were manipulated using the primary and secondary diagrammatic identities, yielding a set of diagrams which, up to further α and β -terms, were precisely cancelled by (85). The $O(p^2)$ diagrams containing additional, non-polynomial, dependence on p each factorized into an un-manipulable component, $[\mathcal{E}_{n-n'}^c]_{\mathcal{F}_M(p)}$, and an n' -loop component of exactly the same form as (85). This allowed us to immediately write down an expression for β_n which is manifestly independent of the seed action and details of the covariantization. Finally, we neatened the expression up by processing the α and β terms, to yield (96).

This expression was derived with the utmost rigour. In particular, all components carrying non-polynomial dependence on p have been retained, even though it is know that they must cancel out. Indeed, it may well be that these cancellations can be demonstrated diagrammatically (this has already been done to some extent at two loops [50, 51]), which would doubtless serve to considerably illuminate underlying features of (96). If one is prepared to simply accept that these contributions do indeed cancel, then (96) can be simplified by focusing on the strictly $O(p^2)$ components of each diagram. This yields the considerably simpler expression (97).

From (97), the diagrammatic expressions for β_1 and β_2 , (98,99), follow directly. In the context of assessing the practical usability of the calculus, the importance of this can hardly be overstated. Recall that the first time β_2 was computed in our ERG framework [51] the derivation of (99) involved the generation of $O(10^4)$ diagrams (!) at intermediate stages of the calculation, almost all of which cancelled to yield the final diagrammatic expression. Although the number of intermediate diagrams can be hugely reduced using the refinements of [52], the benefits of an expression from which the diagrammatic expression can be read off at any loop order is obvious.

The derivation of the new formula for β_n provides insight into two subtle issues, both of which relate to the regularization. First, although the physical $SU(N)$ gauge

theory is properly regularized, care must be taken with the flow equation. In particular, the flow equation generates (non-universal) diagrams in which the kernel ‘bites its own tail’ which are not properly regularized [42–45, 49] (see the discussion around figure 1). Up until [52], these diagrams were excluded, via an imposed constraint on the covariantization. However, as speculated in [51, 52], all explicit instances such non-universal objects should cancel out in the reduction of β -function coefficients to a form with no explicit dependence on either the seed action or details of the covariantization. This has been borne out here, though it should be emphasised that implicit dependence on these objects remains. It thus seems very likely that, ultimately, a suitable constraint on the covariantization is required.

Nonetheless, it is very interesting that the basic structure of the flow equation is sufficient to formally remove certain non-universal objects to β_n , even if these objects are not strictly well defined. This very much strengthens the case that the diagrammatics is driving us towards a new framework formulated directly in terms of functions such as the \mathcal{E}^i , with the seed action and details of the covariantization of the cutoff operating in the background.

The second issue pertaining to the regularization that the new formula for β_n sheds some light on is that of pre-regularization. Recall that, in order the regularization be properly defined, a pre-regulator must be used in $D = 4$ [41] to unambiguously define contributions which are finite only by virtue of the Pauli-Villars regularization provided by the massive regularizing fields. The pre-regulator amounts to a prescription for discarding otherwise non-vanishing surface terms which can be generated by shifting loop momenta. In this paper, dimensional regularization was used. However, the only place that the pre-regulator is explicitly used in practise is to throw away diagrams such as I.122 which possess a sum of momentum derivative with respect to the loop momenta. Thus, for the purposes of the calculation performed in this paper, we could have adopted the prescription that we simply throw away all diagrams of this form. Of course, the diagrammatic functions contributing to β_n require pre-regularization themselves, as they contain diagrams which are finite only by virtue of the PV regularization. It is not immediately obvious that the new prescription suffices in this case but it will be interesting to see in the future if it can, in fact, be adopted in complete generality, thereby allowing us to work directly in $D = 4$.

Whilst the application of the calculus to β -function coefficients was vital in the development of the formalism, it is very important to ask whether the techniques of this paper can be applied in the computation of other quantities. The most obvious extension is to try to calculate the expectation values of gauge invariant variables in perturbation theory; efforts in this direction are underway [59]. Additionally, we should not lose sight of the fact that the current formulation was originally developed with a view to non-perturbative applications [43, 45]. This is hardly surprising, since the ERG has proven itself to be a flexible and powerful tool for addressing such problems in a range of QFTs [4, 5, 8–11, 14, 15, 19, 26, 28–30, 36, 37, 40, 60–65]; furthermore, an interesting link has been recently made between elements of the formalism presented here and the AdS

/ CFT correspondence [66].

A very interesting question to ask from the perspective of this paper is whether it is possible to repeat the type of cancellations seen in the treatment of β_n in a non-perturbative context. An immediate obstacle to this is that non-perturbative ERG treatments typically rely on truncations (in our case of the Wilsonian effective action), after which universality is lost. However, as stated already, it seems that the diagrammatics are driving us towards a more direct framework for performing calculations in QFTs, whilst retaining the advantages of an ERG approach. If this turns out to be the case, then we can hope that the new framework is defined non-perturbatively. Indeed, consider again the expression (96) for β_n . We could imagine formally lifting the diagrammatic expression on the right-hand side to a non-perturbative expression, such that its weak coupling expansion just reproduces (96).

Of course, even if this action is possible (and we note that the presence of reduced vertices in (96) complicates matters) we stress that it would represent only one step towards extracting non-perturbative information. After all, our hypothetical non-perturbative expression for the β -function would presumably still require truncation before any numbers could be computed. Nonetheless, the starting point would surely be far more appealing with the explicit dependence on the seed action and details of the covariantization removed from the start.

Acknowledgments

I would like to thank Daniel Litim for encouragement and useful discussions. I acknowledge financial support from PPARC.

Appendix A. The Diagrammatic Identities

The Primary Diagrammatic Identities

The First Type

$$\text{Diagram with arrow on top} = \text{Diagram with arrow on left} + \text{Diagram with arrow on right} - \text{Diagram with arrow on bottom-left} - \text{Diagram with arrow on bottom-right} + \dots \text{(A.1)}$$

$$\text{Diagram with dot on top} = 0 \text{ (A.2)}$$

$$\text{Diagram with circle on top} = 0 \text{ (A.3)}$$

$$\text{Diagram with circle S} = 0 \text{ (A.4)}$$

$$\text{Diagram with wavy arrow} = \text{Diagram with wavy arrow and dot} + \text{Diagram with wavy arrow and circle} - \text{Diagram with wavy arrow and dot} - \text{Diagram with wavy arrow and circle} + \dots \text{(A.5)}$$

The Second Type

$$2m(m-1) \{ \text{diagram} \}^{>^{m-2}} = - \{ \text{diagram} \}^{\sqcup >^m}. \quad (\text{A.13})$$

$$\begin{aligned} & \sum_{m'=0}^m \left[\text{diagram}_1 - \text{diagram}_2 \right] \\ & - \sum_{m'=0}^m m' C_{m''} \sum_{m''=0}^{m'} \left[\text{diagram}_3 - \text{diagram}_4 \right] = 0 \quad (\text{A.14}) \end{aligned}$$

Appendix B. Diagrammatic Expressions

Decoration of diagram D.6

$$\begin{aligned}
 & \left[\sum_{s=1}^n \sum_{m=0}^{2s} \sum_{j=-1}^{n+s-m-3} \frac{\Upsilon_{j+s+1,j+1}}{m!} \right]_{11\Delta^{j+s+1}>m} \left[\begin{array}{c} \text{D.99} \\ \begin{array}{c} \textcircled{\psi^{k;R}} \\ | \\ \textcircled{\ominus} \\ | \\ \textcircled{\psi^{j+,k;R}} \end{array} \\ \textcircled{n_s, j} \end{array} \right] - \left[\sum_{s=1}^n \sum_{m=0}^{2s-1} \sum_{j=-1}^{n+s-m-2} \frac{\Upsilon_{j+s,j+1}}{m!} \right]_{11\Delta^{j+s}>m} \left[\begin{array}{c} \text{D.100} \\ \begin{array}{c} \textcircled{\ominus} \\ \textcircled{\psi^{j+;R}} \\ \textcircled{n_s, j} \end{array} \end{array} \right] \\
 & -2 \left[\sum_{s=1}^n \sum_{m=1}^{2s} \sum_{j=-1}^{n+s-m-2} \frac{\Upsilon_{j+s,j+1}}{m!} \sum_{m'=1}^m m C_{m'} \right]_{11\Delta^{j+s}>m-m'} \left[\begin{array}{c} \text{D.101} \\ \begin{array}{c} \{ \} >^{m'} \\ | \\ \textcircled{\ominus} \\ | \\ \textcircled{\psi^{j+;R}} \\ \textcircled{n_s, j} \end{array} \end{array} \right] \\
 & + \left[\sum_{s=1}^n \sum_{m=1}^{2s} \sum_{j=-2}^{n+s-m-2} \frac{\Upsilon_{j+s,j+2}}{m!} \sum_{m'=1}^m m C_{m'} \right]_{11\Delta^{j+s}>m-m'} \left[\begin{array}{c} \text{D.102} \quad \text{D.103} \\ \begin{array}{c} m' C_{m''} \sum_{m''=1}^{m'-1} \left\{ \begin{array}{c} \{ \} >^{m'-m''} \\ | \\ \textcircled{\ominus} \\ | \\ \{ \} >^{m''} \end{array} \right. + \left\{ \begin{array}{c} \cup \\ \textcircled{\ominus} \end{array} \right\} >^{m'} \\ \textcircled{\psi^{j+;R}} \\ \textcircled{n_s, j} \end{array} \right]
 \end{aligned}$$

Figure B1. Decoration of diagram D.6 with the differentiated effective propagator.

Trapped gauge remainders

$$\begin{aligned}
 & - \left[\sum_{s=1}^n \sum_{m=0}^{2s-2} \sum_{j=-1}^{n+s-m-4} \frac{\Upsilon_{j+s,j+1}}{m!} \sum_{m'=0}^m \right. \\
 & \quad \left. \begin{array}{c} \text{D.104} \\ \begin{array}{c} \circ \\ \downarrow \\ \{ \} >^{m'} \\ \circ \\ \psi^{j+;R} \\ \circ \\ (n_s, j) \end{array} \end{array} \right]^{11\Delta^{j+s} > m-m'} \\
 & - \left[\sum_{s=1}^n \sum_{m=0}^{2s-2} \sum_{j=-2}^{n+s-m-4} \frac{\Upsilon_{j+s+1,j+2}}{m!} \sum_{m'=0}^m m C_{m'} \right. \\
 & \quad \left. \begin{array}{c} \text{D.105} \\ \begin{array}{c} \circ \\ \downarrow \\ \{ \} >^{m'} \\ \circ \\ 0^2 \\ \circ \\ \psi^{j+;R} \\ \circ \\ (n_s, j) \end{array} \end{array} \right]^{11\Delta^{j+s+1} > m-m'} \\
 & + \left[\sum_{s=1}^n \sum_{m=0}^{2s-2} \sum_{j=-2}^{n+s-m-4} \frac{\Upsilon_{j+s,j+2}}{m!} \sum_{m'=0}^m m C_{m'} \right. \\
 & \quad \left. \begin{array}{c} \text{D.106} \\ \begin{array}{c} \circ \\ \downarrow \\ \{ \} >^{m'} \\ \bullet \\ \circ \\ \psi^{j+;R} \\ \circ \\ (n_s, j) \end{array} \end{array} \right]^{11\Delta^{j+s} > m-m'}
 \end{aligned}$$

Figure B2. Terms spawned by diagrams D.50 and D.51 which possess a trapped gauge remainder.

Diagrams spawned by (85) in which a kernel bites its own tail

$$\begin{aligned}
 & \left[\sum_{s=2}^n \sum_{r=1}^{s-1} \sum_{m=0}^{2(s-r)-2} \sum_{j=-2}^{n+s-2r-m-3} \frac{\Upsilon_{j+s+2-r, j+2}}{m!(r-1)!} \sum_{m'=0}^m m C_{m'} \sum_{m''=0}^{m'} m' C_{m''} \right] \\
 & \left[\begin{array}{c} \text{D.107} \quad \text{D.108} \\ \left[\begin{array}{c} \text{Diagram D.107} \\ \text{Diagram D.108} \end{array} \right] \star^{r-1} \\ \left[\begin{array}{c} \text{Diagram D.107} \\ \text{Diagram D.108} \end{array} \right] p^2 \end{array} \right] \left[\begin{array}{c} \text{Diagram D.107} \\ \text{Diagram D.108} \end{array} \right] \left[\begin{array}{c} \text{Diagram D.107} \\ \text{Diagram D.108} \end{array} \right] \left[\begin{array}{c} \text{Diagram D.107} \\ \text{Diagram D.108} \end{array} \right] \\
 & \left[\sum_{s=2}^n \sum_{r=1}^{s-1} \sum_{m=0}^{2(s-r)-1} \sum_{j=-2}^{n+s-2r-m-3} \frac{\Upsilon_{j+s+2-r, j+2}}{m!(r-1)!} \sum_{m'=0}^m m C_{m'} \right] \\
 & \left[\begin{array}{c} \text{D.109} \quad \text{D.110} \\ \left[\begin{array}{c} \text{Diagram D.109} \\ \text{Diagram D.110} \end{array} \right] \star^{r-1} \\ \left[\begin{array}{c} \text{Diagram D.109} \\ \text{Diagram D.110} \end{array} \right] p^2 \end{array} \right] \left[\begin{array}{c} \text{Diagram D.109} \\ \text{Diagram D.110} \end{array} \right] \left[\begin{array}{c} \text{Diagram D.109} \\ \text{Diagram D.110} \end{array} \right] \left[\begin{array}{c} \text{Diagram D.109} \\ \text{Diagram D.110} \end{array} \right] \\
 & \left[\sum_{s=2}^n \sum_{r=1}^{s-1} \sum_{m=0}^{2(s-r)-1} \sum_{j=-2}^{n+s-2r-m-3} \frac{\Upsilon_{j+s+1-r, j+2}}{m!(r-1)!} \sum_{m'=0}^m m C_{m'} \sum_{m''=0}^{m'} m' C_{m''} \right] \\
 & \left[\begin{array}{c} \text{D.111} \\ \left[\begin{array}{c} \text{Diagram D.111} \end{array} \right] \star^{r-1} \\ \left[\begin{array}{c} \text{Diagram D.111} \end{array} \right] p^2 \end{array} \right] \left[\begin{array}{c} \text{Diagram D.111} \end{array} \right] \left[\begin{array}{c} \text{Diagram D.111} \end{array} \right] \left[\begin{array}{c} \text{Diagram D.111} \end{array} \right]
 \end{aligned}$$

Figure B3. Diagrams spawned by (85) in which a kernel bites its own tail, part 1.

$$2 \left[\left[\sum_{s=2}^n \sum_{r=1}^{s-1} \sum_{m=0}^{2(s-r)-1} \sum_{j=-2}^{n+s-2r-m-3} \frac{\Upsilon_{j+s+1-r, j+2}}{m!(r-1)!} \sum_{m'=0}^m {}^m C_{m'} \right] \right. \\ \left. \left[\begin{array}{c} \text{D.112} \quad \text{D.113} \\ \begin{array}{c} \text{Diagram 1} \\ \text{Diagram 2} \end{array} \end{array} \right] \right]^{*r-1} \left[\begin{array}{c} \text{Diagram 3} \\ \text{Diagram 4} \end{array} \right] \left. \right]^{1\Delta^{j+s+1-r} > m-m'} \\ \left. \right]_{p^2}$$

Figure B4. Diagrams spanned by (85) in which a kernel bites its own tail, part 2.

Subtractions and Additions

$$\pm 4 \left[\left[\sum_{s=1}^n \sum_{m=0}^{2s-1} \sum_{j=-1}^{n+s-m-2} \frac{\Upsilon_{j+s+1, j+1}}{m!} \sum_{m'=0}^m {}^m C_{m'} \right] \right. \\ \left. \left[\begin{array}{c} \text{D.114} \quad \text{D.116} \\ \text{D.115} \quad \text{D.117} \\ \begin{array}{c} \text{Diagram 1} \\ \text{Diagram 2} \end{array} \end{array} \right] \right]^{1\Delta^{j+s+1} > m-m'} \\ \left. \right]_{p^2} \\ \pm 4 \left[\left[\sum_{s=1}^n \sum_{m=0}^{2s-1} \sum_{j=0}^{n+s-m-3} \frac{\Upsilon_{j+s+2, j+1}}{m!} \sum_{m'=0}^m {}^m C_{m'} \right] \right. \\ \left. \left[\begin{array}{c} \text{D.118} \quad \text{D.120} \\ \text{D.119} \quad \text{D.121} \\ \begin{array}{c} \text{Diagram 1} \\ \text{Diagram 2} \end{array} \end{array} \right] \right]^{1\Delta^{j+s+2} > m-m'} \\ \left. \right]_{p^2}$$

Figure B5. Subtractions and additions for diagrams D.67 and D.68, part 1.

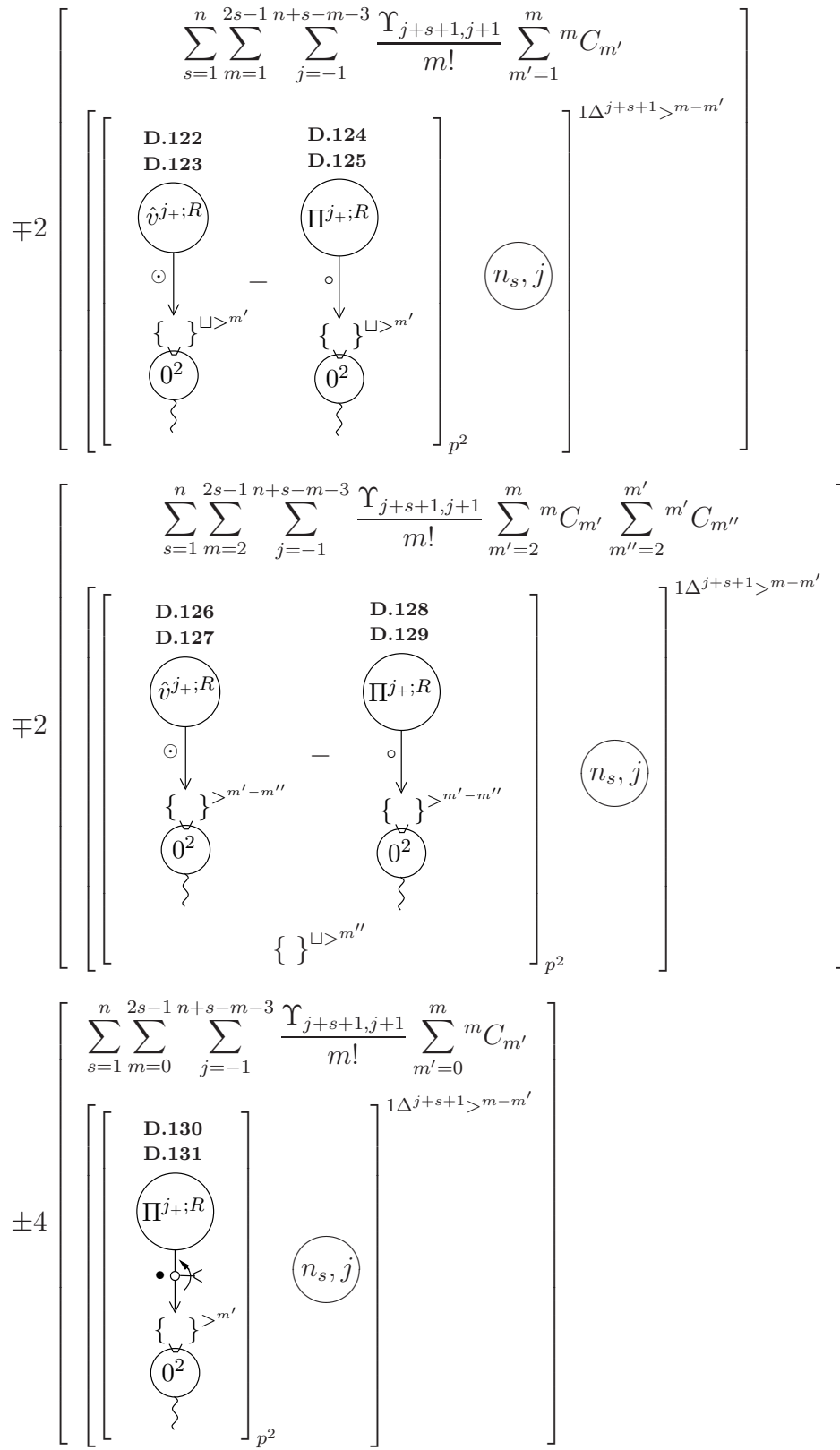


Figure B6. Subtractions and additions for diagrams D.67 and D.68, part 2.

$$\pm \left[\begin{array}{c} \sum_{s=1}^n \sum_{m=2}^{2s-1} \sum_{j=-2}^{n+s-m-3} \frac{\Upsilon_{j+s+1, j+2}}{m!} \sum_{m'=2}^m m C_{m'} \sum_{m''=2}^{m'} m' C_{m''} \\ \left[\begin{array}{c} \text{D.144} \\ \text{D.145} \end{array} \right] \left[\begin{array}{c} \text{D.146} \\ \text{D.147} \end{array} \right] \\ \left[\begin{array}{c} \text{Diagram 1} \\ \text{Diagram 2} \end{array} \right] - 2 \left[\begin{array}{c} \text{Diagram 3} \\ \text{Diagram 4} \end{array} \right] \\ \left[\begin{array}{c} \text{Diagram 5} \\ \text{Diagram 6} \end{array} \right] \\ \left[\begin{array}{c} \text{Diagram 7} \\ \text{Diagram 8} \end{array} \right] \end{array} \right] \begin{array}{l} 1_{\Delta^{j+s+1} > m-m'} \\ p^2 \end{array}$$

Figure B8. Subtractions and additions for diagrams D.70 and D.71, part 2.

$$\mp 4 \left[\begin{array}{c} \sum_{s=1}^n \sum_{m=2}^{2s-1} \sum_{j=-1}^{n+s-m-2} \frac{\Upsilon_{j+s+1, j+1}}{m!} \sum_{m'=2}^m m C_{m'} \sum_{m''=2}^{m'} m' C_{m''} \\ \left[\begin{array}{c} \text{D.148} \\ \text{D.149} \end{array} \right] \\ \left[\begin{array}{c} \text{Diagram 1} \\ \text{Diagram 2} \end{array} \right] \ominus \left[\begin{array}{c} \text{Diagram 3} \\ \text{Diagram 4} \end{array} \right] \\ \left[\begin{array}{c} \text{Diagram 5} \\ \text{Diagram 6} \end{array} \right] \\ \left[\begin{array}{c} \text{Diagram 7} \\ \text{Diagram 8} \end{array} \right] \end{array} \right] \begin{array}{l} 1_{\Delta^{j+s+1} > m-m'} \\ p^2 \end{array}$$

Figure B9. Subtractions and additions for diagram D.72, part 1.

References

- [1] K. Wilson and J. Kogut, Phys. Rep. **12 C** (1974) 75.
- [2] F. J. Wegner and A. Houghton, Phys. Rev. **A 8** (1973) 401.
- [3] J. Polchinski, Nucl. Phys. **B 231** (1984) 269.
- [4] M. E. Fisher, Rev. Mod. Phys. **70** (1998) 653.
- [5] T. R. Morris, Prog. Theor. Phys. Suppl. **131** (1998) 395, [arXiv:hep-th/9802039].
- [6] D. F. Litim and J. M. Pawłowski, in *The Exact Renormalization Group*, eds. A. Krasnitz et al., World Sci (1999) 168, [arXiv:hep-th/9901063].
- [7] K. Aoki, Int. J. Mod. Phys. **B 14** (2000) 1249.
- [8] J. Berges, N. Tetradis and C. Wetterich, Phys. Rept. **363** (2002) 223, [arXiv:hep-ph/0005122].
- [9] C. Bagnuls and C. Bervillier, Phys. Rept. **348** (2001) 91, [arXiv:hep-th/0002034].
- [10] J. Polonyi, Central Eur. J. Phys. **1** (2003) 1, [arXiv:hep-th/0110026].
- [11] M. Salmhofer and C. Honerkamp, Prog. Theor. Phys. **105** (2001) 1.
- [12] B. Delamotte, D. Mouhanna and M. Tissier, Phys. Rev. **B 69** (2004) 134413, [arXiv:cond-mat/0309101].
- [13] M. Reuter and C. Wetterich, Nucl. Phys. **B 417** (1994) 181.
- [14] M. Reuter and C. Wetterich, Phys. Rev. **D 56** (1997) 7893, [arXiv:hep-th/9708051].
- [15] B. Bergerhoff and C. Wetterich, Phys. Rev. **D 57** (1998) 1591, [arXiv:hep-ph/9708425].
- [16] D. F. Litim and J. M. Pawłowski, JHEP 0209 (2002) 049, [arXiv:hep-th/0203005].
- [17] M. Bonini and E. Tricarico, Nucl. Phys. **B 606** (2001) 231, [arXiv:hep-th/0104255].
- [18] F. Freire, D. F. Litim and J. M. Pawłowski, Phys. Lett. **B 495** (256) 2000, [arXiv:hep-th/0009110].
- [19] H. Gies, Phys. Rev. **D 66** (2002) 025006, [arXiv:hep-th/0202207].
- [20] D. F. Litim and J. M. Pawłowski, Phys. Lett. **B 546** (2002) 279, [arXiv:hep-th/0208216].
- [21] C. Becchi, in *Elementary Particles, Field Theory and Statistical Mechanics* (Parma, 1993), [arXiv:hep-th/9607188].
- [22] M. Bonini, M. D'Attanasio and G. Marchesini, Nucl. Phys. **B 421** (1994) 429, [arXiv:hep-th/9312114].
- [23] M. Bonini, M. D'Attanasio and G. Marchesini, Nucl. Phys. **B 437** (1995) 163, [arXiv:hep-th/9410138].
- [24] U. Ellwanger, Phys. Lett. **B 335** (1994) 364, [arXiv:hep-th/9402077].
- [25] U. Ellwanger, M. Hirsch and A. Weber, Z. Phys. **C 69** (1996) 687, [arXiv:hep-th/9506019].
- [26] U. Ellwanger, M. Hirsch and A. Weber, Eur. Phys. J. **C 1** (1998) 563, [arXiv:hep-ph/9606468].
- [27] U. Ellwanger, Z. Phys. **C 76** (1997) 721, [arXiv:hep-ph/9702309].
- [28] U. Ellwanger, Nucl. Phys. **B 531** (1998) 593, [arXiv:hep-ph/9710326].
- [29] U. Ellwanger, Nucl. Phys. **B 560** (1999) 587, [arXiv:hep-th/9906061].
- [30] U. Ellwanger and N. Wschebor, Eur. Phys. J. **C 28** (2003) 415, [arXiv:hep-th/0211014].
- [31] M. D'Attanasio and T. R. Morris, Phys. Lett. **B 378** (1996) 213, [arXiv:hep-th/9602156].
- [32] D. F. Litim and J. M. Pawłowski, Phys. Lett. **B 435** (1998) 181, [arXiv:hep-th/9802064].
- [33] M. Simionato, Int. J. Mod. Phys. **A 15** (2000) 2153, [arXiv:hep-th/9810117].
- [34] M. Simionato, Int. J. Mod. Phys. **A 15** (2000) 4811, [arXiv:hep-th/0005083].
- [35] A. Panza and R. Soldati, Phys. Lett. **B 493** (2000) 197, [arXiv:hep-th/0006170].
- [36] J. M. Pawłowski, D. F. Litim, S. Nedelko and L. von Smekal, Phys. Rev. Lett. **93** (2004) 152002, [arXiv:hep-th/0312324].
- [37] C. S. Fischer and H. Gies, JHEP 0410 (2004) 048. [arXiv:hep-ph/0408089].
- [38] V. Branchina, K. A. Meissner and G. Veneziano, Phys. Lett. **B 574** (2003) 319, [arXiv:hep-th/0309234].
- [39] J. M. Pawłowski, [arXiv:hep-th/0310018].
- [40] J. M. Pawłowski, [arXiv:hep-th/0512261].
- [41] S. Arnone, Y. A. Kubyshin, T. R. Morris and J. F. Tighe, Int. J. Mod. Phys. **A 17** (2283) 2002, [arXiv:hep-th/0106258].

- [42] T. R. Morris, in *The Exact Renormalization Group*, eds. A. Krasnitz *et al*, World Sci (1999) 1, [arXiv:hep-th/9810104].
- [43] T. R. Morris, Nucl. Phys. **B 573** (2000) 97, [arXiv:hep-th/9910058].
- [44] T. R. Morris, JHEP 0012 (2000) 012, [arXiv:hep-th/0006064].
- [45] S. Arnone, A. Gatti and T. R. Morris, Phys. Rev. **D 67** (2003) 085003, [arXiv:hep-th/0209162].
- [46] V. N. Gribov, Nucl. Phys. **B 139** (1978) 1.
- [47] J. I. Latorre and T. R. Morris, JHEP 0011 (2000) 004, [arXiv:hep-th/0008123].
- [48] J. I. Latorre and T. R. Morris, Int. J. Mod. Phys. **A 16** (2001) 2071, [arXiv:hep-th/0102037].
- [49] S. Arnone, T. R. Morris and O. J. Rosten, [arXiv:hep-th/0507154].
- [50] T. R. Morris and O. J. Rosten, Phys. Rev. **D 73** (2006) 065003, [arXiv:hep-th/0508026].
- [51] O. J. Rosten, ‘The Manifestly Gauge Invariant Exact Renormalisation Group’, Ph.D. Thesis, [arXiv:hep-th/0506162].
- [52] O. J. Rosten, J. Phys. **A: Math. Gen.** 39 (2006) 8699-8726, [arXiv:hep-th/0507166].
- [53] O. J. Rosten, J. Phys. **A: Math. Gen.** 39 (2006) 8141-8155, [arXiv:hep-th/0511107].
- [54] S. Arnone, A. Gatti and T. R. Morris, JHEP 0205 (2002) 059, [arXiv:hep-th/0201237].
- [55] S. Arnone, A. Gatti, T. R. Morris and O. J. Rosten, Phys. Rev. **D 69** (2004) 065009, [arXiv:hep-th/0309242].
- [56] S. Arnone, T. R. Morris and O. J. Rosten, JHEP 0510 (2005) 115, [arXiv:hep-th/0505169].
- [57] L. P. Kadanoff, Physics **2** (1966) 263.
- [58] See *e.g.* S. Weinberg, *The Quantum Theory of Fields* (Cambridge University Press, Cambridge 1996), Vol. 2.
- [59] O. J. Rosten, Phys. Rev. **D 74** (2006) 125006, [arXiv:hep-th/0604183].
- [60] K. G. Wilson, Phys. Rev. **D 10** (1974) 2445.
- [61] A. Hasenfratz and P. Hasenfratz, Nucl. Phys. **B 270** (1986) 687.
- [62] C. Wetterich, Phys. Lett. **B 301** (1993) 90.
- [63] B. Bergerhoff, D. Litim, S. Lola and C. Wetterich, Int. J. Mod. Phys. **A 11** (1996) 4273, [arXiv:cond-mat/9502039].
- [64] B. Bergerhoff, F. Freire, D. Litim, S. Lola and C. Wetterich, Phys. Rev. **B 53** (1996) 5734, [arXiv:hep-ph/9503334].
- [65] K. I. Aoki, K. i. Morikawa, J. I. Sumi, H. Terao and M. Tomoyose, Prog. Theor. Phys. **97** (1997) 479, [arXiv:hep-ph/9612459].
- [66] N. Evans, T. R. Morris and O. J. Rosten, Phys. Lett. **B 635** (2006) 148, [arXiv:hep-th/0601114].